Astronomy 233 Spring 2011

Physical Cosmology

Week 6

Structure Formation

Joel Primack

University of California, Santa Cruz

Astro 233 - Spring 2011

Physical Cosmology

Week	Topics
1	Introduction
2	General Relativistic Cosmology
3	Big Bang Nucleosynthesis
4	Recombination, Dark Matter (DM)
5	DM Detection, Cosmic Microwave Background
6	Structure Formation
7	Galaxy Formation and Evolution
8	Galaxy Formation and Cosmic Inflation
9	Before and After Cosmic Inflation
10	Early Universe: Baryogenesis, Strings, ...
11	Student Presentations of Term Projects

Late Cosmological Epochs

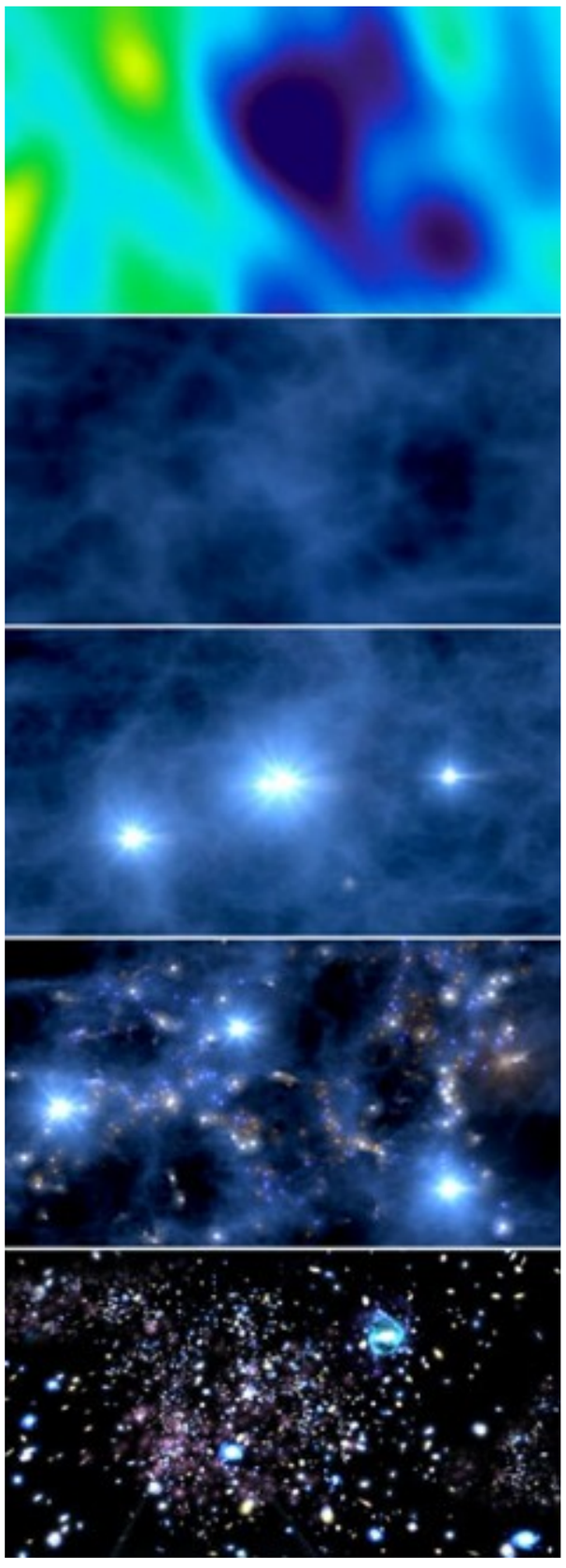

380 kyr z~1000

recombination
last scattering

dark ages

~100 Myr z~30

first stars

~480 Myr z~10

reionization

galaxy formation

13.7 Gyr z=0

today

Gravitational instability

small-amplitude fluctuations:

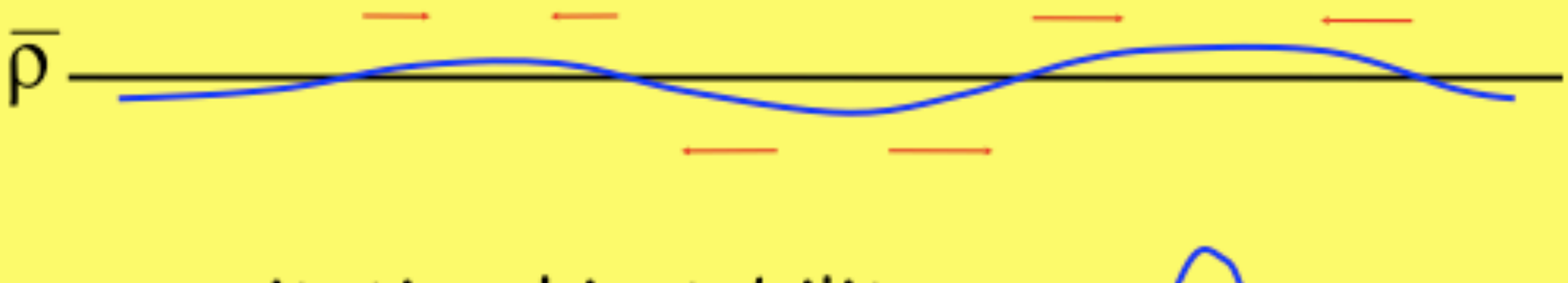

gravitational instability:

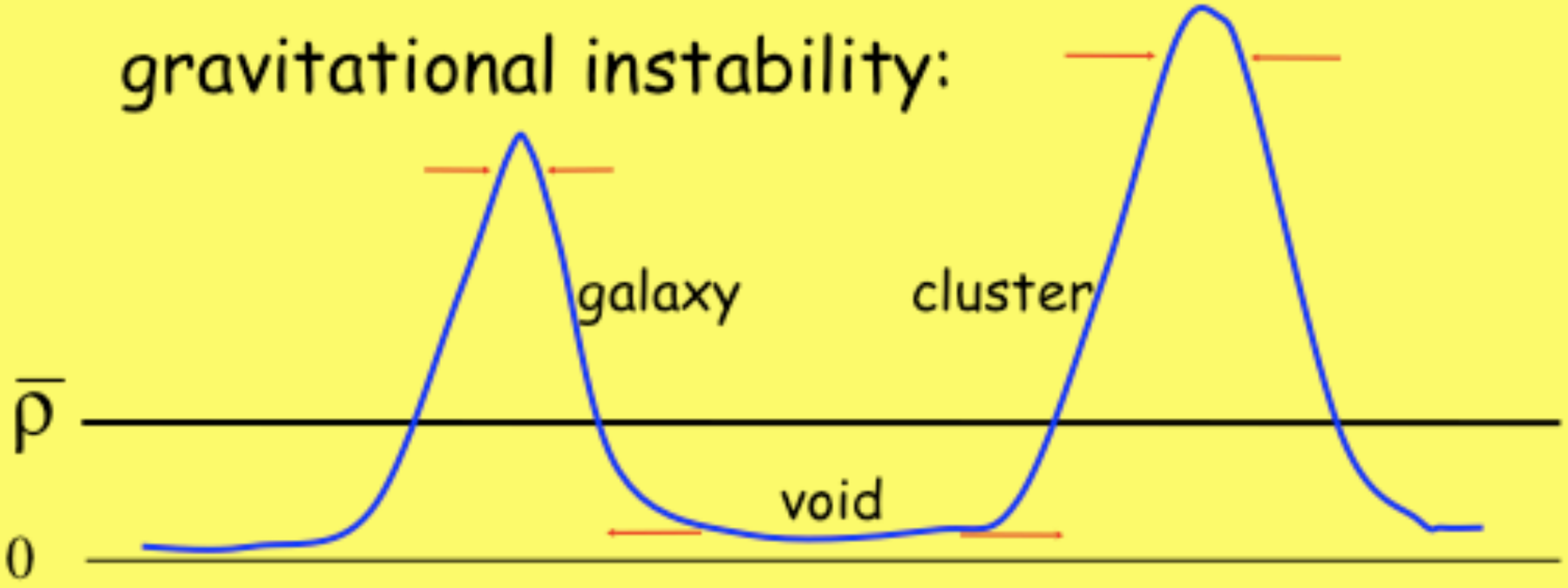

FLUCTUATIONS: LINEAR THEORY

Recall: $E(ii) - E(00) \Rightarrow \frac{2\ddot{a}}{a} = -\frac{8\pi}{3}G\rho - 8\pi G p + \frac{2}{3}\Lambda$ (here a = R, Λ=0)

"TOP HAT MODEL"

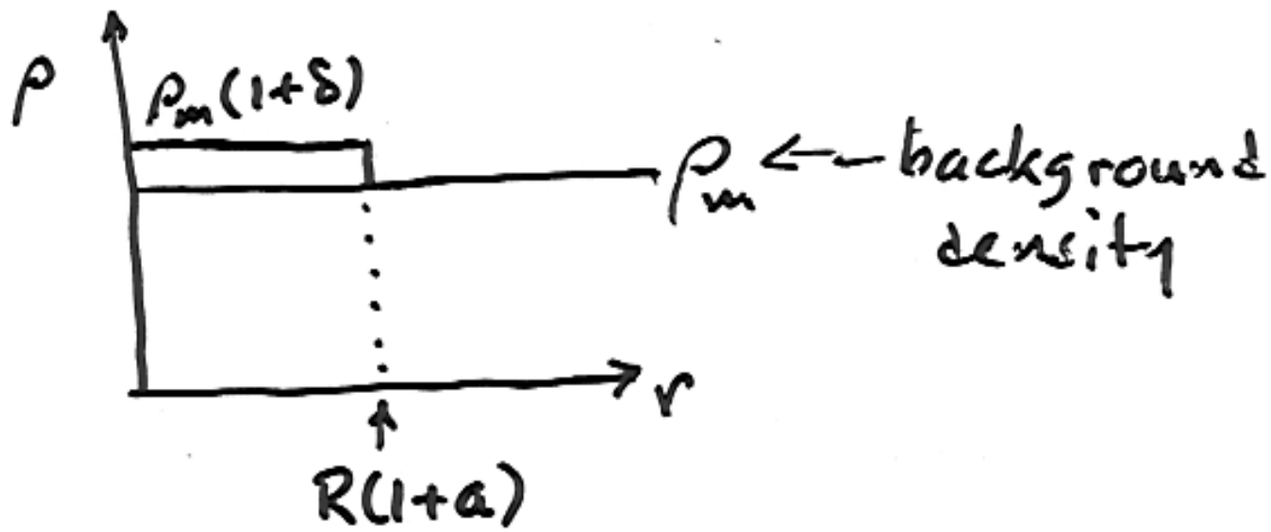

MASS CONS. ⇒

$\rho_m (1+\delta) R^3 (1+a)^3 = \text{const.} \Rightarrow$

$\delta = -3a$

GRAVITY: $\ddot{R} = -\frac{4\pi G}{3}(\rho + 3p)R$ APPLIED BOTH TO FLUCT. + BCG. ⇒

$$\ddot{\delta} + 2\frac{\dot{R}}{R}\dot{\delta} = 4\pi G \rho_m \delta$$

Try $\delta = t^\alpha$

RAD ERA $\dot{R}/R = \frac{1}{2}t^{-1}$,

MATTER ERA $= \frac{2}{3}t^{-1}$,

$\delta = At + Bt^{-1} = AR^2 + BR^{-2}$

$\delta = At^{2/3} + Bt^{-1} = AR + BR^{-3/2}$

GROWING MODE

CDM Structure Formation: Linear Theory

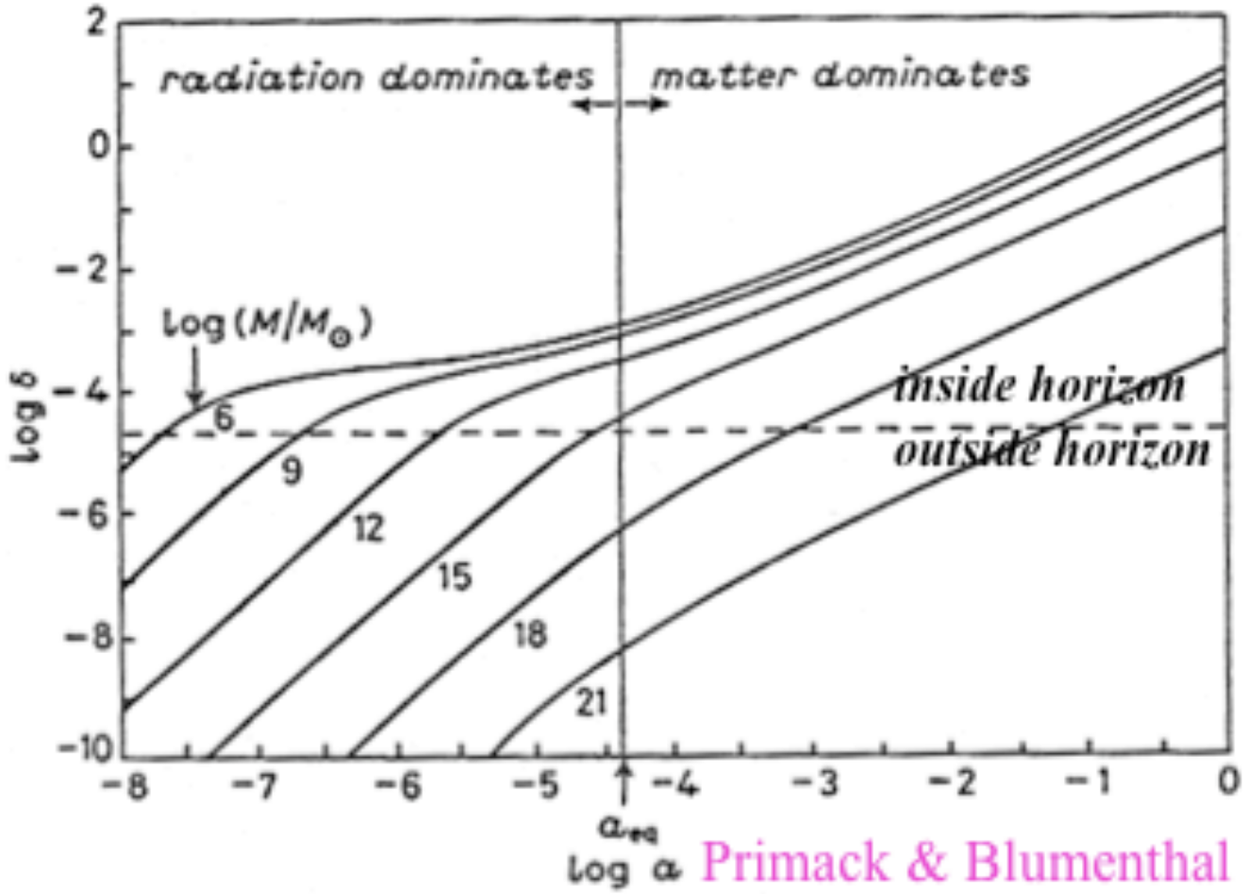

Primack & Blumenthal 1983

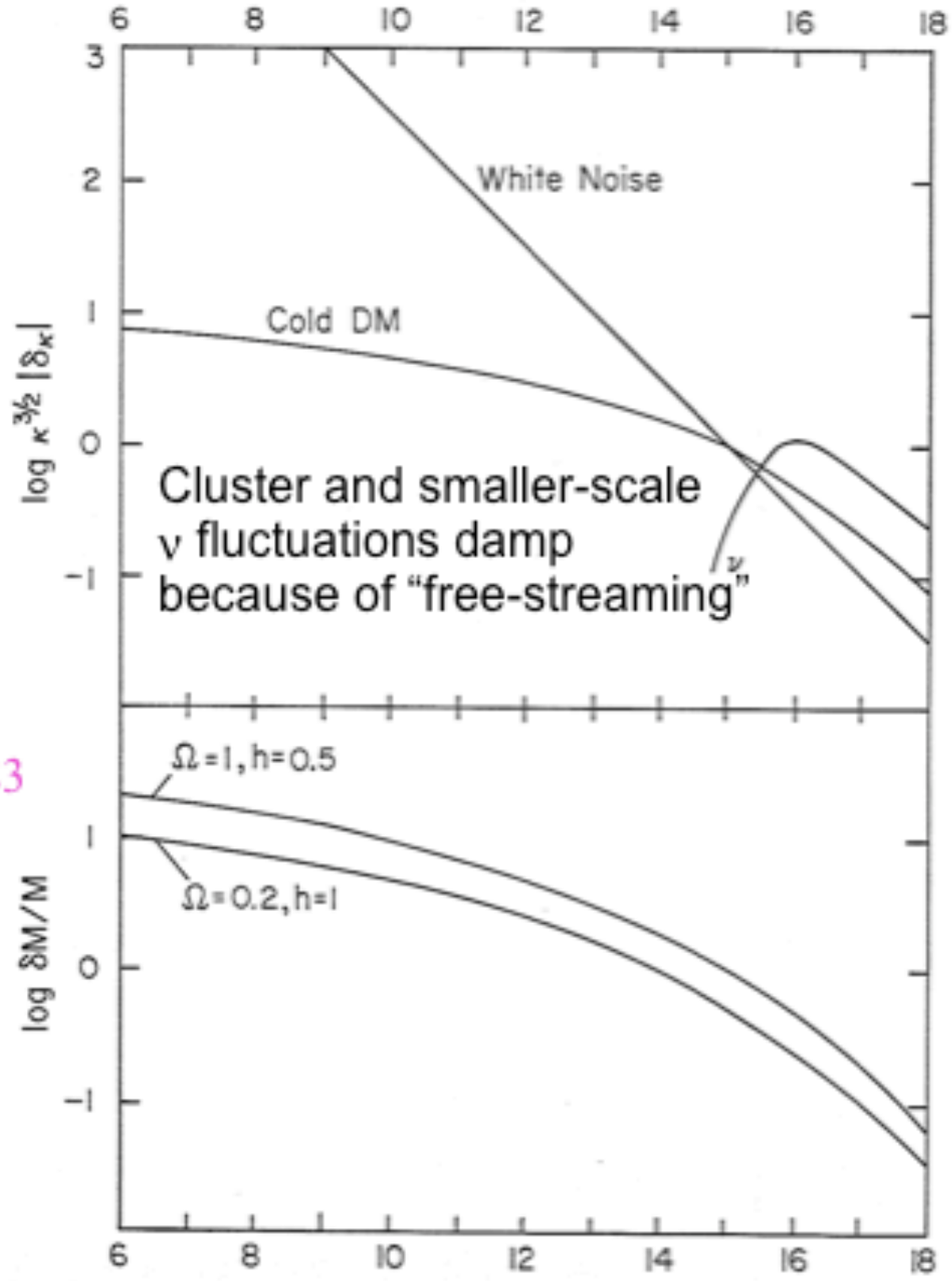

Blumenthal, Faber, Primack, & Rees 1984

Matter fluctuations that enter the horizon during the radiation dominated era, with masses less than about $10^{15} M_\odot$, grow only $\propto \log a$, because they are not in the gravitationally dominant component. But matter fluctuations that enter the horizon in the matter-dominated era grow $\propto a$. This explains the characteristic shape of the CDM fluctuation spectrum, with $\delta(k) \propto k^{-n/2-2} \log k$ for $k >> k_{eq}$.

The Initial Fluctuations

At Inflation: Gaussian, adiabatic

Fourier transform:

$$\delta(\vec{x}) = \sum_{\vec{k}} \delta_{\vec{k}}\ e^{i\vec{k}\cdot\vec{x}}$$

Power Spectrum:

$$P(k) \equiv <|\,\tilde{\delta}(\vec{k})\,|^2> \ \propto k^n$$

rms perturbation:

$$\delta_{rms} = <\delta^{\,2}>^{1/2} \propto \int_{k=0}^{k_{\max}} P_k\ d^3k \quad \propto M^{-(n+3)/6}$$

Correlation function:

$$\xi(r) \equiv <\delta(\vec{x})\delta(\vec{x}+\vec{r})> \ \propto \int |\,\tilde{\delta}(\vec{k})\,|^2\ e^{-i\vec{k}\cdot\vec{r}}\, d^3k \ \propto r^{-(n+3)}$$

$$dP = [1+\xi(r)]\, n\, dV$$

Gravitational Instability

Small fluctuations: $\delta, v, \varphi \quad (x,t)$ comoving coordinates

$$r = a(t)x \quad \text{etc.}$$

Continuity: $\dot{\delta} + \nabla \times v + \nabla \times (v\delta) = 0$

Euler: $\dot{v} + 2Hv + (v \times \nabla)v = -\nabla\varphi$

$$H \equiv \dot{a}/a, \quad \Omega(t)$$

matter era

Poisson: $\nabla^2\varphi = (3/2)H^2\Omega\delta$

Linear approximation: $\ddot{\delta} + 2H\dot{\delta} = (3/2)H^2\Omega\delta$

growing mode: $\delta \propto D(t) = t^{2/3} \xrightarrow[\Omega_m \to 0]{} t^0$

$$\delta = -\nabla \cdot v / [Hf(\Omega)] \qquad f(\Omega) \equiv \dot{D}/(HD) \approx \Omega^{0.6}$$

irrotational, potential flow: $\nabla \times v = 0 \quad v = -\nabla\varphi_v$

Thus far, we have considered only the evolution of fluctuations in the dark matter. But of course we have to consider also the ordinary matter, known in cosmology as "baryons" (implicitly including the electrons). See Piero Madau's lectures "The Astrophysics of Early Galaxy Formation" (http://arxiv.org/abs/0706.0123v1) and Avi Loeb's *How Did the First Stars and Galaxies Form?* (2010) for recent summaries. We have already seen that the baryons are primarily in the form of atoms after z ~ 1000, with a residual ionization fraction of a few x 10^{-4}. They become fully reionized by z ~ 6, but they were not reionized at z~20 since the COBE satellite found that "Compton parameter" $y \leq 1.5 \times 10^{-5}$, where

$$y = \int_0^z \frac{k_B T_e}{m_e c^2} \frac{d\tau_e}{dz} dz$$

This implies that $\langle x_e T_e \rangle [(1+z)^{3/2} - 1] < 4 \times 10^7 \, \mathrm{K}$. Thus, for example, a universe that was reionized and reheated at z = 20 to (x_e, T_e) = (1, > 4×10^5 K) would violate the COBE y-limit.

The figure at right shows the evolution of the radiation (dashed line, labeled CMB) and matter (solid line, labeled GAS) temperatures after recombination, in the absence of any reheating mechanism.
(From Madau's lectures.)

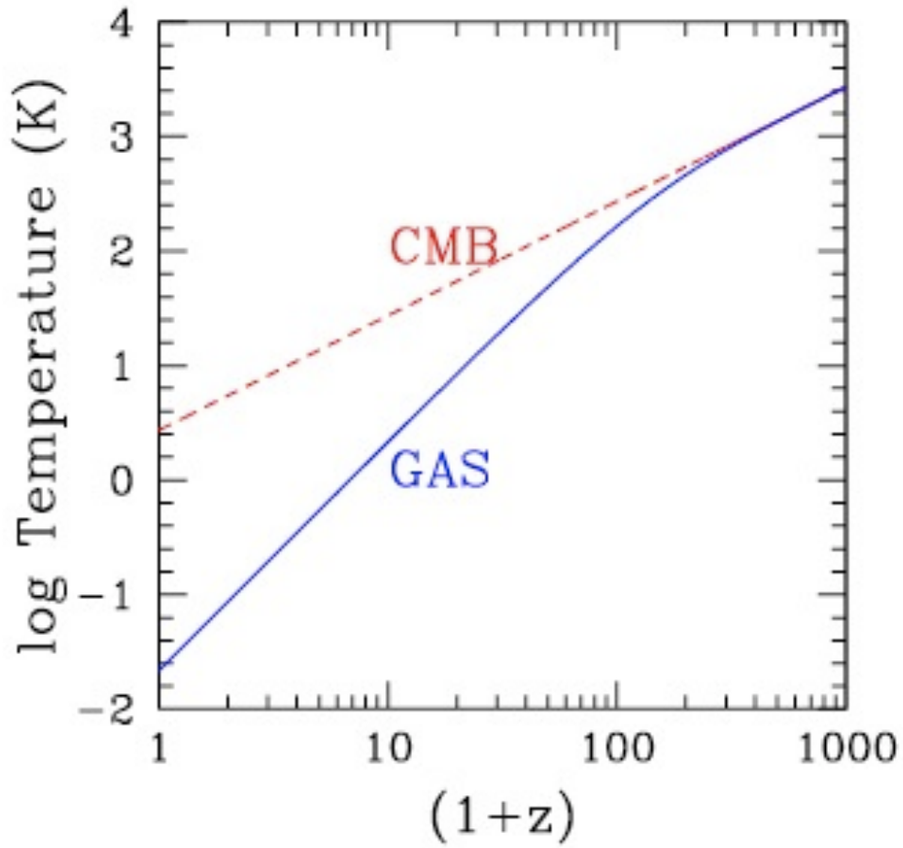

The linear evolution of sub-horizon density perturbations in the dark matter-baryon fluid is governed in the matter-dominated era by two second-order differential equations:

$$\ddot{\delta}_{\rm dm} + 2H\dot{\delta}_{\rm dm} = \frac{3}{2}H^2\Omega_m^z\left(f_{\rm dm}\delta_{\rm dm} + f_b\delta_b\right) \qquad (1)$$

for the dark matter, and

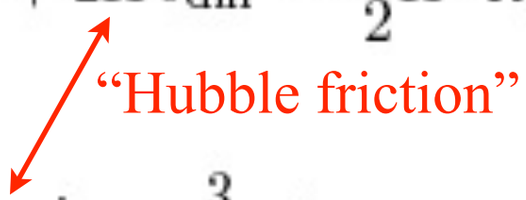

$$\ddot{\delta}_b + 2H\dot{\delta}_b = \frac{3}{2}H^2\Omega_m^z\left(f_{\rm dm}\delta_{\rm dm} + f_b\delta_b\right) - \frac{c_s^2}{a^2}k^2\delta_b$$

for the baryons, where dm(k) and b(k) are the Fourier components of the density fluctuations in the dark matter and baryons,† f_{dm} and f_b are the corresponding mass fractions, c_s is the gas sound speed, k is the (comoving) wavenumber, and the derivatives are taken with respect to cosmic time. Here

$$\Omega_m^z \equiv 8\pi G\rho(t)/3H^2 = \Omega_m(1+z)^3/[\Omega_m(1+z)^3+\Omega_\Lambda] \qquad (2)$$

is the time-dependent matter density parameter, and ρ(t) is the total background matter density. Because there is ~5 times more dark matter than baryons, it is the former that defines the pattern of gravitational wells in which structure formation occurs. If it were true that $f_b \simeq 0$ and the universe were static (H = 0), equation (1) above becomes

---

† For each fluid component (i = b, dm) the real space fluctuation in the density field, $\delta_i(\mathbf{x}) \equiv \delta\rho_i(\mathbf{x})/\rho_i$, can be written as a sum over Fourier modes,

$$\delta_i(\mathbf{x}) = \int d^3\mathbf{k}\,(2\pi)^{-3}\,\delta_i(\mathbf{k})\,\exp i\mathbf{k}\cdot\mathbf{x}.$$

$$\ddot{\delta}_{\rm dm} = 4\pi G\rho\delta_{\rm dm} \equiv \frac{\delta_{\rm dm}}{t_{\rm dyn}^2},$$

where t_{dyn} denotes the dynamical timescale. This equation admits solution

$$\delta_{\rm dm} \;=\; A_1 \exp(t/t_{\rm dyn}) + A_2 \exp(-t/t_{\rm dyn}).$$

After a few dynamical times, only the exponentially growing term is significant: gravity tends to make small density fluctuations in a static pressureless medium grow exponentially with time. Sir James Jeans (1902) was the first to discuss this.

The additional term $\propto H\dot{\delta}_{\rm dm}$ present in an expanding universe can be thought as a "Hubble friction" term that acts to slow down the growth of density perturbations. Equation (1) admits the general solution for the growing mode:

$$\delta_{\rm dm}(a) = \frac{5\Omega_m}{2}\, H_0^2\, H \int_0^a \frac{da'}{(\dot{a}')^3}, \qquad (3)$$

so that an Einstein-de Sitter universe gives the familiar scaling δ_{dm}(a) = a with coefficient unity. The right-hand side of equation (3) is called the linear growth factor D(a) = D_+(a). Different values of Ω_m, Ω_Λ lead to different linear growth factors.

Growing modes actually decrease in density, but not as fast as the average universe. Note how, in contrast to the exponential growth found in the static case, the growth of perturbations even in the case of an Einstein-de Sitter (Ω_m =1) universe is just algebraic (power-law) not exponential. This was discovered by the Russian physicist Lifshitz (1946).

Since cosmological curvature is at most marginally important at the present epoch, it was negligible during the radiation-dominated era and at least the beginning of the matter-dominated era. But for $k = -1$, i.e. $\Omega < 1$, the growth of δ slows for $(R/R_o) \gtrsim \Omega_o$, as gravity becomes less important and the universe begins to expand freely. To discuss this case, it is convenient to introduce the variable

$$x \equiv \Omega^{-1}(t) - 1 = (\Omega_o^{-1} - 1)R(t)/R_o. \tag{2.55}$$

(Note that $\Omega(t) \longrightarrow 1$ at early times.) The general solution in the matter-dominated era is then (Peebles, 1980, §11)

$$\delta = \tilde{A}D_1(t) + \tilde{B}D_2(t), \tag{2.56}$$

where the growing solution is

$$D_1 = 1 + \frac{3}{x} + \frac{3(1+x)^{1/2}}{x^{3/2}} \ln\left[(1+x)^{1/2} - x^{1/2}\right] \tag{2.57}$$

and the decaying solution is

$$D_2 = (1+x)^{1/2}/x^{3/2}. \tag{2.58}$$

These agree with the Einstein-de Sitter results (2.53) at early times ($t \ll t_o, x \ll 1$). For late times ($t \gg t_o, x \gg 1$) the solutions approach

$$D_1 = 1, D_2 = x^{-1}; \tag{2.59}$$

in this limit the universe is expanding freely and the amplitude of fluctuations stops growing.

The consequence is that dark matter fluctuations grow proportionally to the scale factor a(t) when matter is the dominant component of the universe, but only logarithmically when radiation is dominant. Thus there is not much difference in the amplitudes of fluctuations of mass $M < 10^{15}\ M_{sun}$, which enter the horizon before $z_{mr} \sim 3.5 \times 10^3$, while there is a stronger dependance on M for fluctuations with $M > 10^{15}\ M_{sun}$.

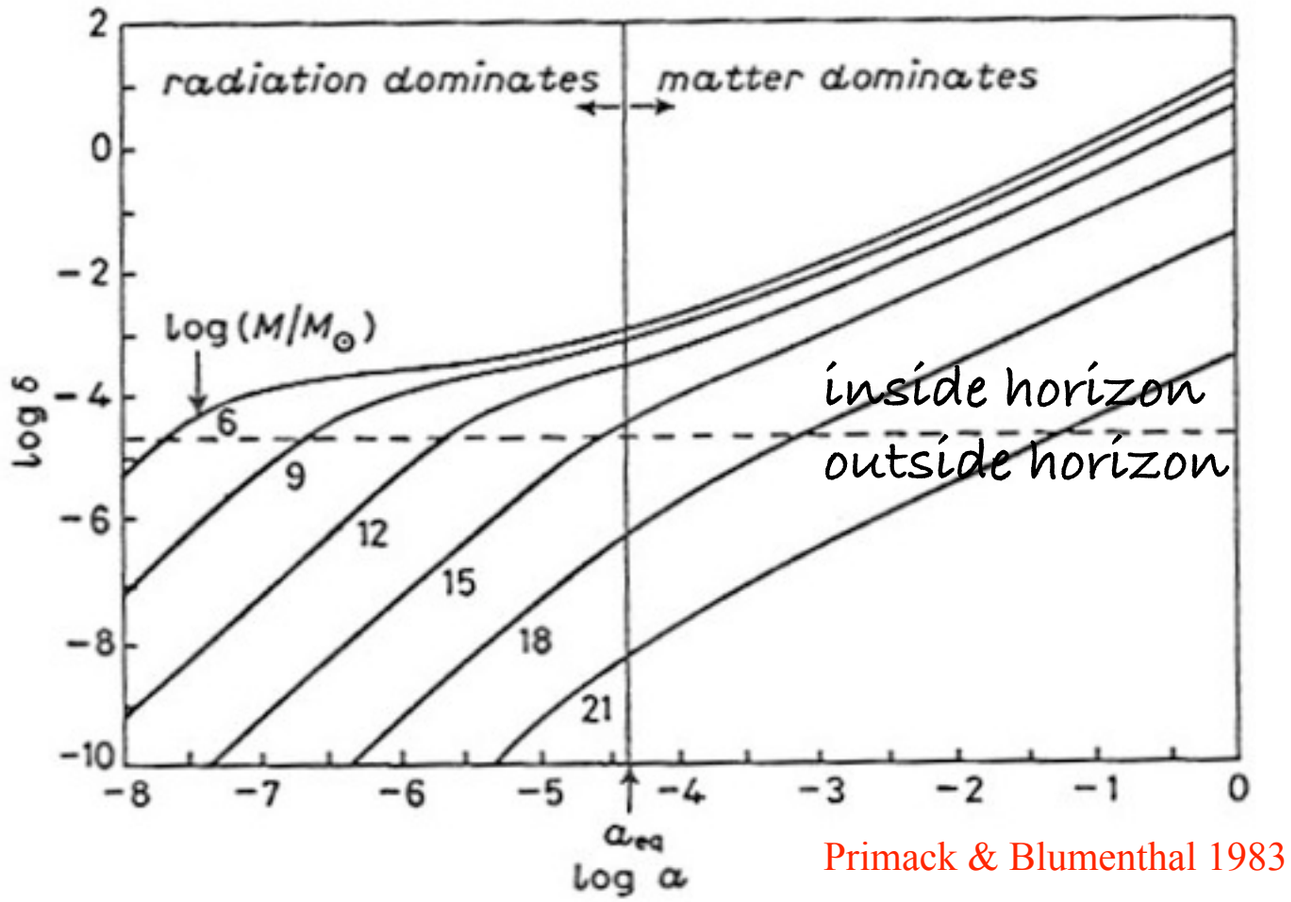

Primack & Blumenthal 1983

There is a similar suppression of the growth of matter fluctuations once the gravitationally dominant component of the universe is the dark energy, for example a cosmological constant. Lahav, Lilje, Primack, & Rees (1991) showed that the growth factor in this case is well approximated by

$$\delta_{\rm dm}(a) = D(a) \simeq \frac{5\Omega_m^z}{2(1+z)}\left[(\Omega_m^z)^{4/7} - \frac{(\Omega_m^z)^2}{140} + \frac{209}{140}\Omega_m^z + \frac{1}{70}\right]^{-1}.$$

Here Ω_m^z is again given by $\Omega_m^z \equiv 8\pi G\rho(t)/3H^2 = \Omega_m(1+z)^3/[\Omega_m(1+z)^3 + \Omega_\Lambda]$

The Linear Transfer Function T(k)

The observed uniformity of the CMB guarantees that density fluctuations must have been quite small at decoupling, implying that the evolution of the density contrast can be studied at $z \lesssim z_{\rm dec}$ using linear theory, and each mode $\delta(k)$ evolves independently. The inflationary model predicts a scale-inv$\approx$iant primordial power spectrum of density fluctuations $P(k) \equiv \langle|\delta(k)|^2\rangle \propto k^n$, with $n = 1$ (the so-called Harrison-Zel'dovich spectrum). It is the index n that governs the balance between large and small-scale power. In the case of a Gaussian random field with zero mean, the power spectrum contains the complete statistical information about the density inhomogeneity. It is often more convenient to use the dimensionless quantity $\Delta_k^2 \equiv [k^3 P(k)/2\pi^2]$, which is the power per logarithmic interval in wavenumber k. In the matter-dominated epoch, this quantity retains its initial primordial shape ($\Delta_k^2 \propto k^{n+3}$) only on very large scales. Small wavelength modes enter the horizon earlier on and their growth is suppressed more severely during the radiation-dominated epoch: on small scales the amplitude of Δ_k^2 is essentially suppressed by four powers of k (from k^{n+3} to k^{n-1}). If $n = 1$, then small scales will have nearly the same power except for a weak, logarithmic dependence. Departures from the initially scale-free form are described by the transfer function $T(k)$, defined such that $T(0) = 1$:

$$P(k, z) = Ak^n \left[\frac{D(z)}{D(0)}\right]^2 T^2(k),$$

where A is the normalization.

An approximate fitting function for T(k) in a ΛCDM universe is (Bardeen et al. 1986)

$$T_k = \frac{\ln(1+2.34q)}{2.34q}\left[1+3.89q+(16.1q)^2+(5.46q)^3+(6.71q)^4\right]^{-1/4},$$

where (Sugayama 1995)

$$q \equiv \frac{k/\mathrm{Mpc}^{-1}}{\Omega_m h^2 \exp(-\Omega_b - \Omega_b/\Omega_m)}.$$

For accurate work, for example for starting high-resolution N-body simulations, it is best to use instead of fitting functions the numerical output of highly accurate integration of the Boltzmann equations, for example from CMBFast, which is available at
http://lambda.gsfc.nasa.gov/toolbox/ which points to
http://lambda.gsfc.nasa.gov/toolbox/tb_cmbfast_ov.cfm

W e l c o m e to the CMBFAST Website!

This is the most extensively used code for computing cosmic microwave background anisotropy, polarization and matter power spectra. The code has been tested over a wide range of cosmological parameters. We are continuously testing and updating the code based on suggestions from the cosmological community. Do not hesitate to contact us if you have any questions or suggestions.

U. Seljak & M. Zaldarriaga

CMB Toolbox Overview

We provide links to a number of useful tools for CMB and Astronomy in general.

CMB Tools

- CMB Simulations - High-resolution, full-sky microwave temperature simulations including secondary anisotropies.

- Contributed Software is an archive at a LAMBDA partner site for tools built by members of the community.
- CMBFast - A tool that computes spectra for the cosmic background for a given set of CMB parameters. LAMBDA provides a web-based interface for this tool. Seljak and Zaldarriaga
- CAMB - Code for Anisotropies in the Microwave Background that computes spectra for a set of CMB parameters. LAMBDA provides a web-based interface for this tool. Lewis and Challinor
- CMBEASY - A C++ package, initially based on CMBFAST, now featuring a parameter likelihood package as well. Doran
- CMBview - A Mac OS X program for viewing HEALPix-format CMB data on an OpenGL-rendered sphere. Portsmouth
- COMBAT - A set of computational tools for CMB analysis. Borrill et al.
- CosmoMC - A Markov-Chain Monte-Carlo engine for exploring cosmological parameter space. Lewis and Bridle
- CosmoNet - Accelerated cosmological parameter estimation using Neural Networks.
- GLESP - Gauss-Legendre sky pixelization package. Doroshkevich, et al.
- GSM - Predicted all-sky maps at any frequency from 10 MHz to 100 GHz. de Oliveira-Costa.
- HEALPix - A spherical sky pixelization scheme. The Wilkinson Microwave Anisotropy Probe (WMAP) data skymap products are supplied in this form. Górski et al.
- IGLOO - A sky pixelization package. Crittenden and Turok
- MADCAP - Microwave Anisotropy Data Computational Analysis Package. Borrill et al.
- PICO - Integrates with CAMB and/or CosmoMC for cosmological parameter estimation using machine learning. Wandelt and Fendt
- RADPACK - Radical Compression Analysis Package. Knox
- RECFAST- Software to calculate the recombination history of the Universe. Seager, Sasselov, and Scott
- SkyViewer - A LAMBDA-developed OpenGL-based program to display HEALPix-based skymaps stored in FITS format files. Phillips
- SpiCE - Spatially Inhomogenous Correlation Estimator. Szapudi et al.
- WMAPViewer - A LAMBDA-developed web-based CMB map viewing tool using a technology similar to that found on maps.google.com. Phillips
- WOMBAT - Microwave foreground emission tools. Gawiser, Finkbeiner, Jaff et al.

Likelihood Software

- SDSS LRG DR7 Likelihood Software - A software package that computes likelihoods for Luminous Red Galaxies (LRG) data from the seventh release of the Sloan Digital Sky Survey (SDSS).
- WMAP Likelihood Software - A software library used by the WMAP team to compute Fisher and Master matrices and to compute the likelihoods of various models. This is the same software found on the WMAP products list; more information may be found here.

Other Tools

- WMAP Effective Frequency Calculator - A tool that calculates the effective frequencies of the five WMAP frequency bands.
- CFITSIO - A library of C and Fortran routines for reading and writing data in the FITS format.
- IDL Astro - The IDL Astronomy Users Library.
- Conversion Utilities - A small collection of astronomical conversion utilities.
- Calculators - A list of links to calculators.

This collection of tools can only be extended and improved with your input! Please feel free to send us suggestions and comments.

Scale-Invariant Spectrum (Harrison-Zel'dovich)

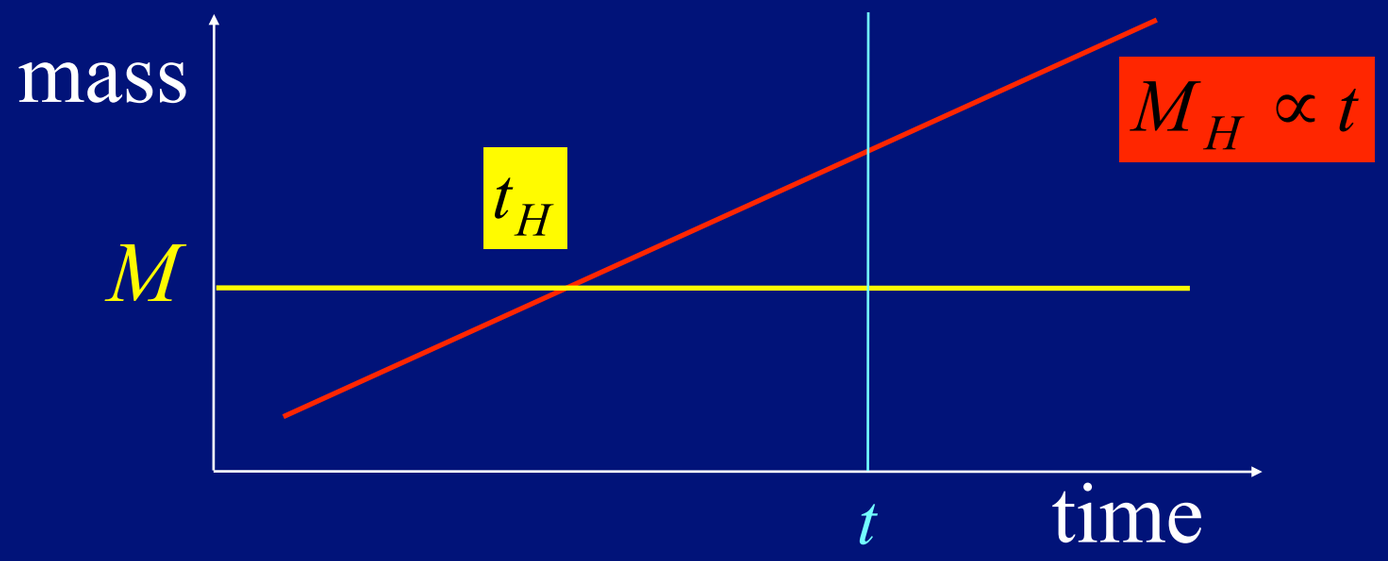

$$\delta(M,t) = \delta_H \left(\frac{t}{t_H(M)} \right)^{2/3} \propto M^{-2/3} t^{2/3}$$

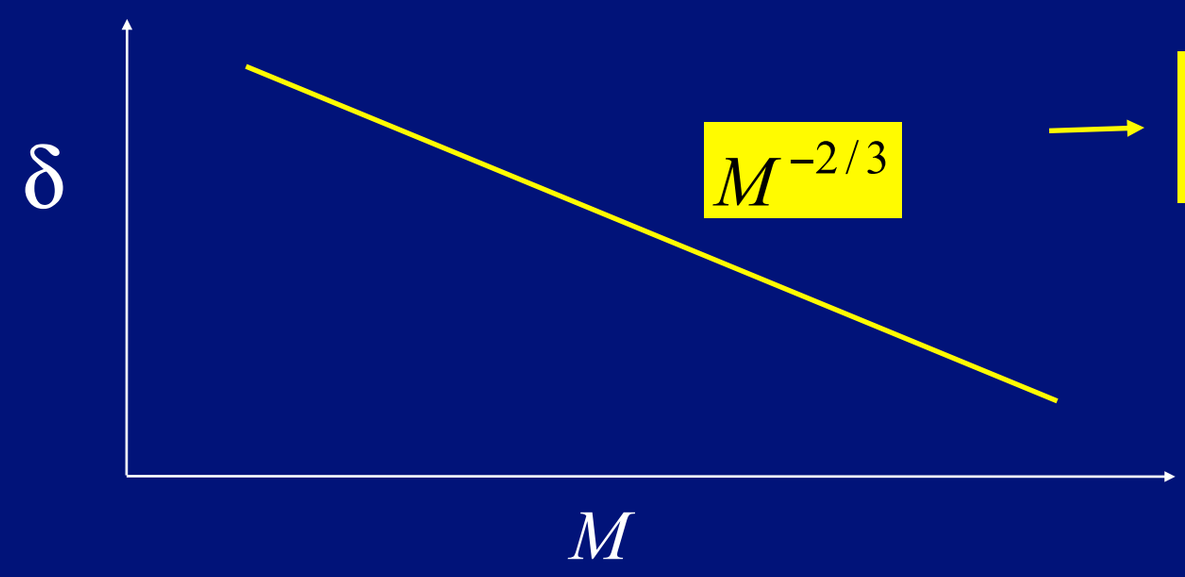

$$\rightarrow \quad n = +1 \quad P_k \propto k$$

CDM Power Spectrum

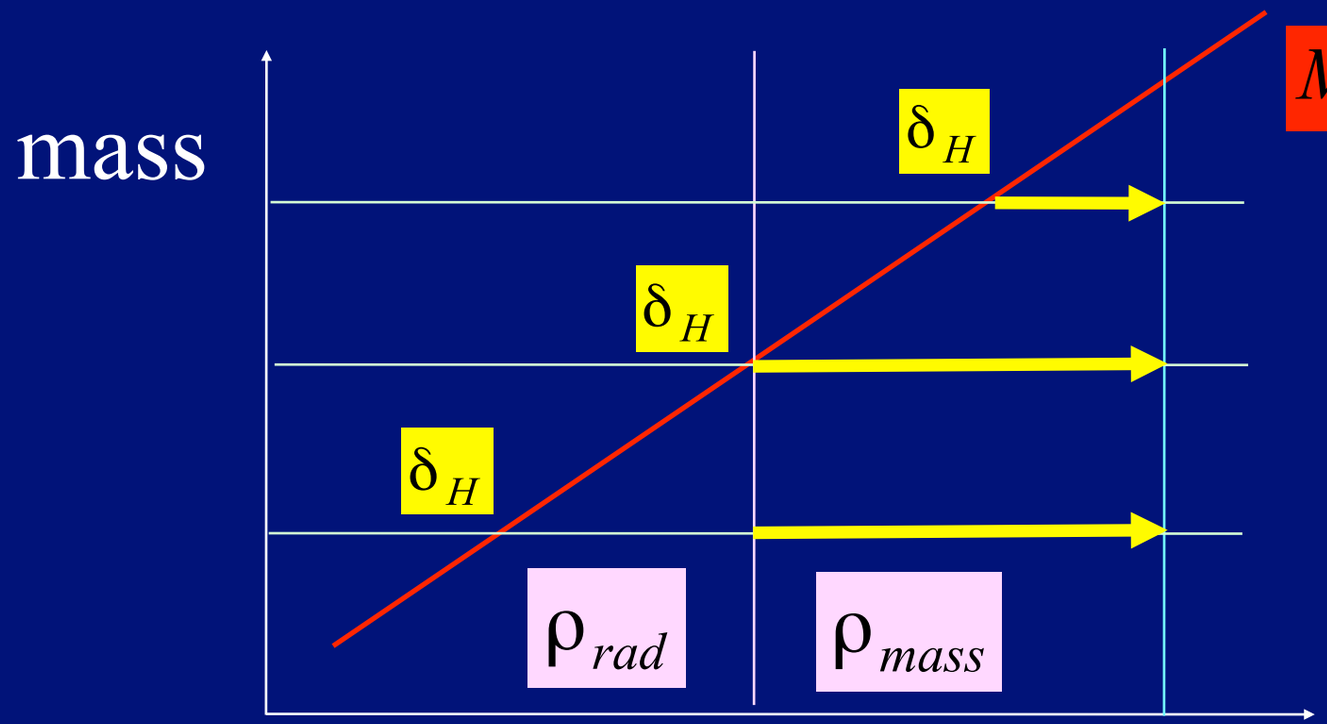

δ growth when matter is self-gravitating

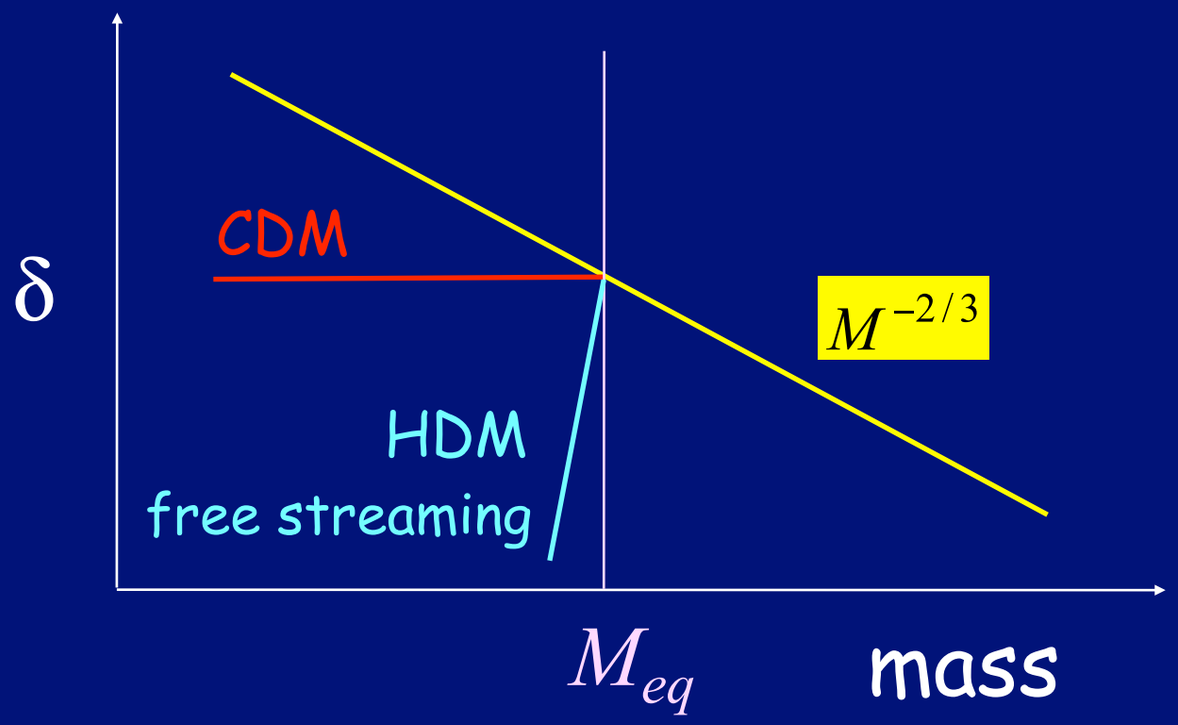

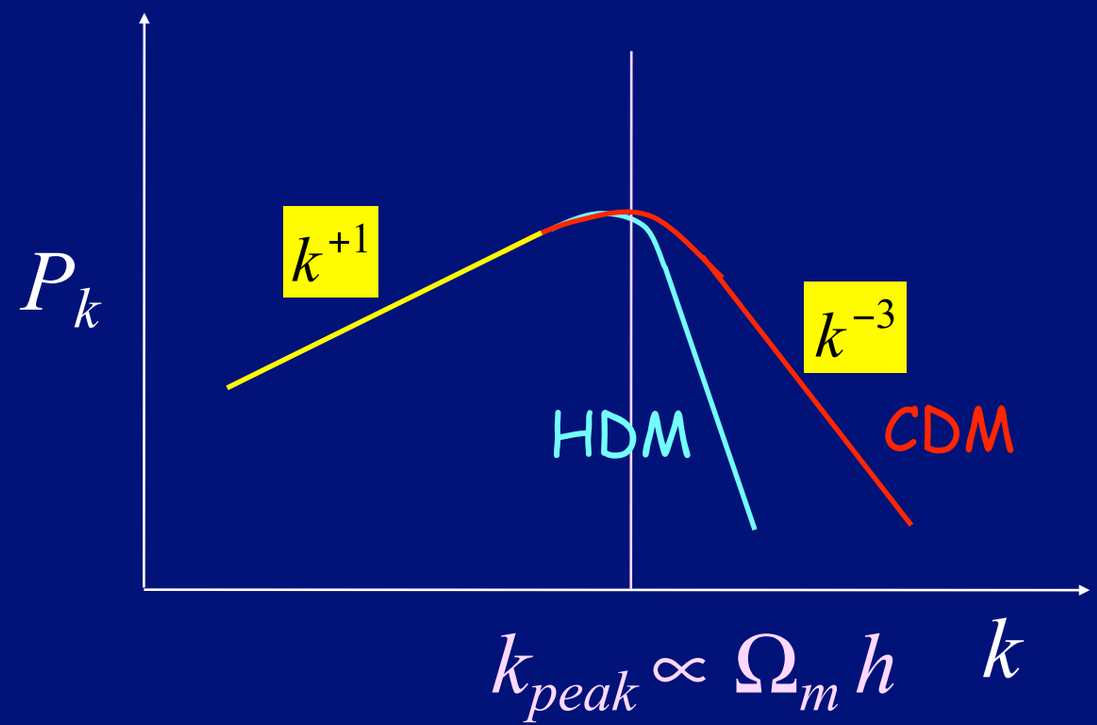

Formation of Large-Scale Structure

Fluctuation growth in the linear regime: $\delta << 1 \longrightarrow \delta \propto t^{2/3}$

rms fluctuation at mass scale M: $\delta \propto M^{-\alpha} \quad 0 < \alpha \leq 2/3$

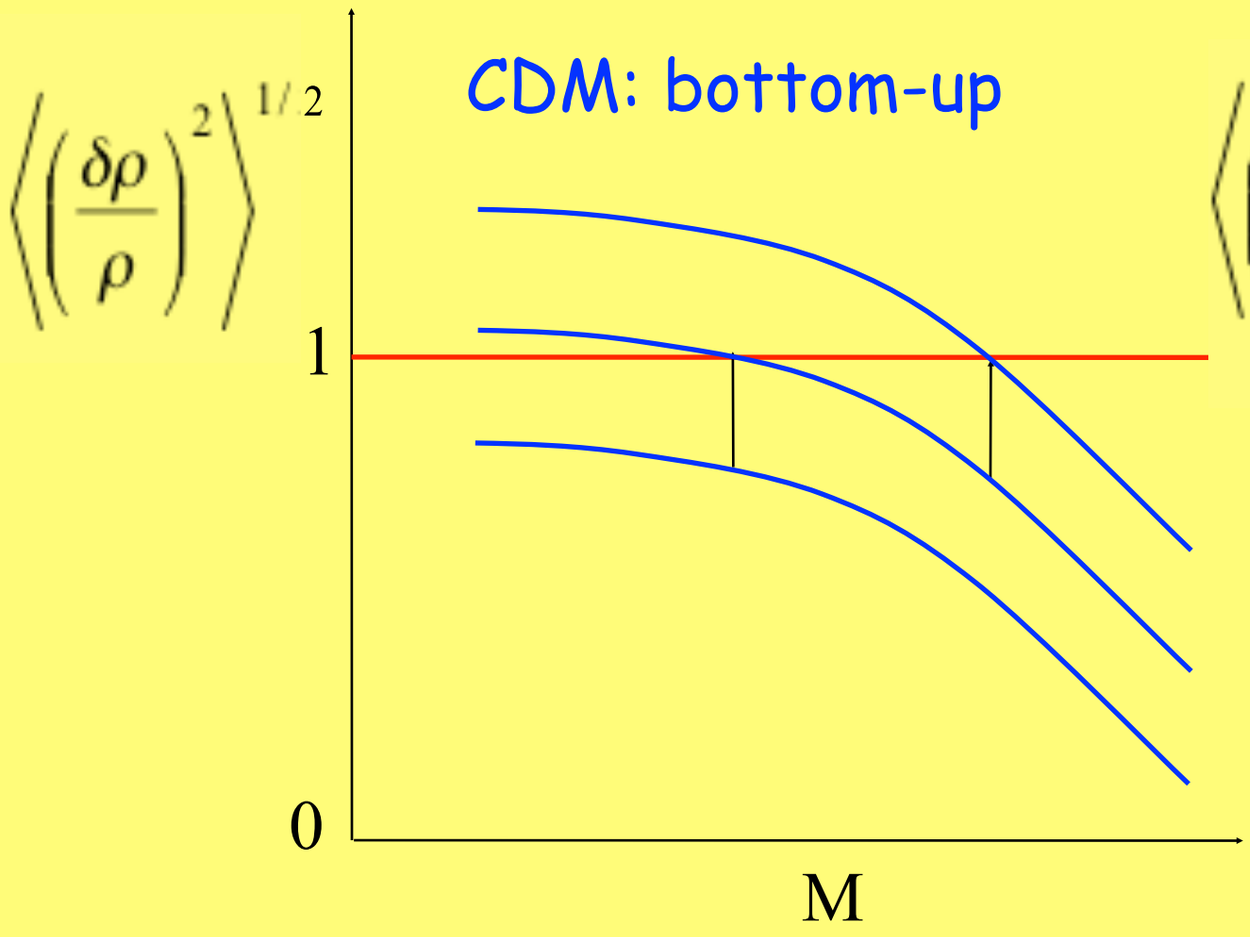

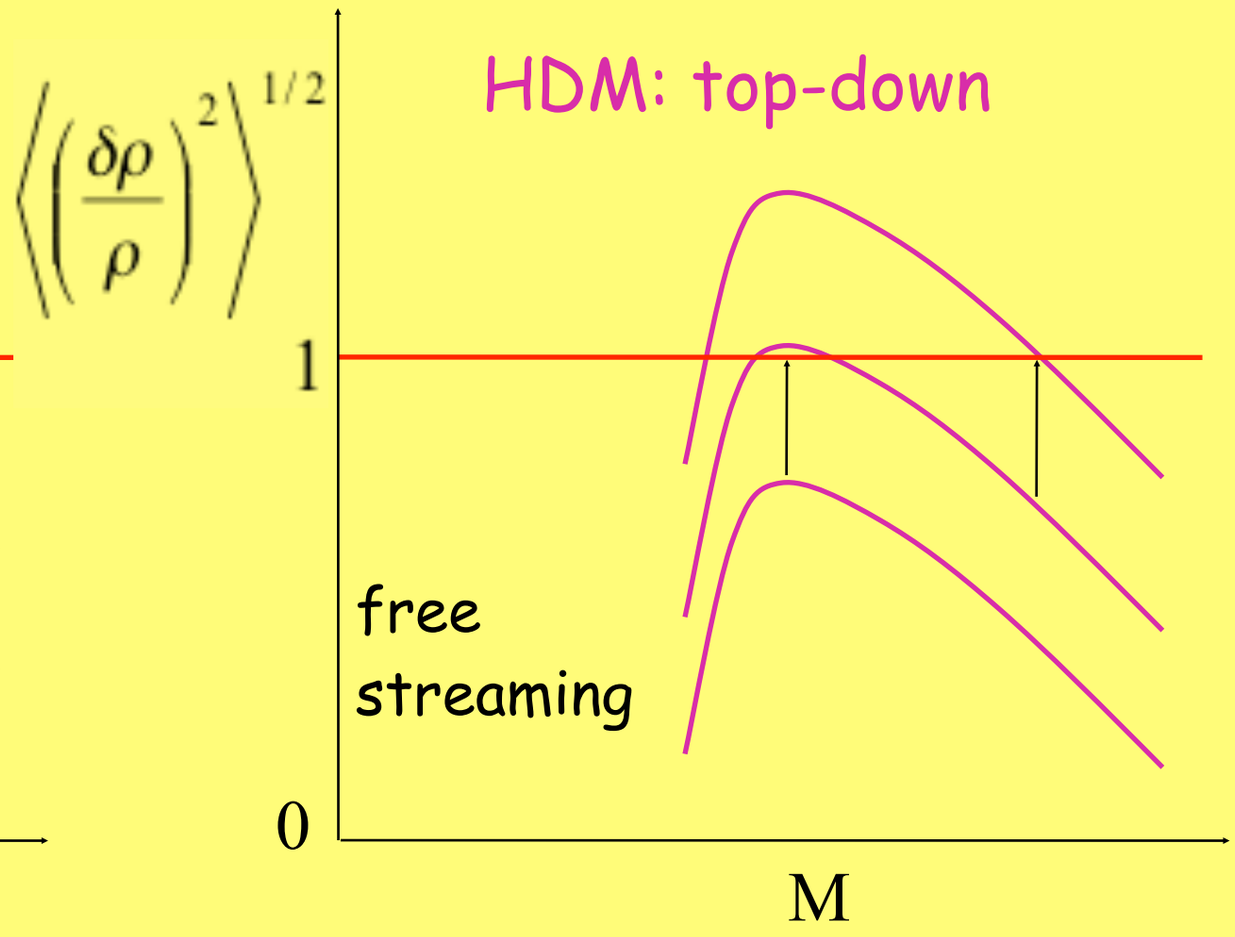

Structure forms earliest in Open, next in Benchmark, latest in EdS model.

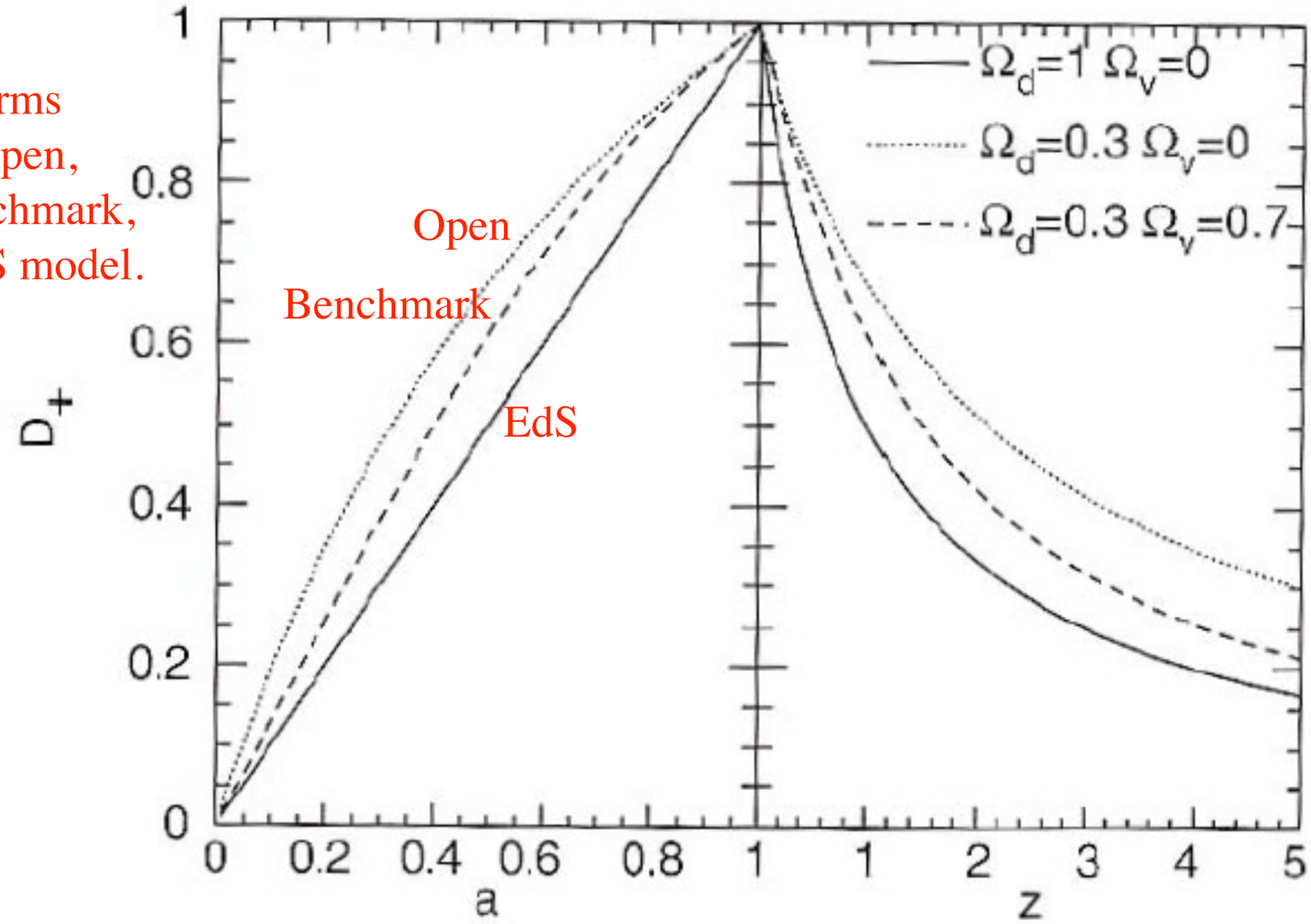

Einstein-de Sitter

Open universe

Benchmark model

Fig. 7.3. Growth factor D_+ for three different cosmological models, as a function of the scale factor a (left panel) and of redshift (right panel). It is clearly visible how quickly D_+ decreases with increasing redshift in the EdS model, in comparison to the models of lower density

From Peter Schneider, *Extragalactic Astronomy and Cosmology* (Springer, 2006)

Linear Growth Rate Function $D(a)$

For completeness, here we present some approximations used in the text. For the family of flat cosmologies ($\Omega_{\rm m}+\Omega_\Lambda=1$) an accurate approximation for the value of the virial overdensity $\Delta_{\rm vir}$ is given by the analytic formula (Bryan & Norman 1998):

$$\Delta_{\rm vir} = (18\pi^2 + 82x - 39x^2)/\Omega(z), \tag{A1}$$

where $\Omega(z) \equiv \rho_{\rm m}(z)/\rho_{\rm crit}$ and $x \equiv \Omega(z) - 1$.

The linear growth-rate function $\delta(a)$, used in eqs. (14-15) and also in $\sigma_8(a)$ is defined as

$$\delta(a) = D(a)/D(1), \tag{A2}$$

where $a = 1/(1+z)$ is the expansion parameter and $D(a)$ is:

$$D(a) = \frac{5}{2}\left(\frac{\Omega_{\rm m,0}}{\Omega_{\Lambda,0}}\right)^{1/3} \frac{\sqrt{1+x^3}}{x^{3/2}} \int_0^x \frac{x^{3/2}dx}{[1+x^3]^{3/2}}, \tag{A3}$$

$$x \equiv \left(\frac{\Omega_{\Lambda,0}}{\Omega_{\rm m,0}}\right)^{1/3} a, \tag{A4}$$

where $\Omega_{\rm m,0}$ and $\Omega_{\Lambda,0}$ are density contributions of matter and cosmological constant at $z=0$. For $\Omega_{\rm m} > 0.1$ the growth rate factor $D(a)$ can be accurately approximated by the following expressions (Lahav et al. 1991; Carroll et al. 1992):

$$D(a) = \frac{(5/2)a\Omega_{\rm m}}{\Omega_{\rm m}^{4/7} - \Omega_\Lambda + (1+\Omega_{\rm m}/2)(1+\Omega_\Lambda/70)}, \tag{A5}$$

$$\Omega_{\rm m}(a) = \Omega_{\rm m,0}/(1+x^3), \tag{A6}$$

$$\Omega_\Lambda(a) = 1 - \Omega_{\rm m}(a) \tag{A7}$$

For $\Omega_{\rm m,0} = 0.27$ the error of these approximation is less than 7×10^{-4}.

From Klypin, Trujillo, Primack - Bolshoi paper I - Appendix A

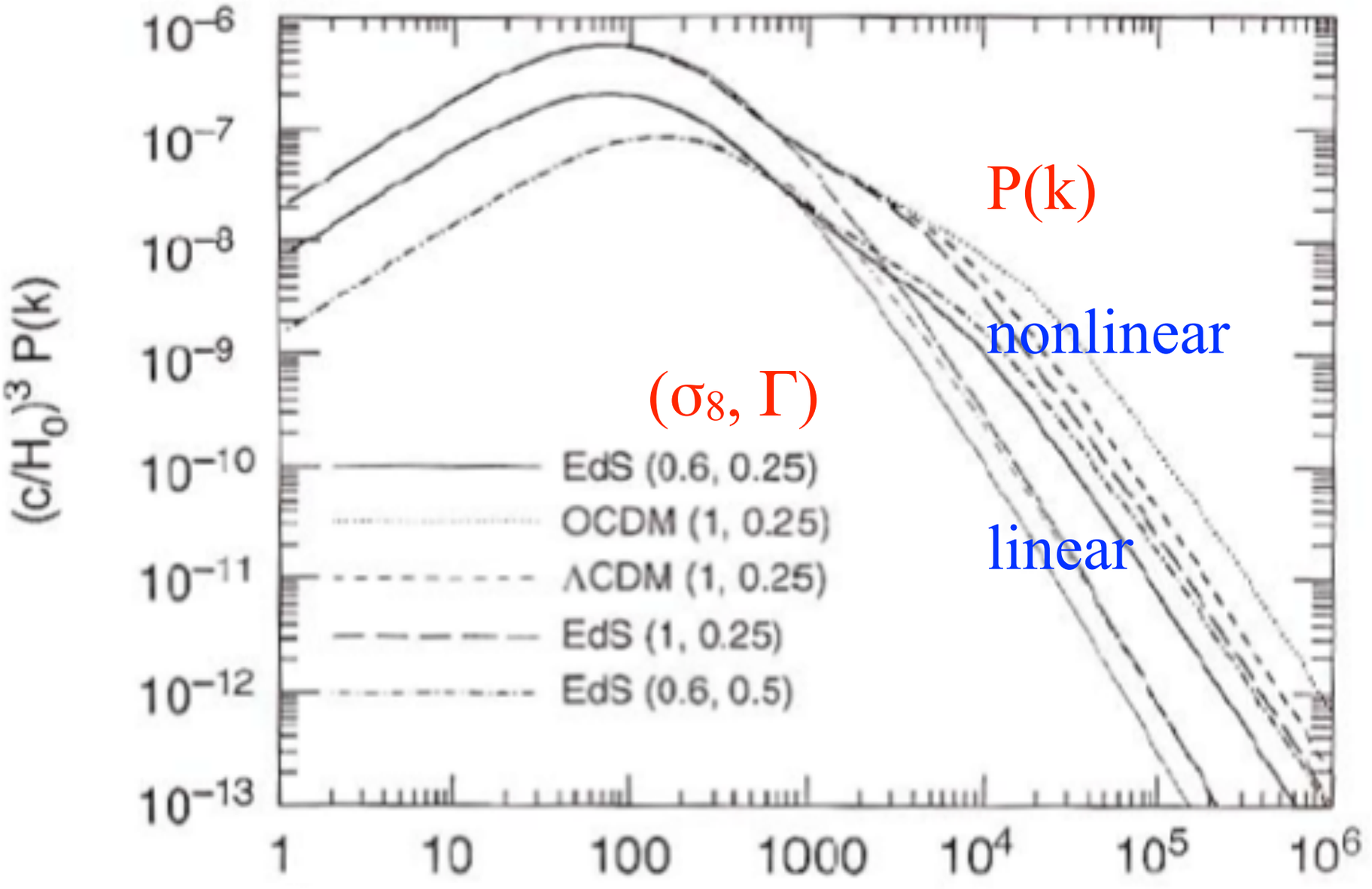

Fig. 7.6. The current power spectrum of density fluctuations for CDM models. The wave number k is given in units of H_0/c, and $(H_0/c)^3\ P(k)$ is dimensionless. The various curves have different cosmological parameters: EdS: $\Omega_m = 1$, $\Omega_\Lambda = 0$; OCDM: $\Omega_m = 0.3$, $\Omega_\Lambda = 0$; ΛCDM: $\Omega_m = 0.3$, $\Omega_\Lambda = 0.7$. The values in parentheses specify (σ_8, Γ), where σ_8 is the normalization of the power spectrum (which will be discussed below), and where Γ is the shape parameter. The thin curves correspond to the power spectrum $P_0(k)$ linearly extrapolated to the present day, and the bold curves take the non-linear evolution into account

From Peter Schneider, *Extragalactic Astronomy and Cosmology* (Springer, 2006)

On large scales (k small), the gravity of the dark matter dominates. But on small scales, pressure dominates and growth of baryonic fluctuations is prevented. Gravity and pressure are equal at the Jeans scale

$$k_J = \frac{a}{c_s}\sqrt{4\pi G\rho}.$$

The Jeans mass is the dark matter + baryon mass enclosed within a sphere of radius $\pi a/k_J$,

$$M_J = \frac{4\pi}{3}\rho\left(\frac{\pi a}{k_J}\right)^3 = \frac{4\pi}{3}\rho\left(\frac{5\pi k_B T_e}{12G\rho m_p \mu}\right)^{3/2} \approx 8.8\times 10^4\ \mathrm{M}_\odot \left(\frac{aT_e}{\mu}\right)^{3/2},$$

where μ is the mean molecular weight. The evolution of M_J is shown below, assuming that reionization occurs at z=15:

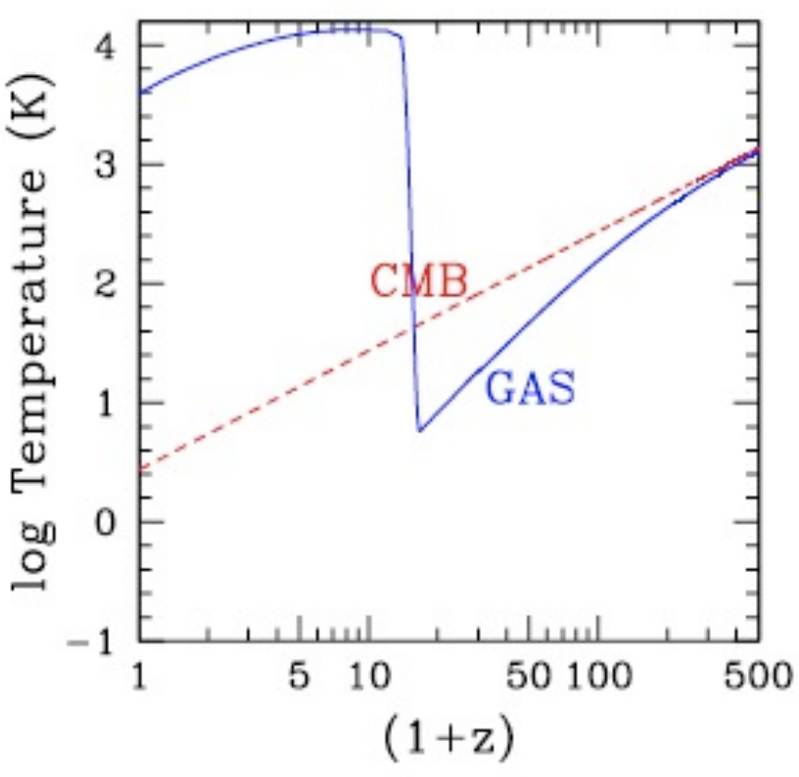

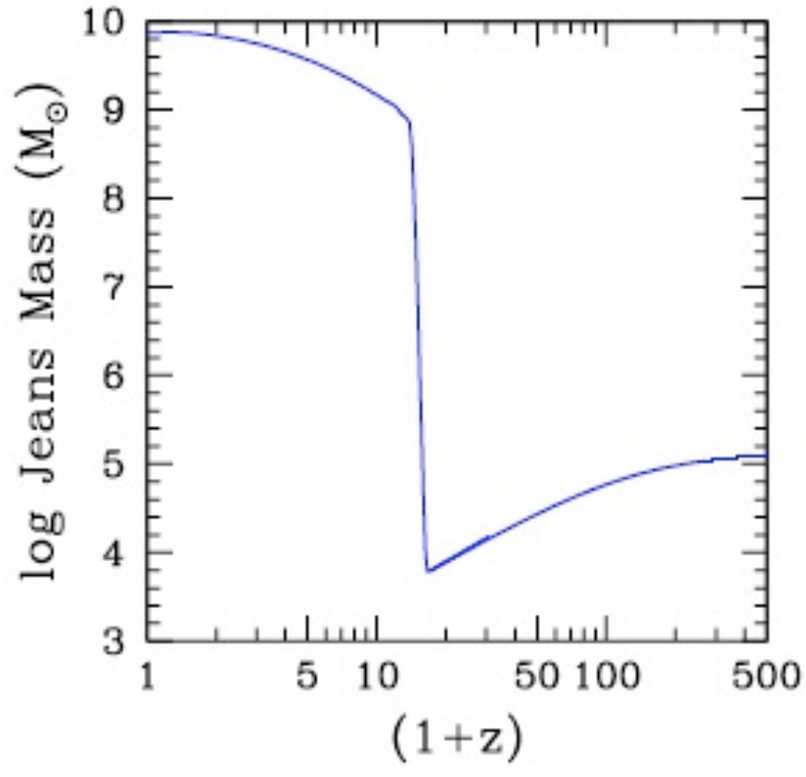

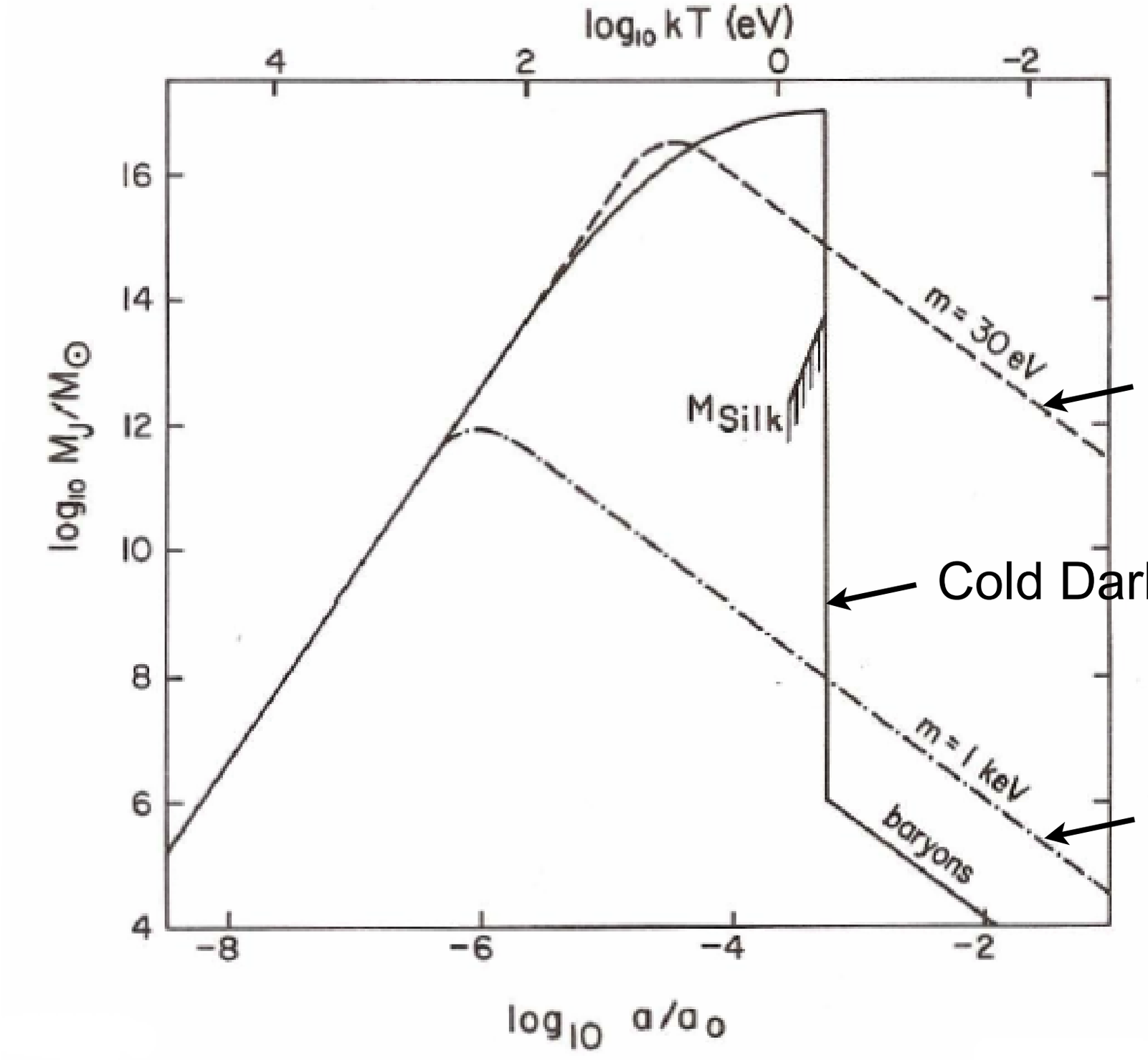

Hot Dark Matter

Cold Dark Matter

Warm Dark Matter

Jeans-type analysis for HDM, WDM, and CDM

GRAVITY – The Ultimate Capitalist Principle

Astronomers say that a region of the universe with more matter is "richer." Gravity magnifies differences—if one region is slightly denser than average, it will expand slightly more slowly and grow relatively denser than its surroundings, while regions with less than average density will become increasingly less dense. The rich always get richer, and the poor poorer.

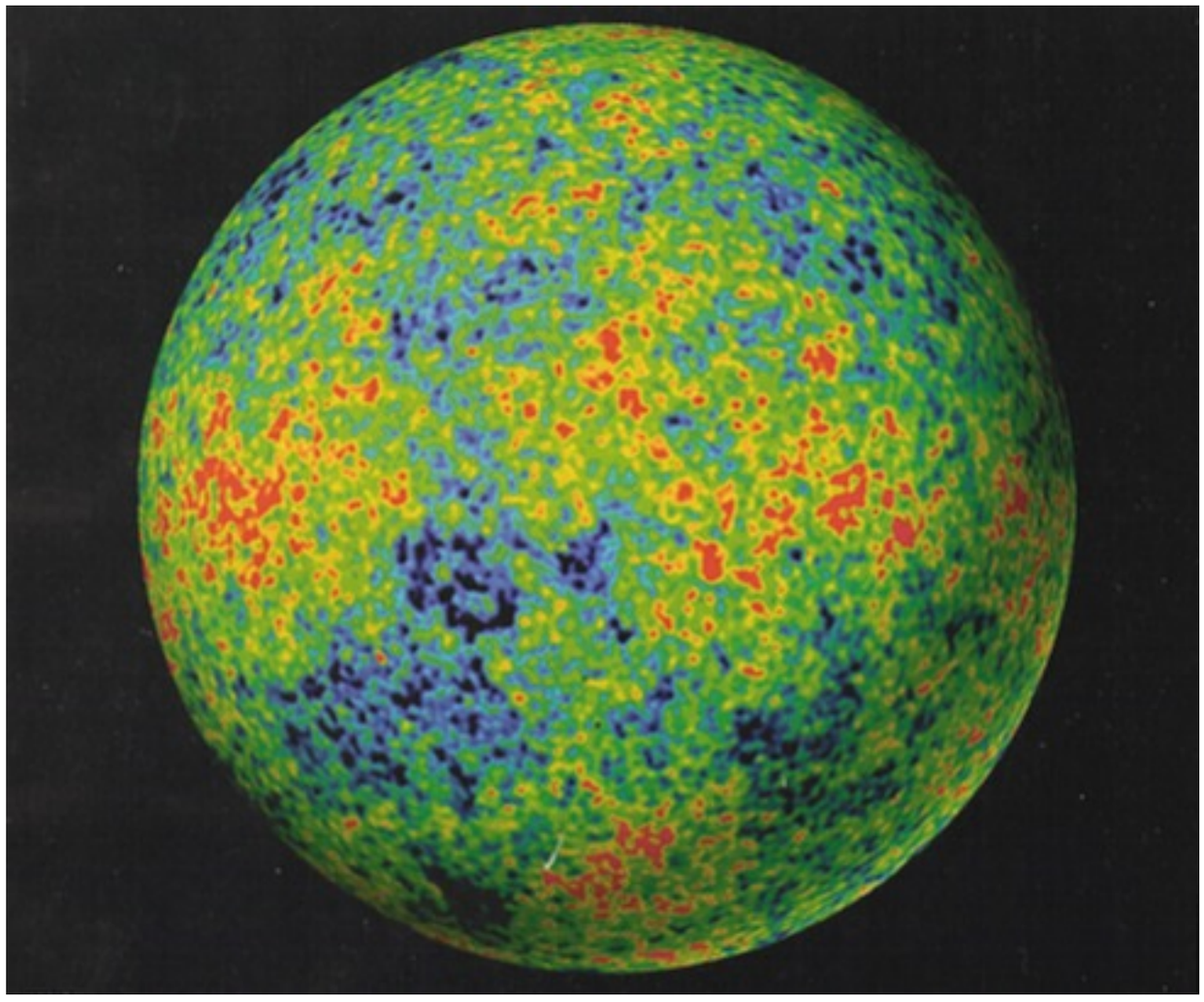

Temperature map at 380,000 years after the Big Bang. Blue (cooler) regions are slightly denser. From NASA's WMAP satellite, 2003.

The early universe expands *almost* perfectly uniformly. But there are small differences in density from place to place (about 30 parts per million). Because of gravity, denser regions expand more slowly, less dense regions more rapidly. Thus gravity amplifies the contrast between them, until…

Structure Formation by Gravitational Collapse

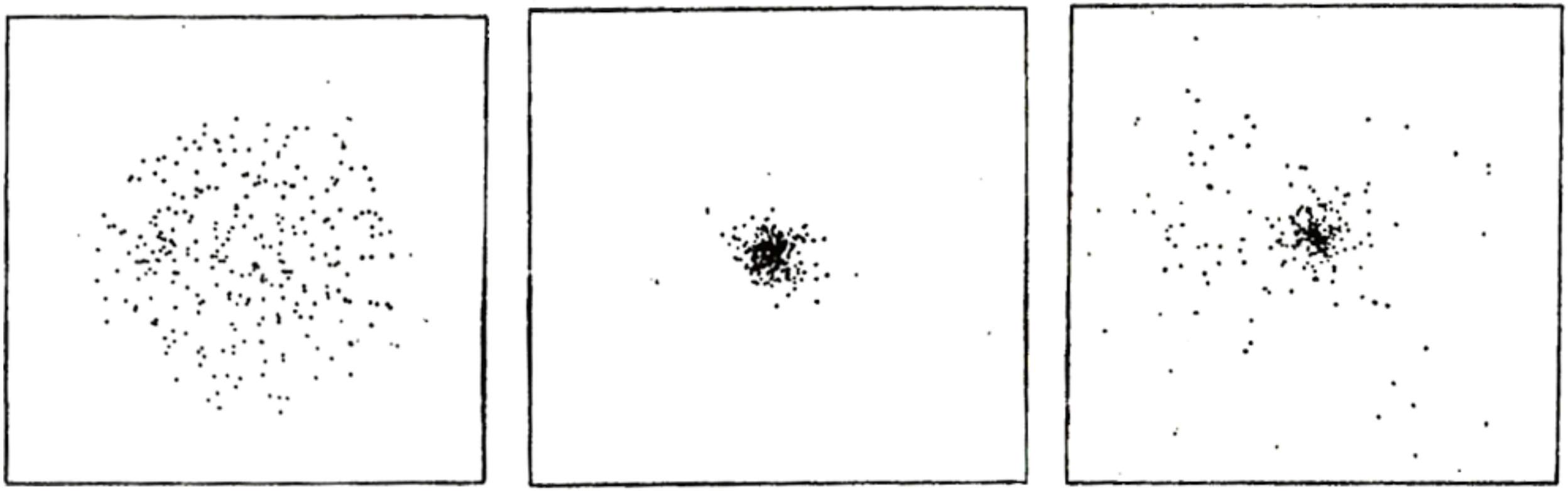

When any region becomes about twice as dense as typical regions its size, it reaches a maximum radius, *stops expanding*,

and starts falling together. The forces between the subregions generate velocities which *prevent* the material from *all falling toward the center*.

Through Violent Relaxation the dark matter quickly reaches a *stable configuration* that's about half the maximum radius but denser in the center.

Simulation of top-hat collapse: P.J.E. Peebles 1970, ApJ, 75, 13.

Used in my 1984 summer school lectures "Dark matter, Galaxies, and Large Scale Structure," http://tinyurl.com/3bjknb3

TOP HAT
Max Expansion

VIOLENT RELAXATION

VIRIALIZED

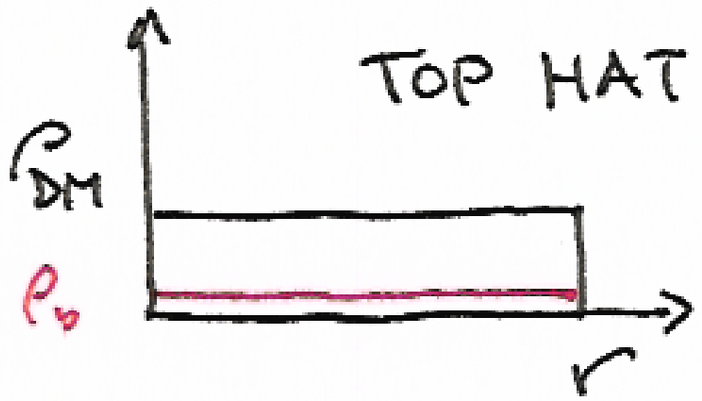

Virial Theorem: $\langle K \rangle = -\frac{1}{2}\langle W \rangle$

$W_m = \frac{c}{r_m}$, so after virialization

$$\frac{c}{r_m} = E = W + K = \frac{1}{2}\langle W \rangle = \frac{c}{2r_v}$$

$$\Rightarrow r_v = \frac{1}{2} r_m, \quad \rho_v = 8\rho_m \approx 50\,\bar{\rho}(t_m)$$

$$\langle v^2 \rangle \approx \frac{GM}{r_v}$$

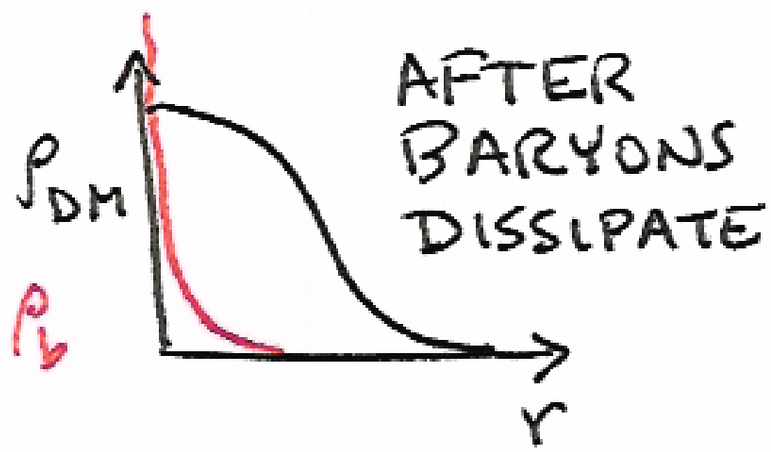

Growth and Collapse of Fluctuations

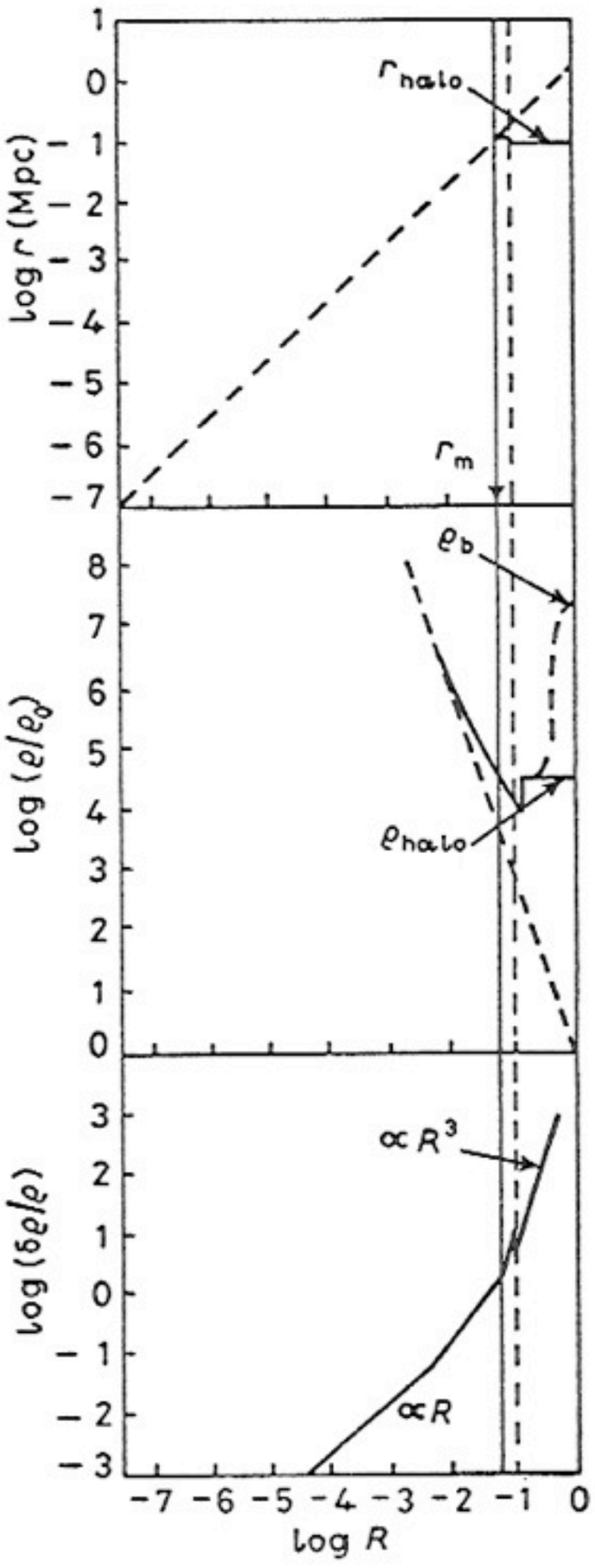

Schematic sketches of radius, density, and density contrast of an overdense fluctuation. It initially expands with the Hubble expansion, reaches a maximum radius (solid vertical line), and undergoes violent relaxation during collapse (dashed vertical line), which results in the dissipationless matter forming a stable halo. Meanwhile the ordinary matter ρb continues to dissipate kinetic energy and contract, thereby becoming more tightly bound, until dissipation is halted by star or disk formation, explaining the origin of galactic spheroids and disks.

(This was the simplified discussion of BFPR84; the figure is from my 1984 lectures at the Varenna school. Now we take into account halo growth by accretion, and the usual assumption is that spheroids form mostly as a result of galaxy mergers Toomre 1977.)

Halo and Galaxy Merging and Spheroid Formation

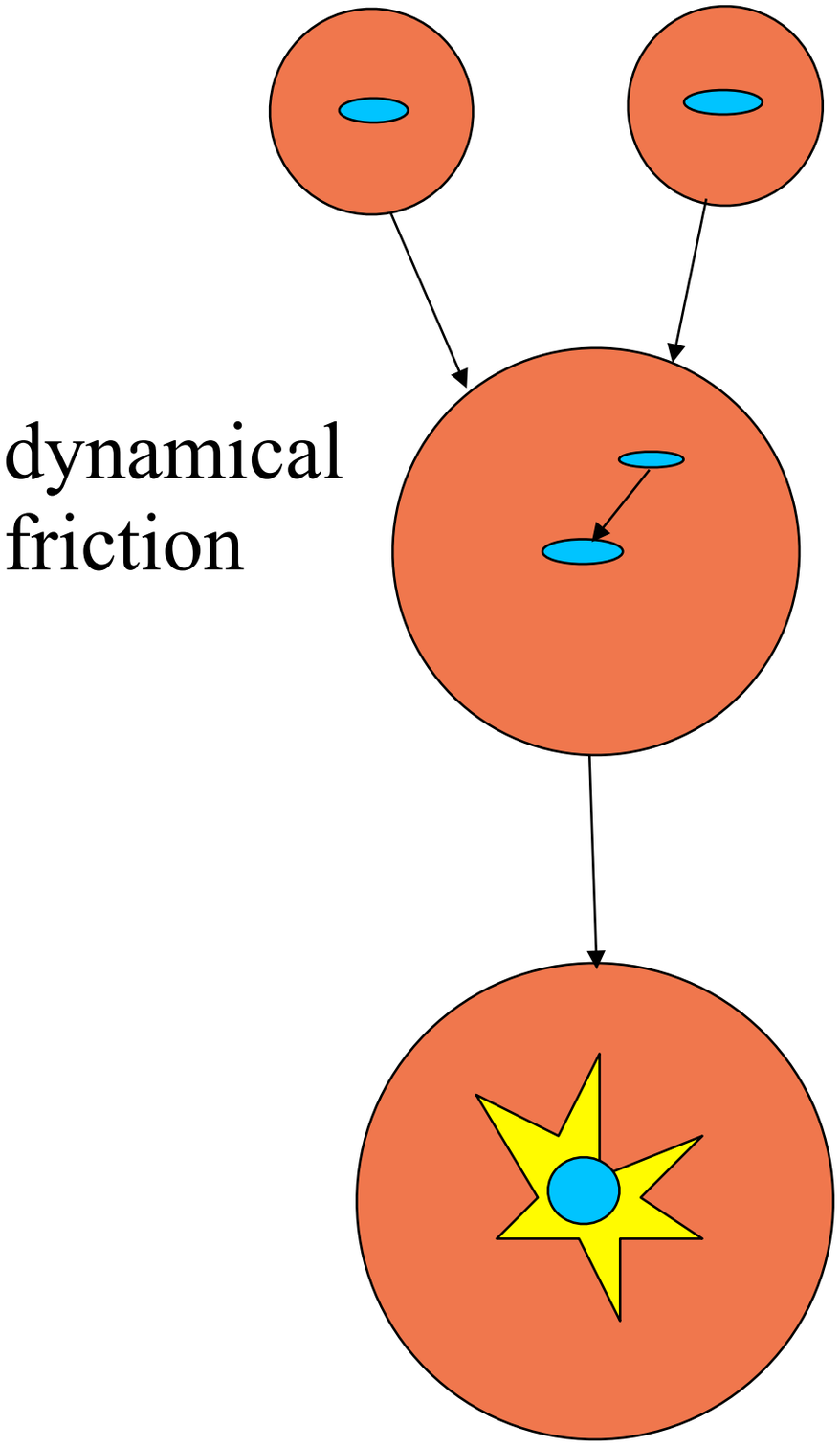

mergers can trigger starburst, forming spheroid

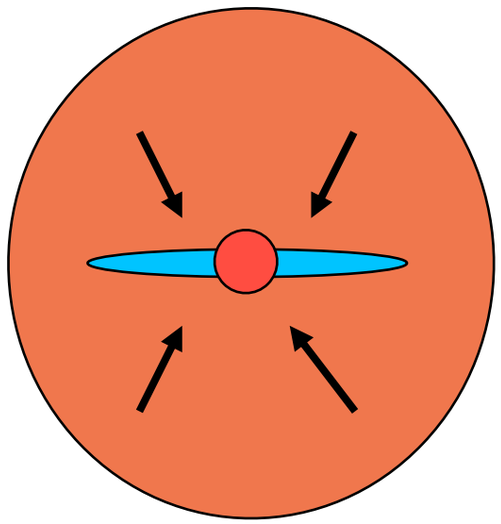

subsequent cooling forms disk

Spherical Collapse

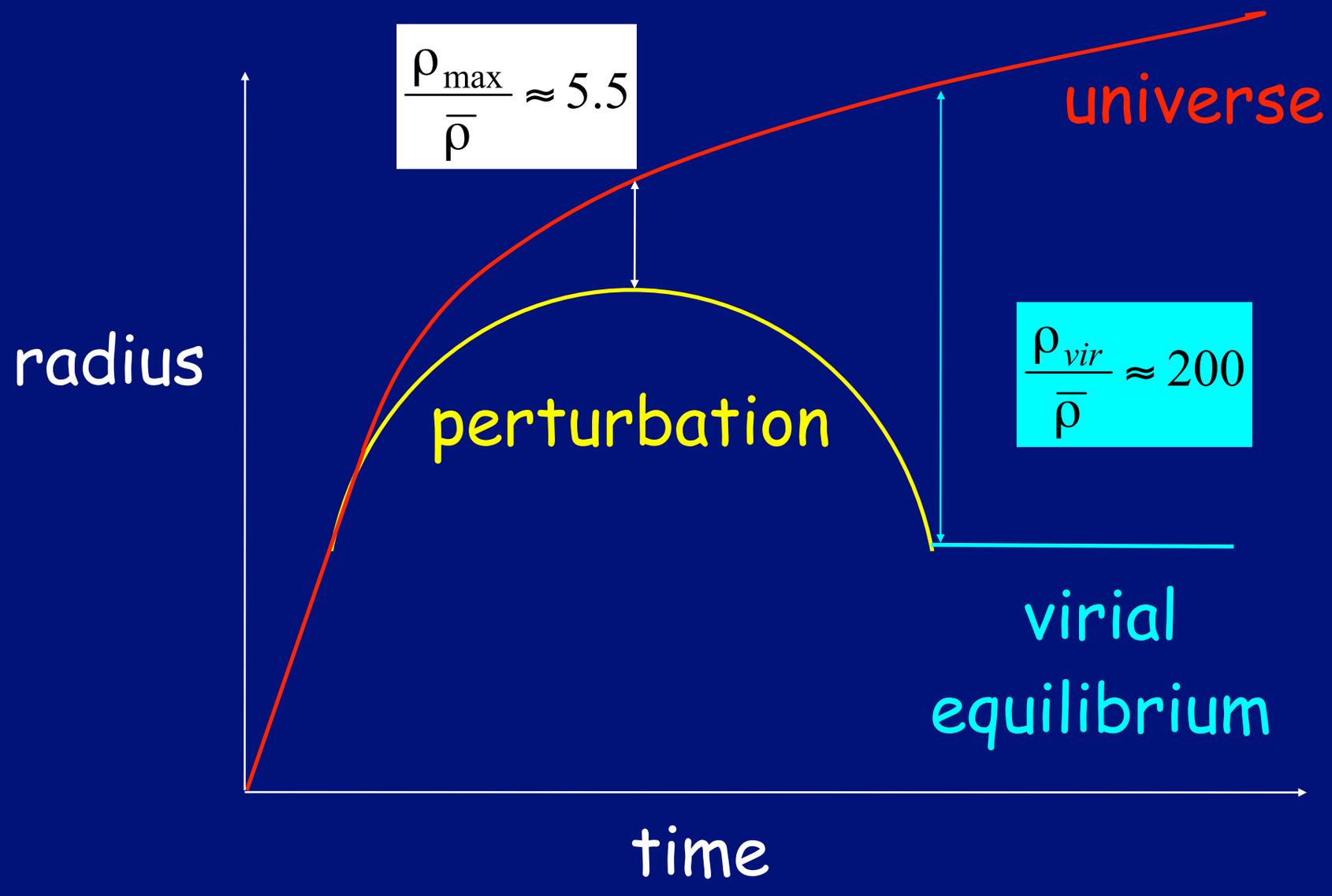

virial equilibrium: $E = -\frac{1}{2}\frac{GM}{R_{vir}} = -\frac{GM}{R_{\max}}$

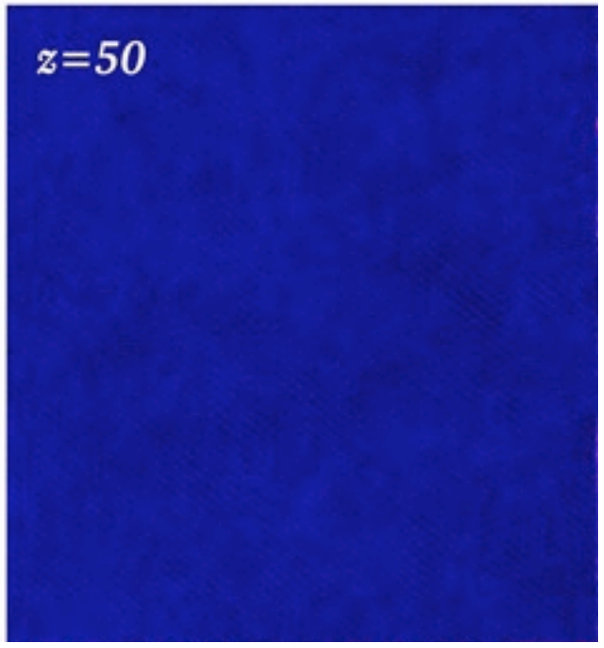

N-body simulation

ΛCDM

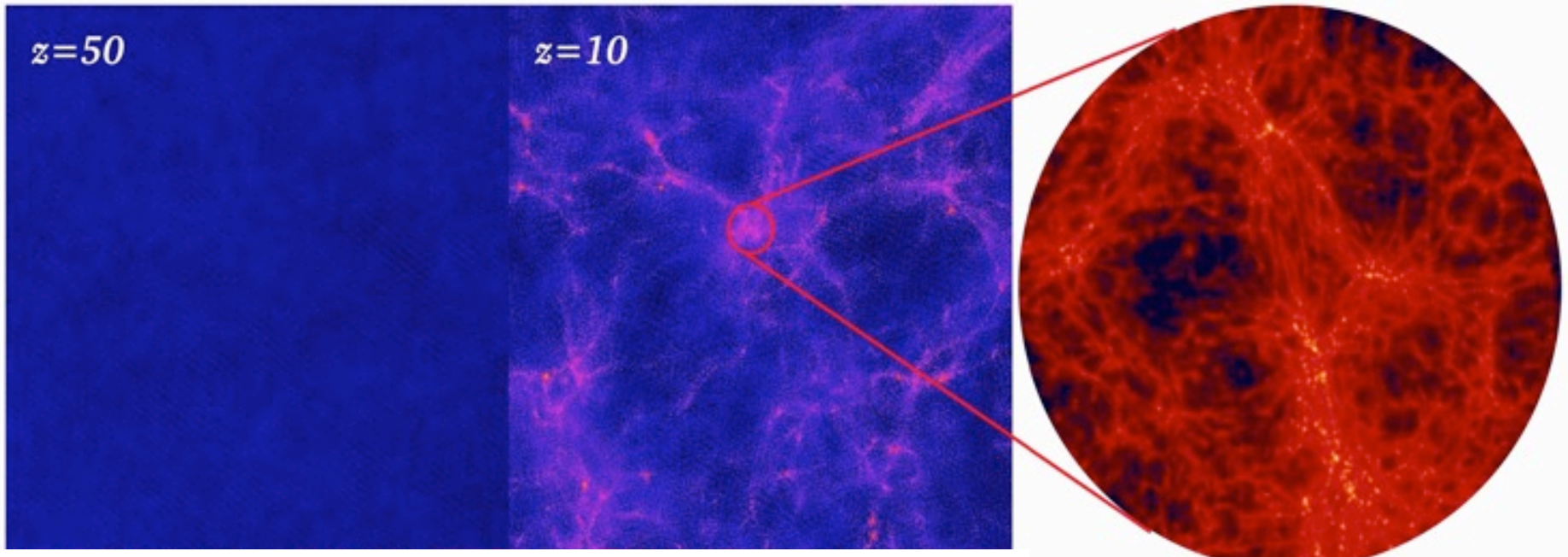
z=50
z=10

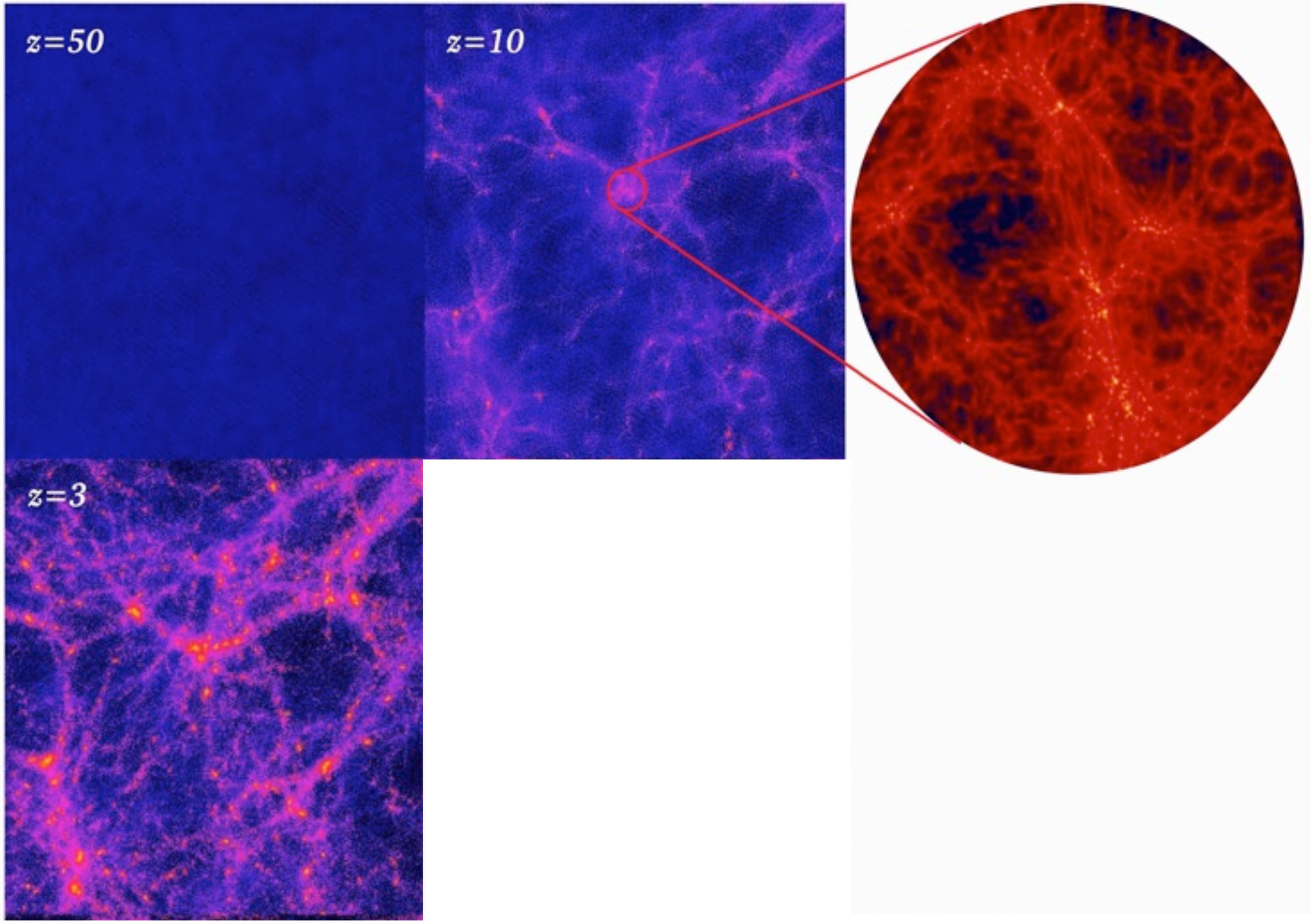
z=50
z=10
z=3

z=49.000

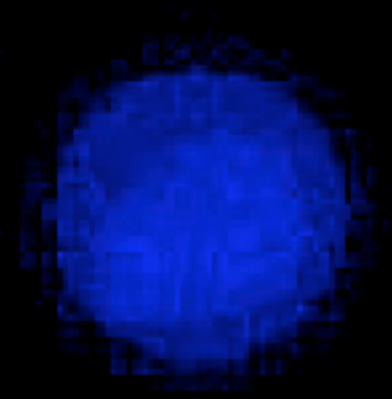

Thursday, May 5, 2011

Expansion....

z=49.0t
=49 Myr

z=12.0
t=374Myr

z=2.95
t=2.23 Gyr

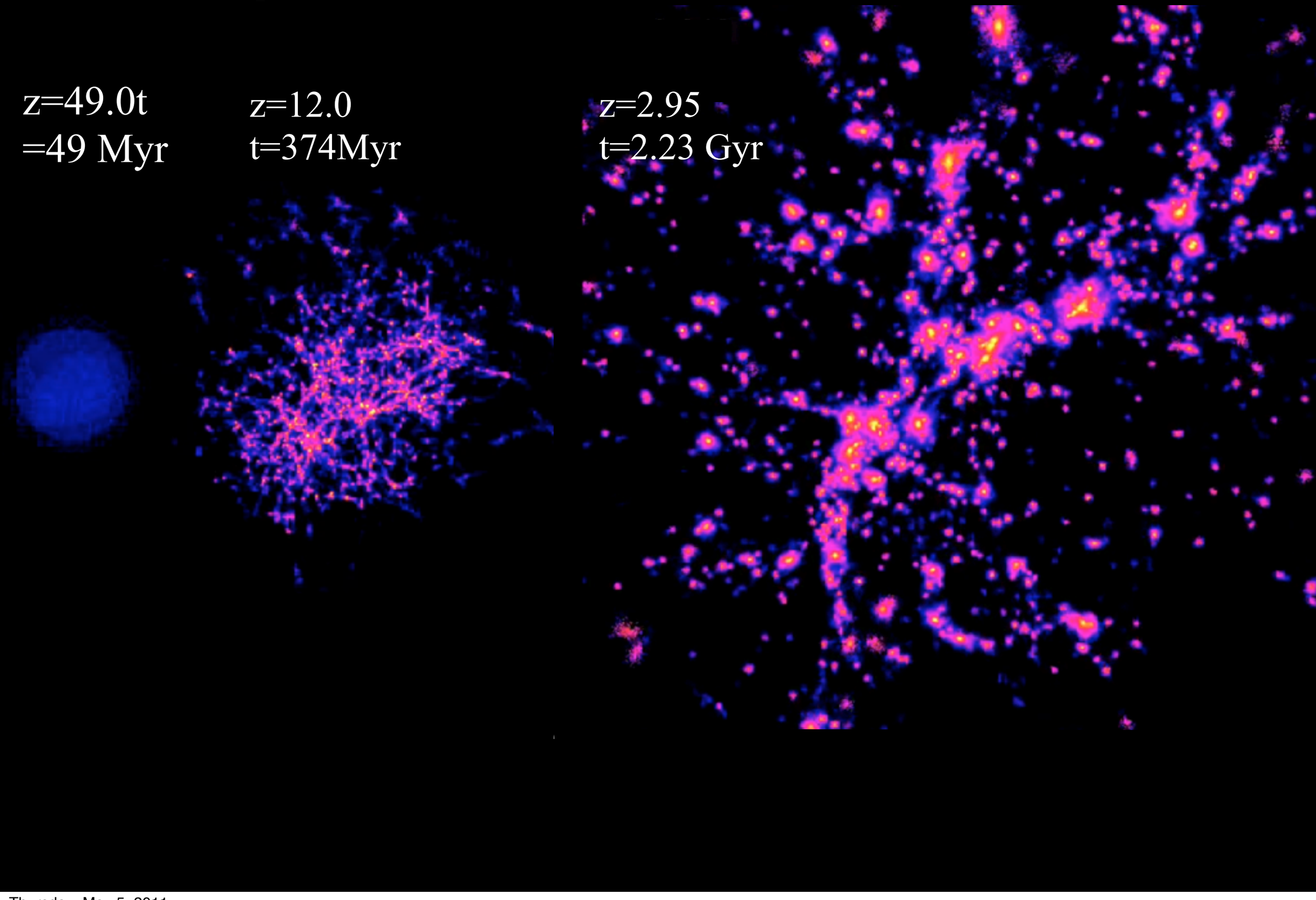

z= 0.837 t= 6.66 Gyr

End of expansion for this halo

z= 0.391 t= 9.48 Gyr

Wild Space

Tame Space

z= 0.391 t= 9.48 Gyr

Wild Space

Tame Space

z= 0.000 t= 13.7 Gyr (today)

Wild Space

Tame Space

Micro-Macro Connection

Cold Dark Matter

Hot Dark Matter

ν

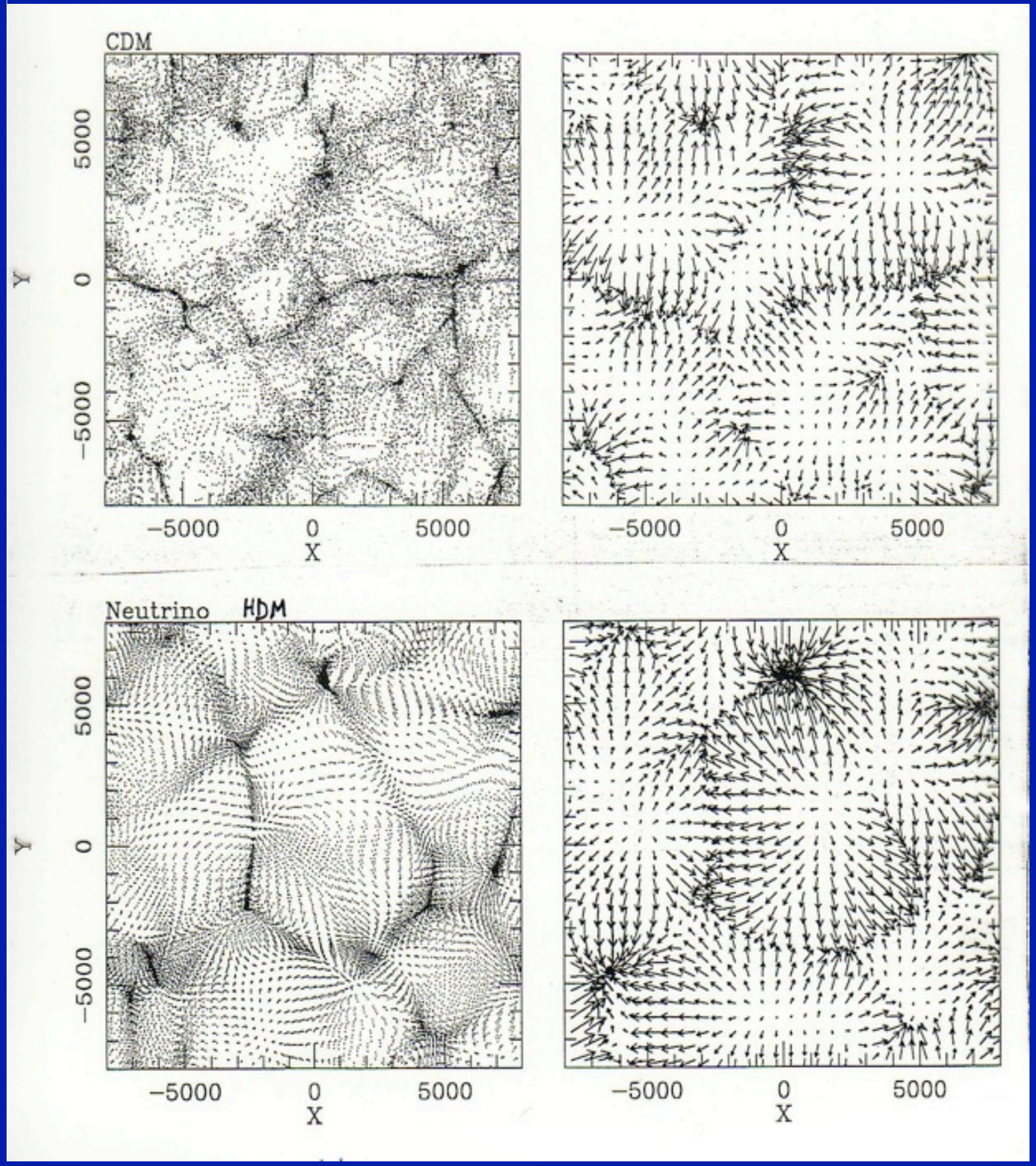

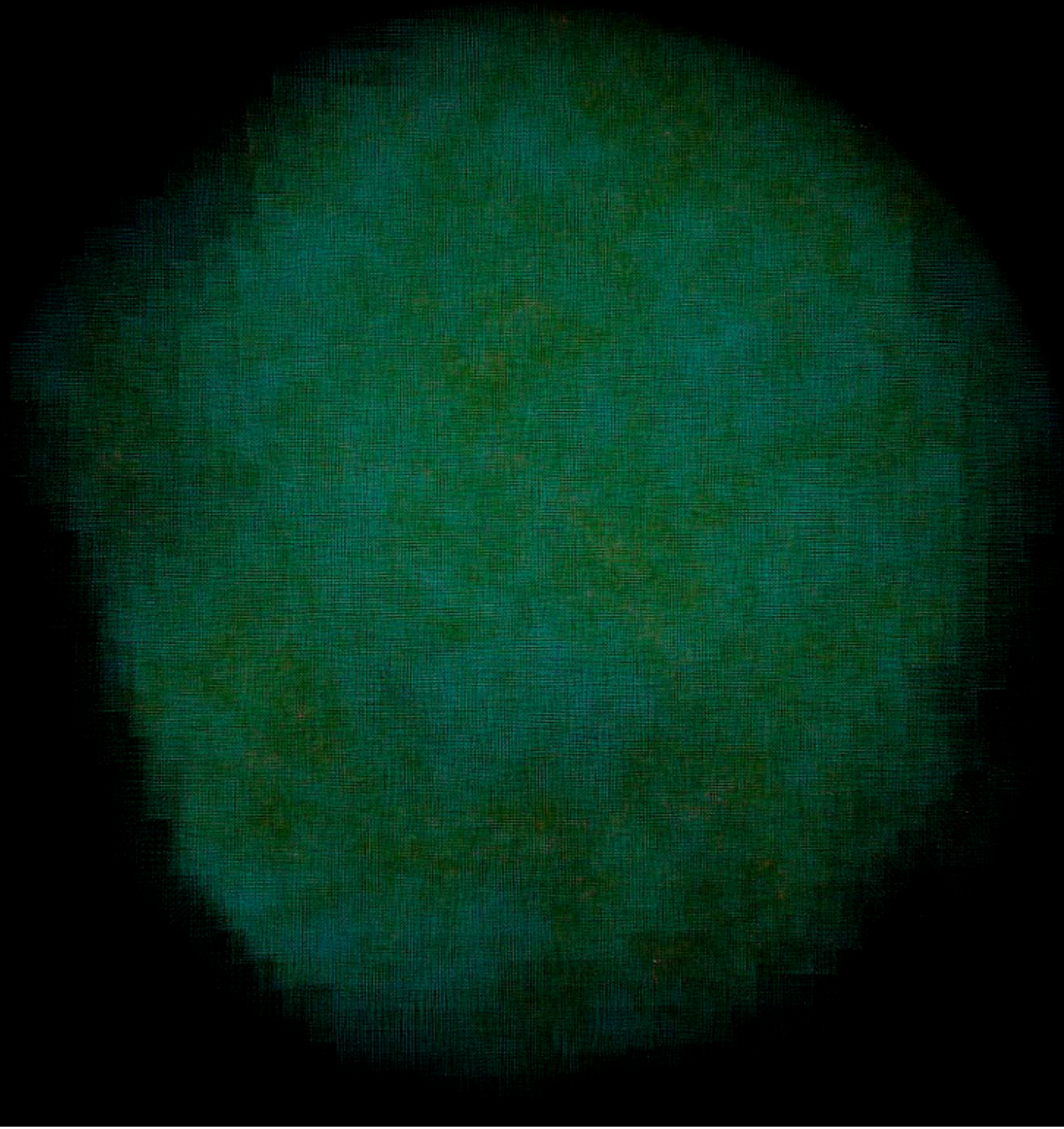

Columbia
Supercomputer
NASA Ames

Simulation:
Brandon
Allgood &
Joel Primack

Visualization:
Chris Henze

(rotation to
show 3D)

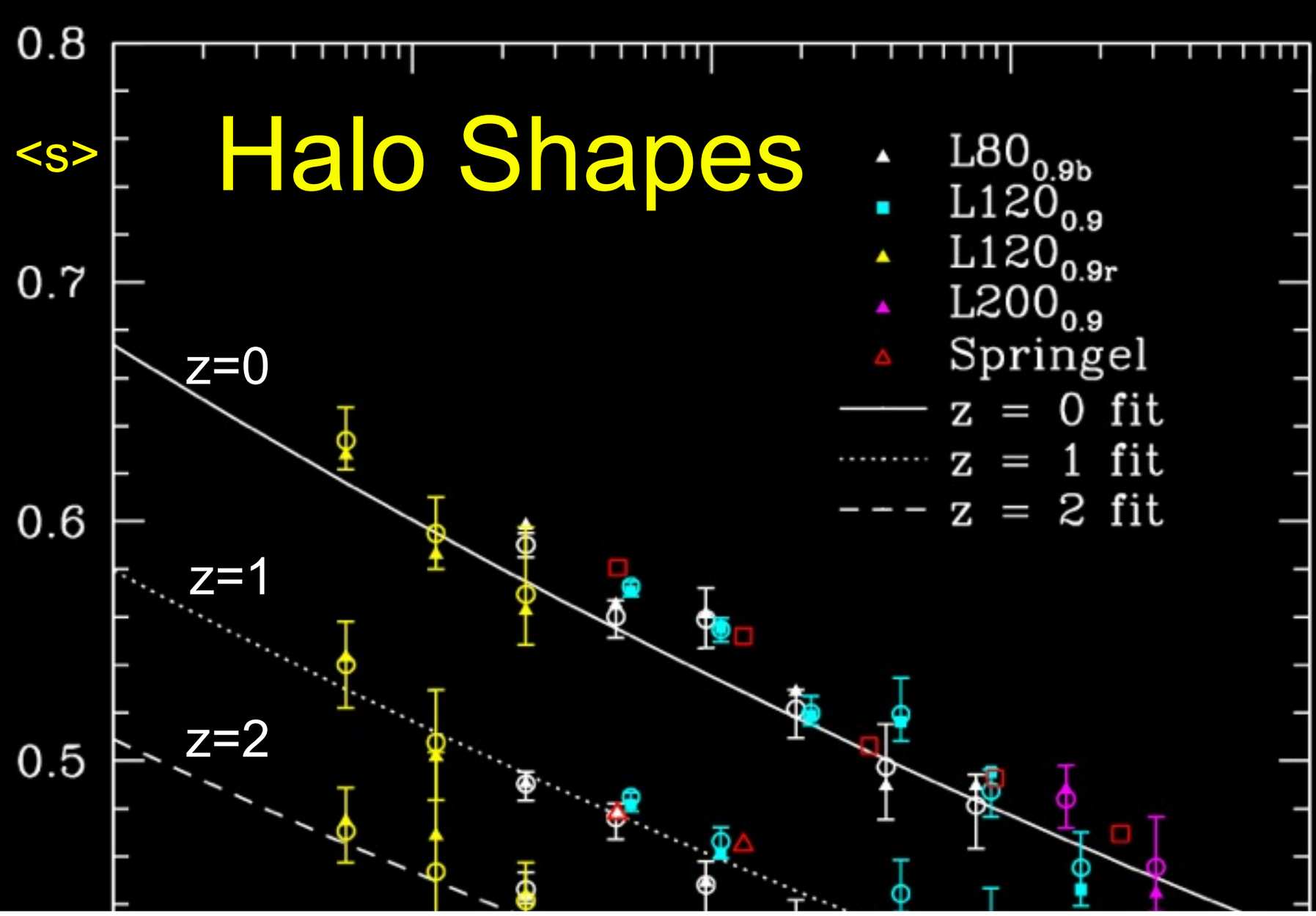

A simple formula describes these results, as well dependence on epoch and cosmological parameter σ_8 :

$$\langle s \rangle (M_{\rm vir}, z = 0) = \alpha \left(\frac{M_{\rm vir}}{M_*} \right)^{\beta}$$

with best fit values

$$\alpha = 0.54 \pm 0.03, \ \beta = -0.050 \pm 0.003.$$

<s> = short / long axis of dark halos vs. mass and redshift. Dark halos are more elongated the more massive they are and the earlier they form. We found that the halo <s> scales as a power-law in Mhalo/M*. Halo shape is also related to the Wechsler halo formation scale factor a_c.

Allgood+2006

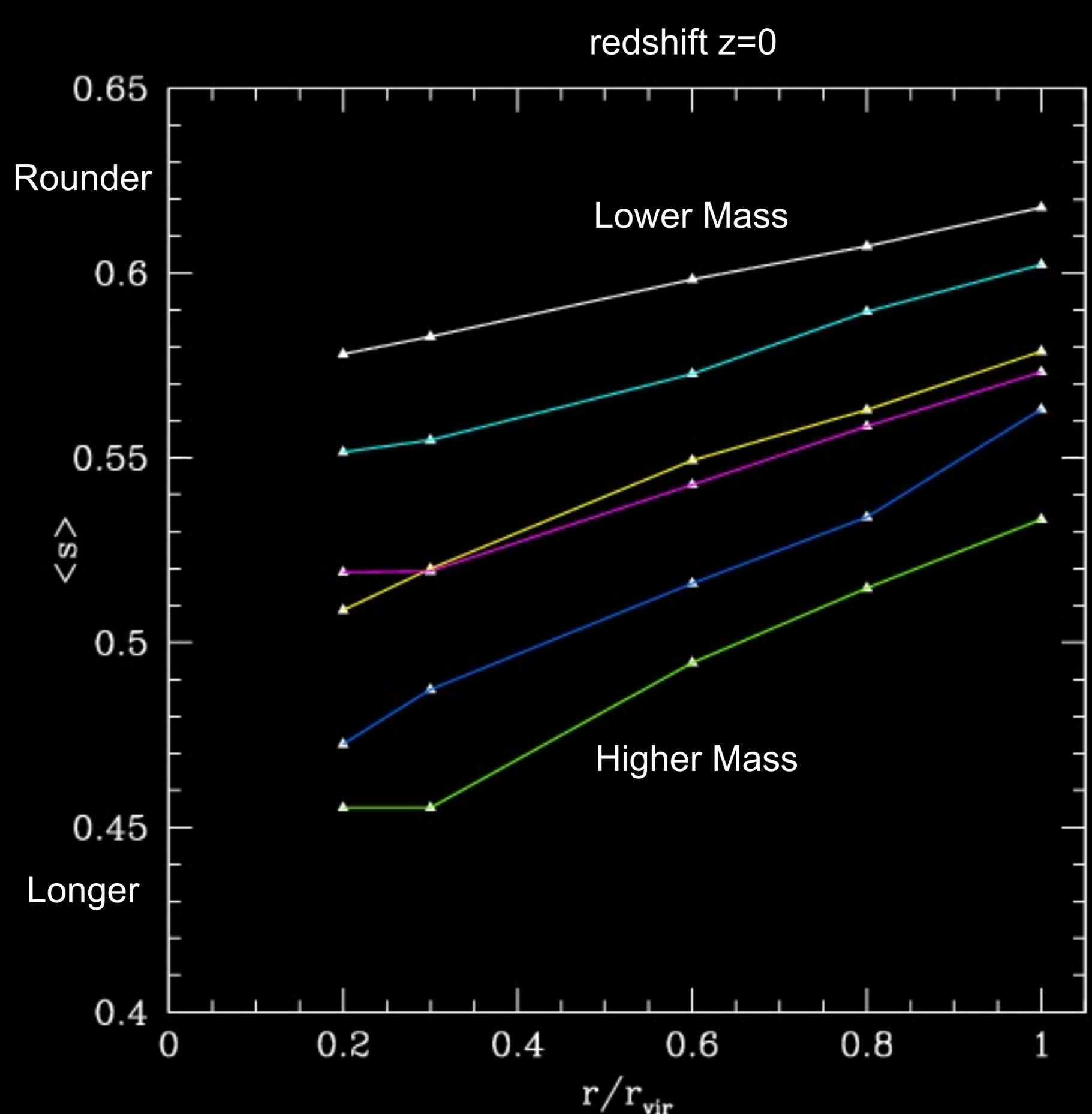

Halos become more spherical at larger radius and smaller mass. As before,

$$s = \frac{\text{short axis}}{\text{long axis}}$$

These predictions can be tested against cluster X-ray data and galaxy weak lensing data.

Allgood+2006

CONSTRAINED LOCAL UNIVERSE SIMULATION

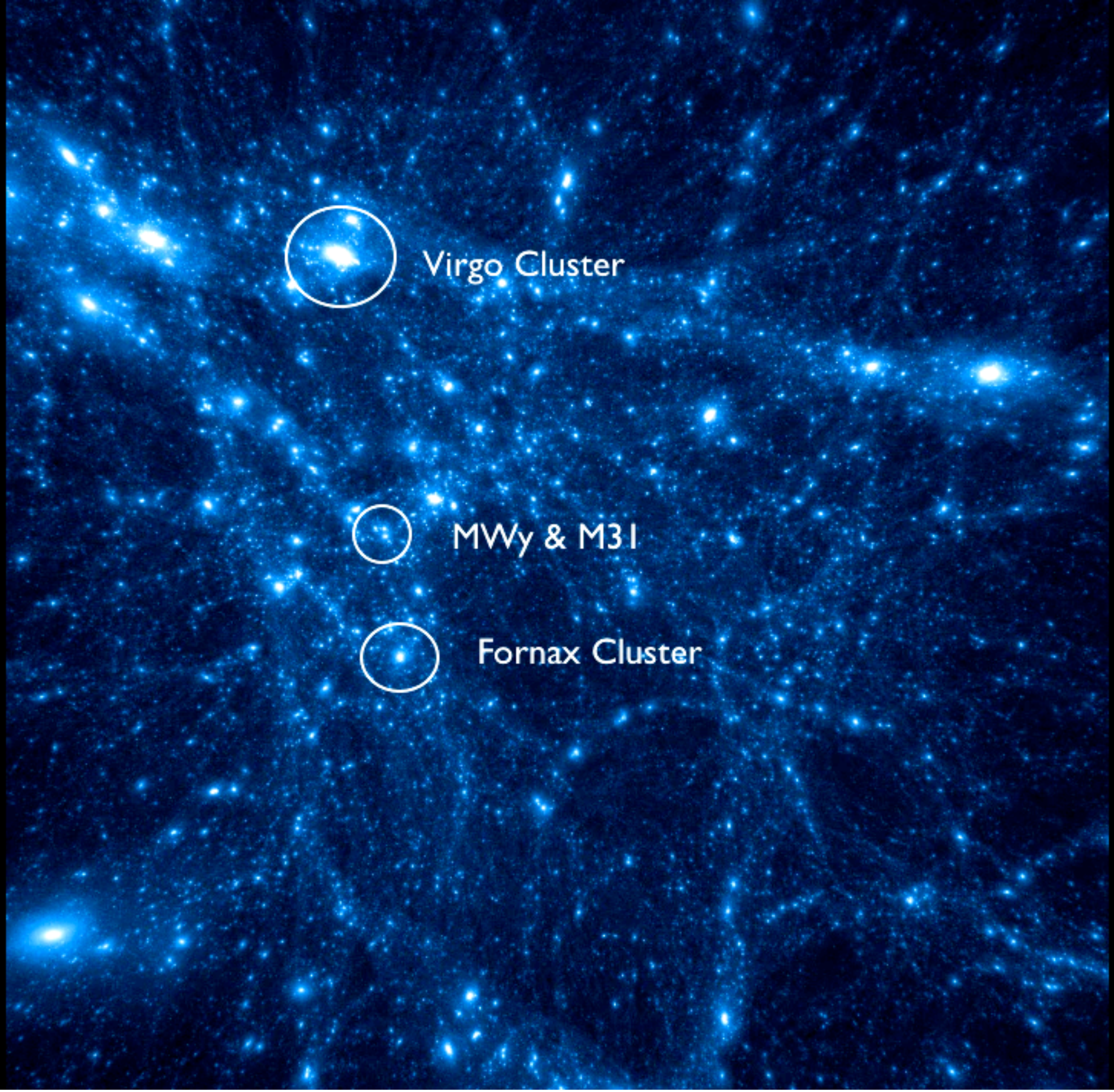
Virgo Cluster
MWy & M31
Fornax Cluster

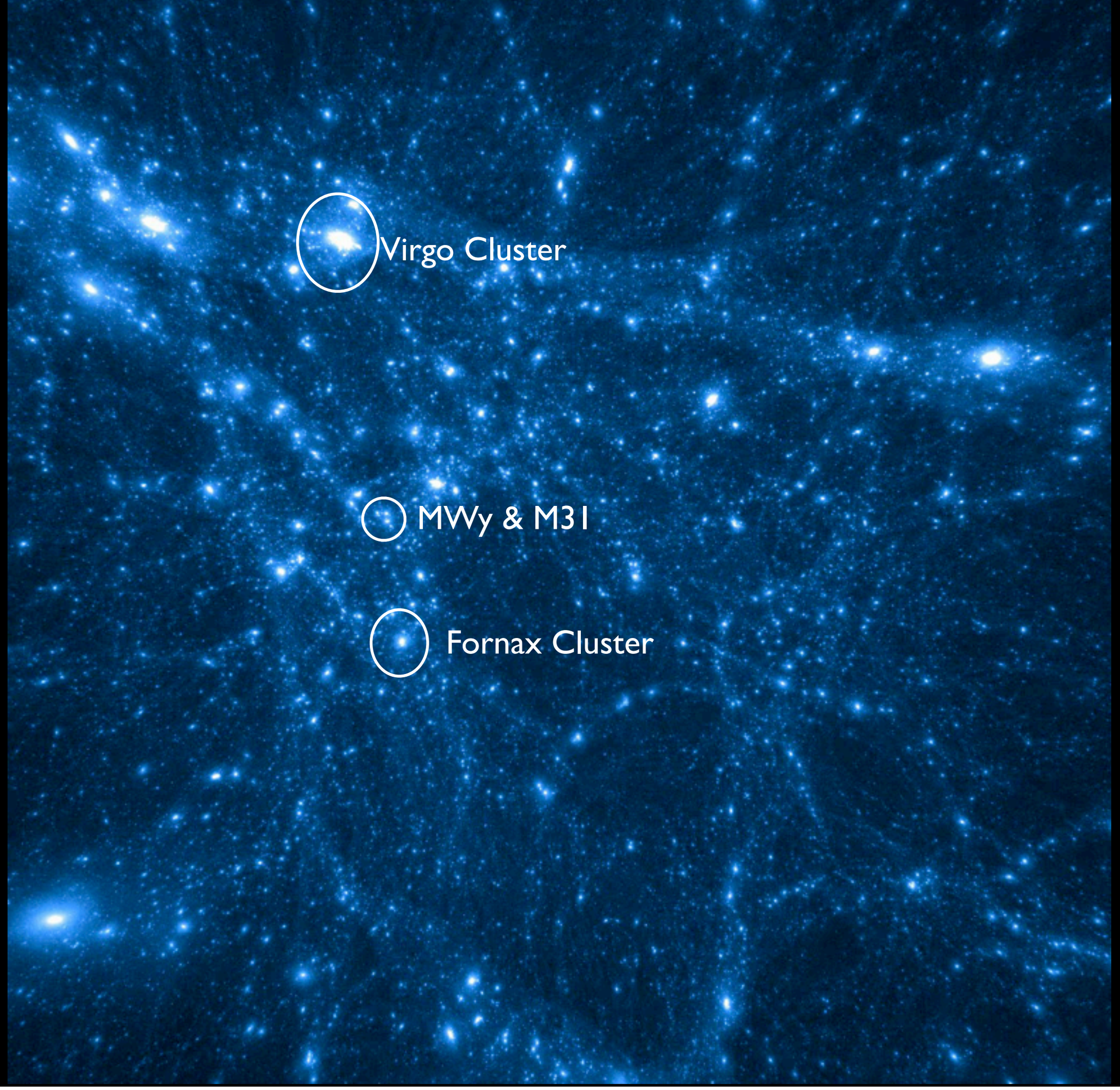
Virgo Cluster
MWy & M31
Fornax Cluster

2dF redshift survey

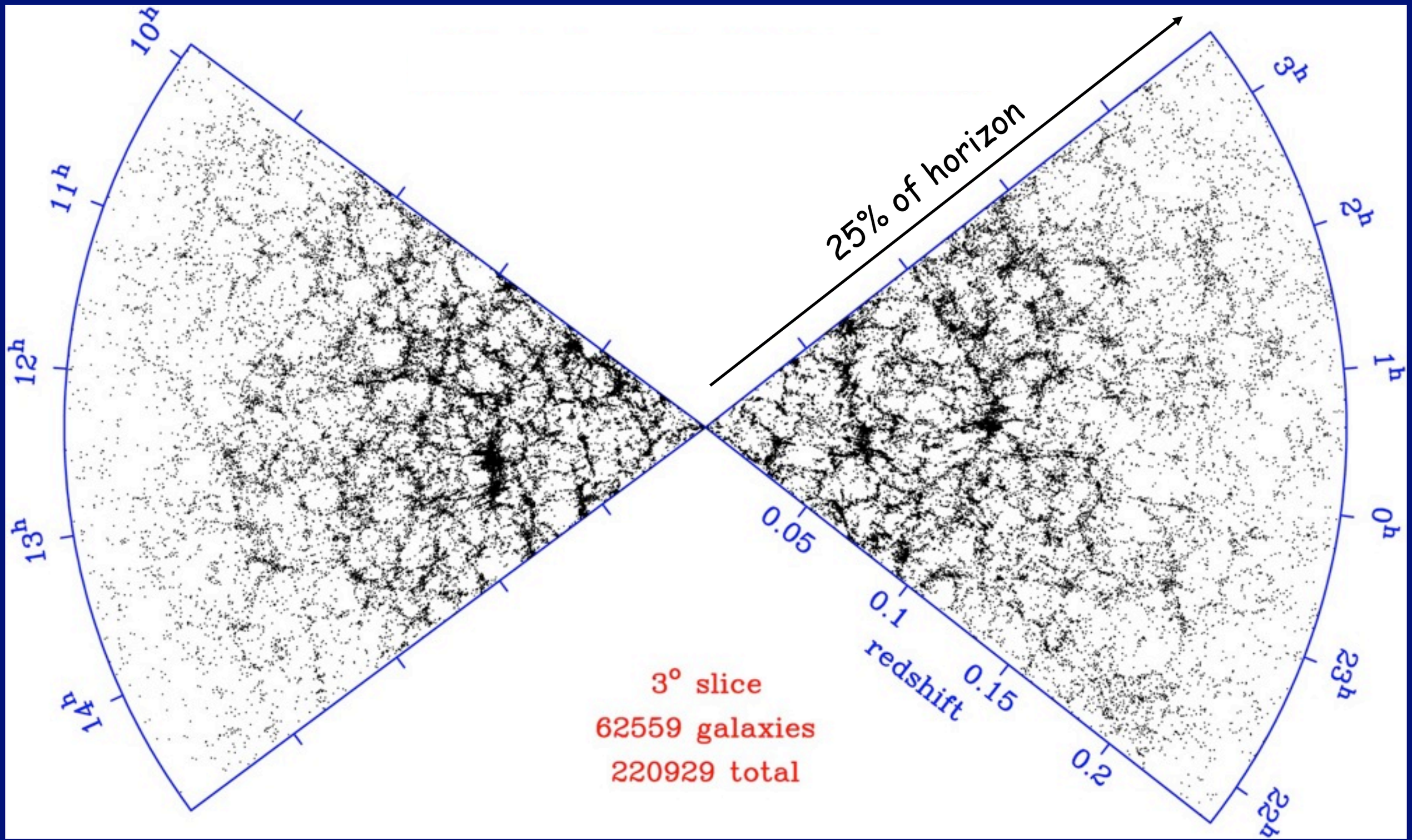

2dF and Mocks

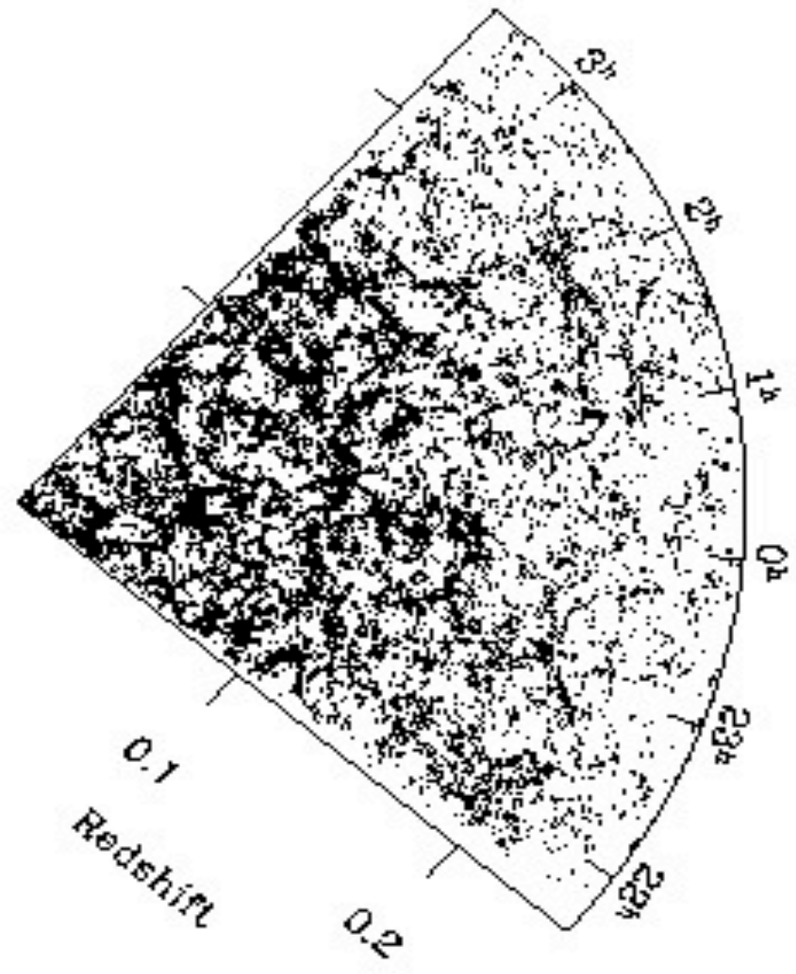

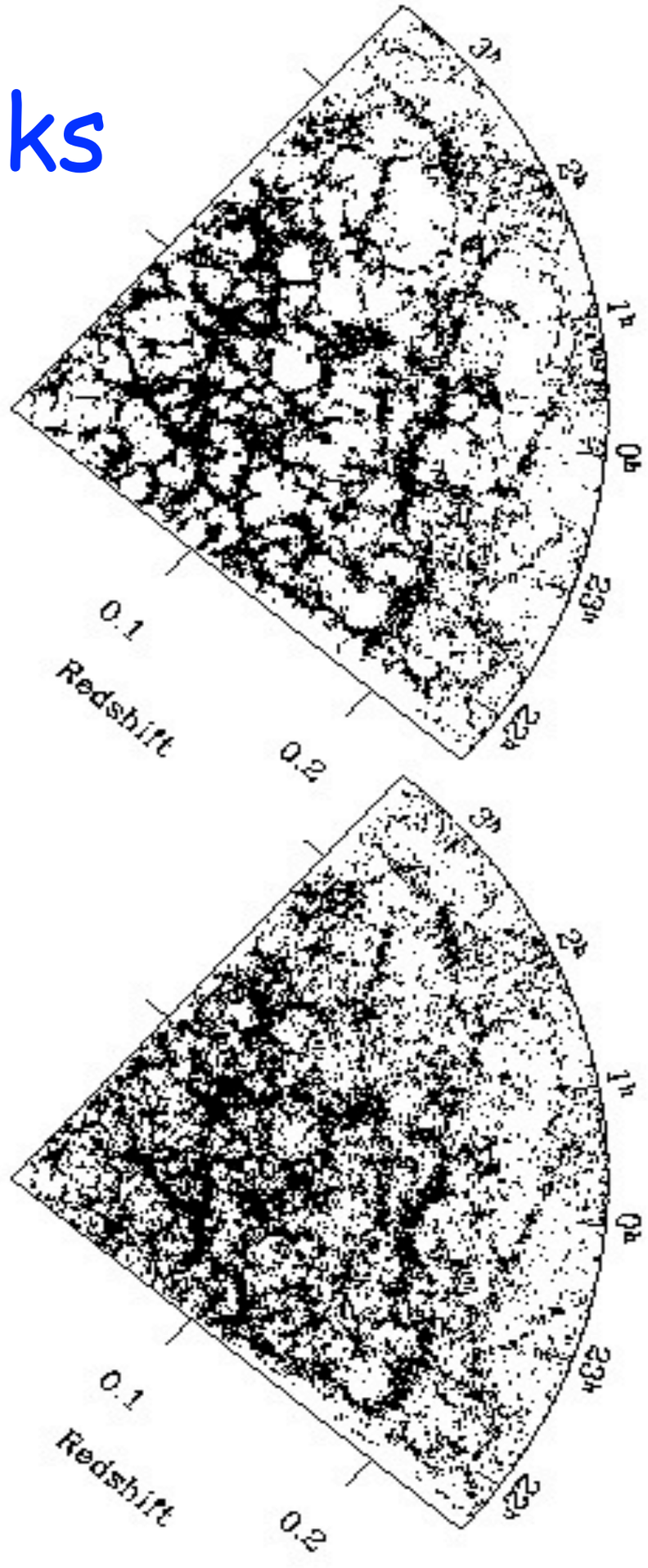

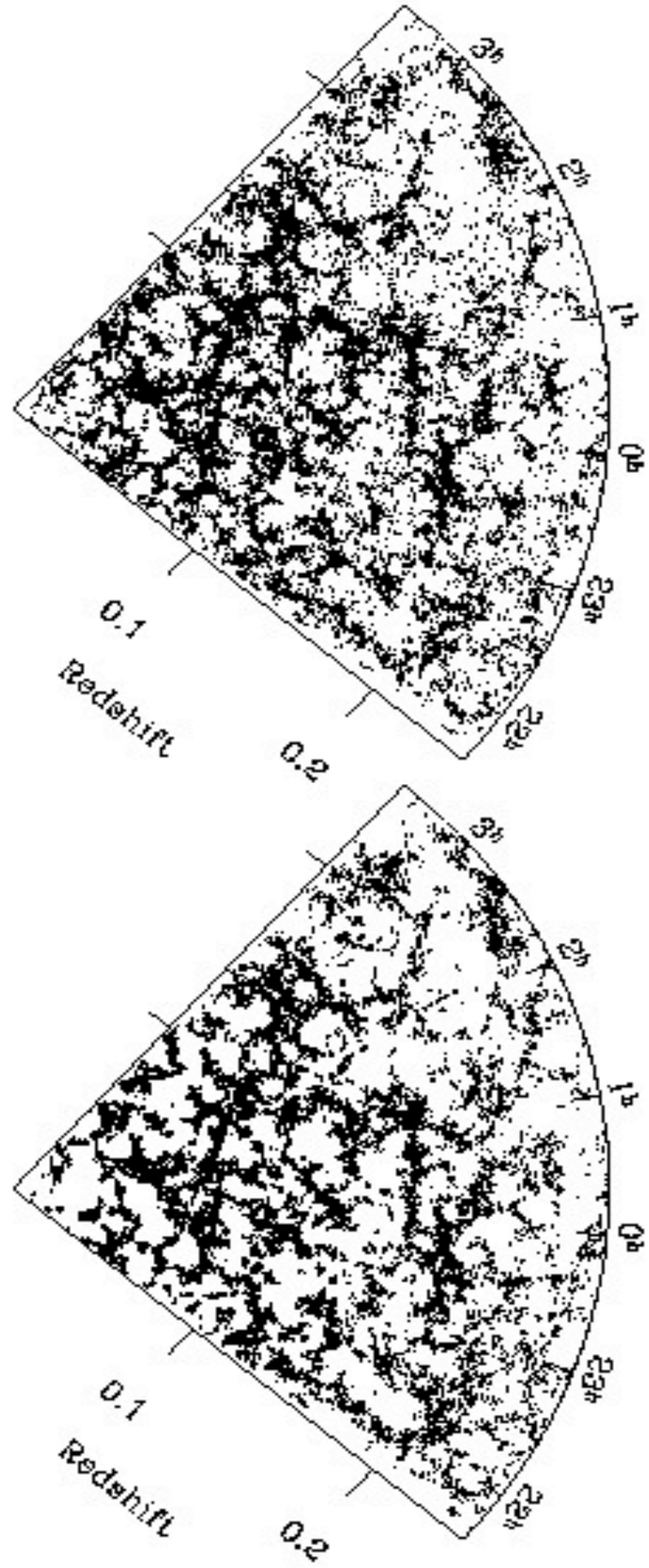

ΛCDM Fluctuation Spectrum

Agrees with Observations!

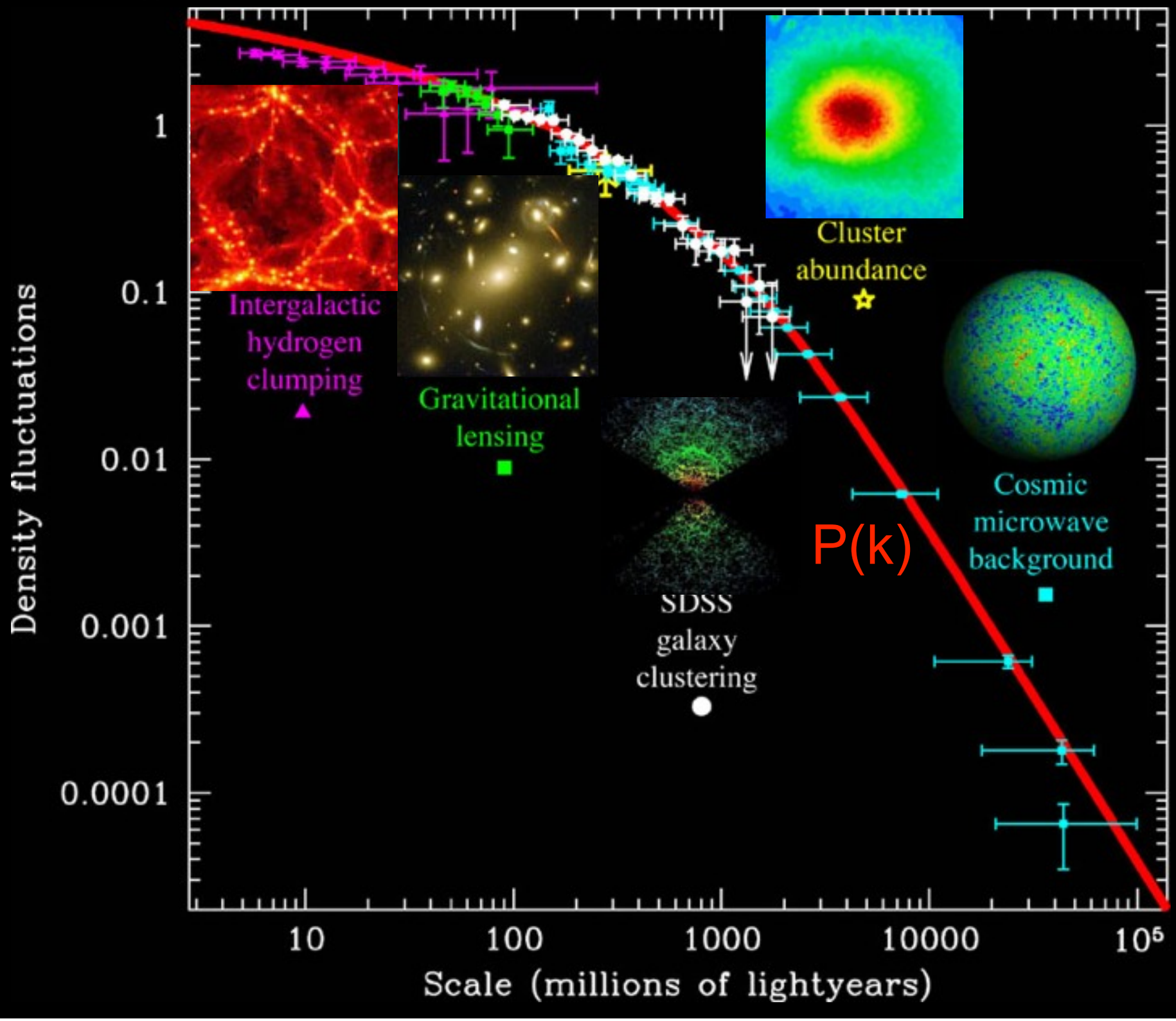

Max Tegmark

Filamentary Structure: Zel'dovich Approximation

displacement from initial position: $x(q,t) = q - D(t)\,\nabla\phi(q)$

Growth Factor

continuity: $\rho(x,t)\,d^3x = \rho_q d^3q \quad \rightarrow$

$$\rightarrow \rho(x,t) = \rho_q \,/\, \| \partial\vec{x} / \partial\vec{q} \|$$

$$= \frac{\rho_q}{(1-D(t)\lambda_1)(1-D(t)\lambda_2)(1-D(t)\lambda_3)}$$

eigenvalues of deformation tensor: $\lambda_i \equiv \frac{\partial^2\phi}{\partial^2 q_i}, \quad \lambda_1 \geq \lambda_2 \geq \lambda_3$

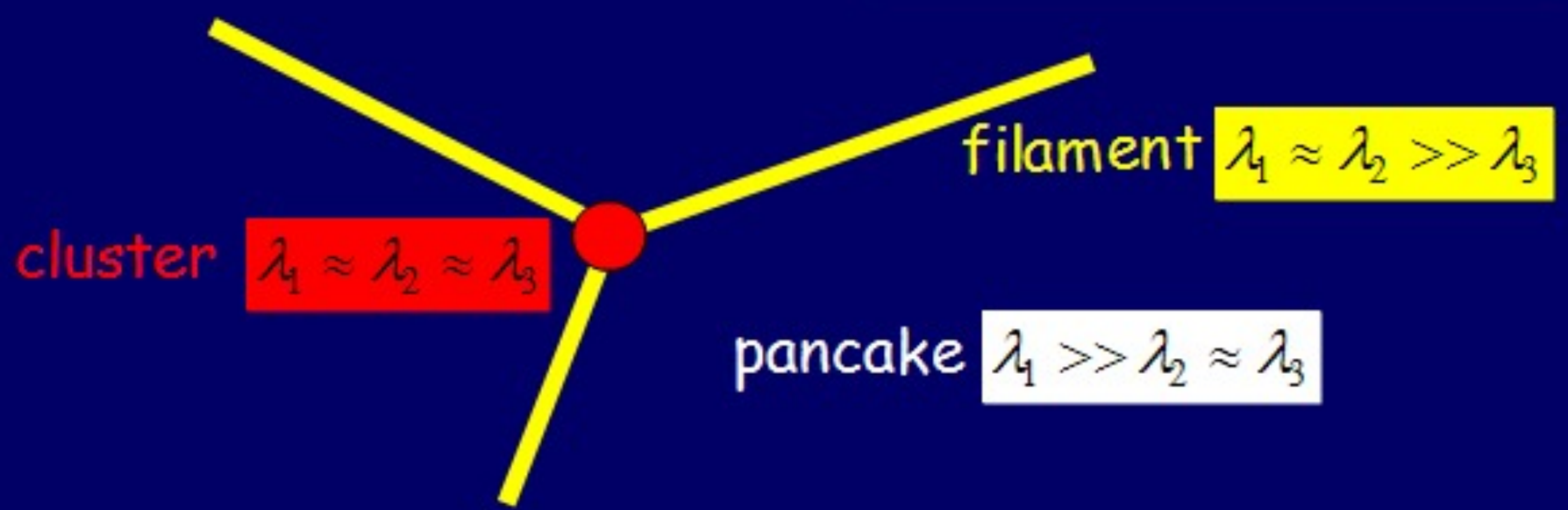

H. J. Mo, S.D.M. White
MNRAS 336 (2002) 112

The abundance and clustering of dark haloes in the standard Lambda CDM cosmogony

We define the characteristic properties of a dark halo within a sphere of radius r_{200} chosen so that the mean enclosed density is 200 times the mean cosmic value. Then

$$r_{200} = \left[\frac{GM}{100\Omega_{\rm m}(z)H^2(z)}\right]^{1/3}, \quad \text{and} \quad V_c = \left(\frac{GM}{r_{200}}\right)^{1/2}, R(M) \equiv \left(\frac{3M}{4\pi\bar{\rho}_0}\right)^{1/3}, \quad \sigma^2(R) = \frac{1}{2\pi^2}\int_0^\infty k^3 P(k)\tilde{W}^2(kR)\frac{{\rm d}k}{k},$$

According to the argument first given by Press & Schechter (1974, hereafter PS), the abundance of haloes as a function of mass and redshift, expressed as the number of haloes per unit comoving volume at redshift z with mass in the interval $(M, M + dM)$, may be written as

$$n(M,z){\rm d}M = \sqrt{\frac{2}{\pi}}\frac{\bar{\rho}_0}{M}\frac{{\rm d}\nu}{{\rm d}M}\exp\left(-\frac{\nu^2}{2}\right){\rm d}M\,. \tag{9}$$

Here $\nu \equiv \delta_c/[D(z)\sigma(M)]$, where $\delta_c \approx 1.69$ and the growth factor is $D(z) = g(z)/[g(0)(1+z)]$ with

$$g(z) \approx \frac{5}{2}\Omega_{\rm m}\left[\Omega_{\rm m}^{4/7} - \Omega_\Lambda + (1+\Omega_{\rm m}/2)(1+\Omega_\Lambda/70)\right]^{-1}, \ \Omega_{\rm m} \equiv \Omega_{\rm m}(z), \quad \Omega_\Lambda \equiv \Omega_\Lambda(z) = \frac{\Omega_{\Lambda,0}}{E^2(z)}.$$

$$E(z) = \left[\Omega_{\Lambda,0} + (1-\Omega_0)(1+z)^2 + \Omega_{{\rm m},0}(1+z)^3\right]^{\frac{1}{2}}.$$

Lahav, Lilje, Primack, & Rees 1991

Press & Schechter derived the above mass function from the *Ansatz* that the fraction F of all cosmic mass which at redshift z is in haloes with masses exceeding M is *twice* the fraction of randomly placed spheres of radius $R(M)$ which have linear overdensity at that time exceeding δ_c, the value at which a spherical perturbation collapses. Since the linear fluctuation distribution is gaussian this hypothesis implies

$$F(>M,z) = {\rm erfc}\left(\frac{\nu}{\sqrt{2}}\right), \tag{12}$$

and equation (9) then follows by differentiation.

The PS formula is $$n(M,z)\mathrm{d}M = \sqrt{\frac{2}{\pi}}\frac{\bar{\rho}_0}{M}\frac{\mathrm{d}\nu}{\mathrm{d}M}\exp\left(-\frac{\nu^2}{2}\right)\mathrm{d}M \quad (9)$$

Numerical simulations show that although the scaling properties implied by the PS argument hold remarkably well for a wide variety of hierarchical cosmogonies, substantially better fits to simulated mass functions are obtained if the error function in equation (12) is replaced by a function of slightly different shape. Sheth & Tormen (1999) suggested the following modification of equation (9)

$$n(M,z)\mathrm{d}M = A\left(1+\frac{1}{\nu'^{2q}}\right)\sqrt{\frac{2}{\pi}}\frac{\bar{\rho}}{M}\frac{\mathrm{d}\nu'}{\mathrm{d}M}\exp\left(-\frac{\nu'^2}{2}\right)\mathrm{d}M, \quad (14)$$

where $\nu' = \sqrt{a}\nu$, $a = 0.707$, $A \approx 0.322$ and $q = 0.3$.

[See Sheth, Mo & Tormen (2001) and Sheth & Tormen (2002) for a justification of this formula in terms of an ellipsoidal model for perturbation collapse.] The fraction of all matter in haloes with mass exceeding M can be obtained by integrating equation (14). To good approximation,

$$F(>M,z) \approx 0.4\left(1+\frac{0.4}{\nu^{0.4}}\right)\mathrm{erfc}\left(\frac{0.85\nu}{\sqrt{2}}\right)$$

In a detailed comparison with a wide range of simulations, Jenkins et al. (2001) confirmed that this model is indeed a good fit provided haloes are defined at the same density contrast relative to the mean in all cosmologies. This is for FOF halo finding -- but Klypin, Trujillo, Primack 2010 find that the more physical Bound Density Maximum (BDM) halo finder results in 10x lower halo number density at z=10.

Comoving Halo Number Density $n(M_{halo})$

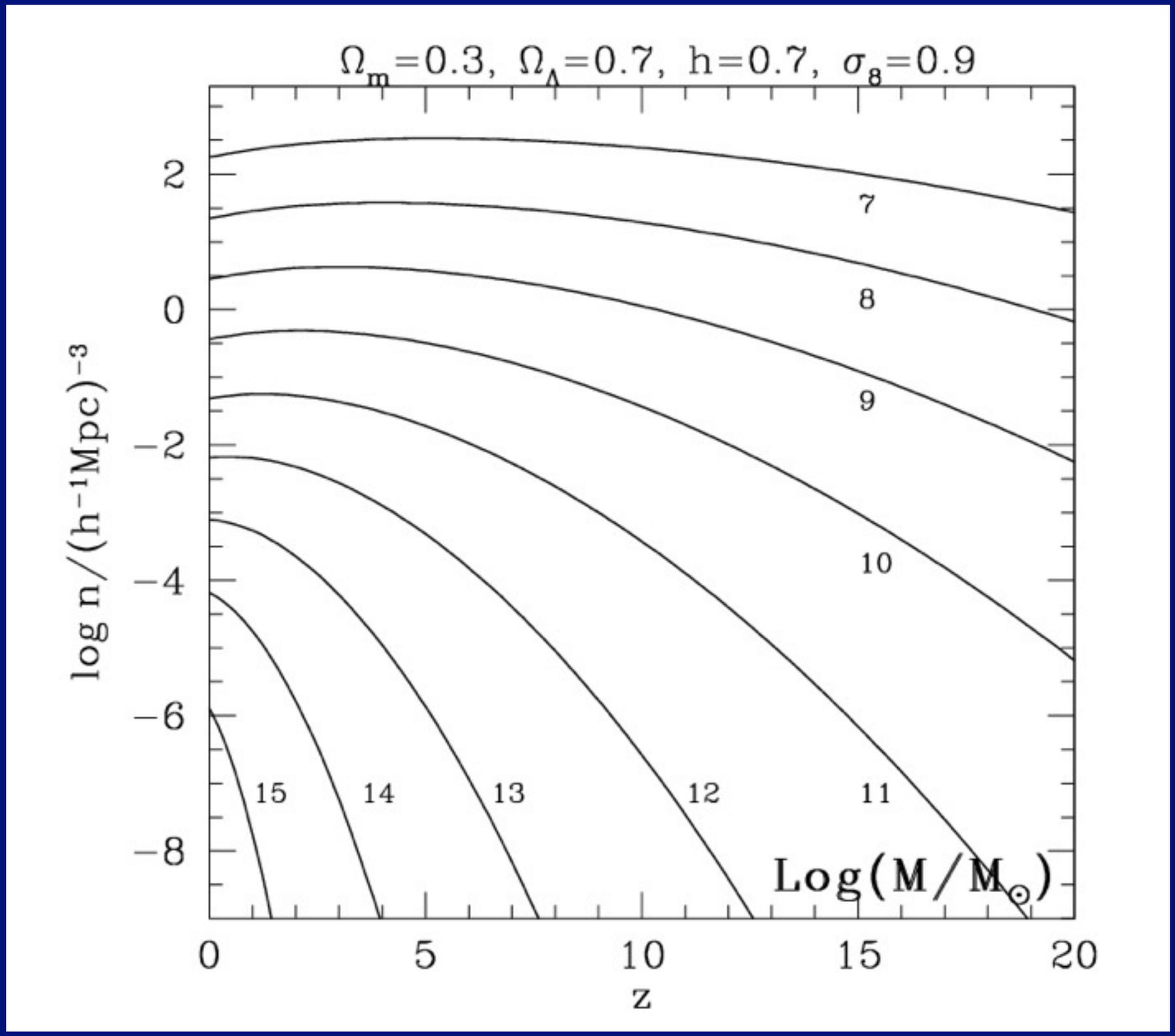

Mo & White 2002

Comoving Halo Number Density n(M_{halo})

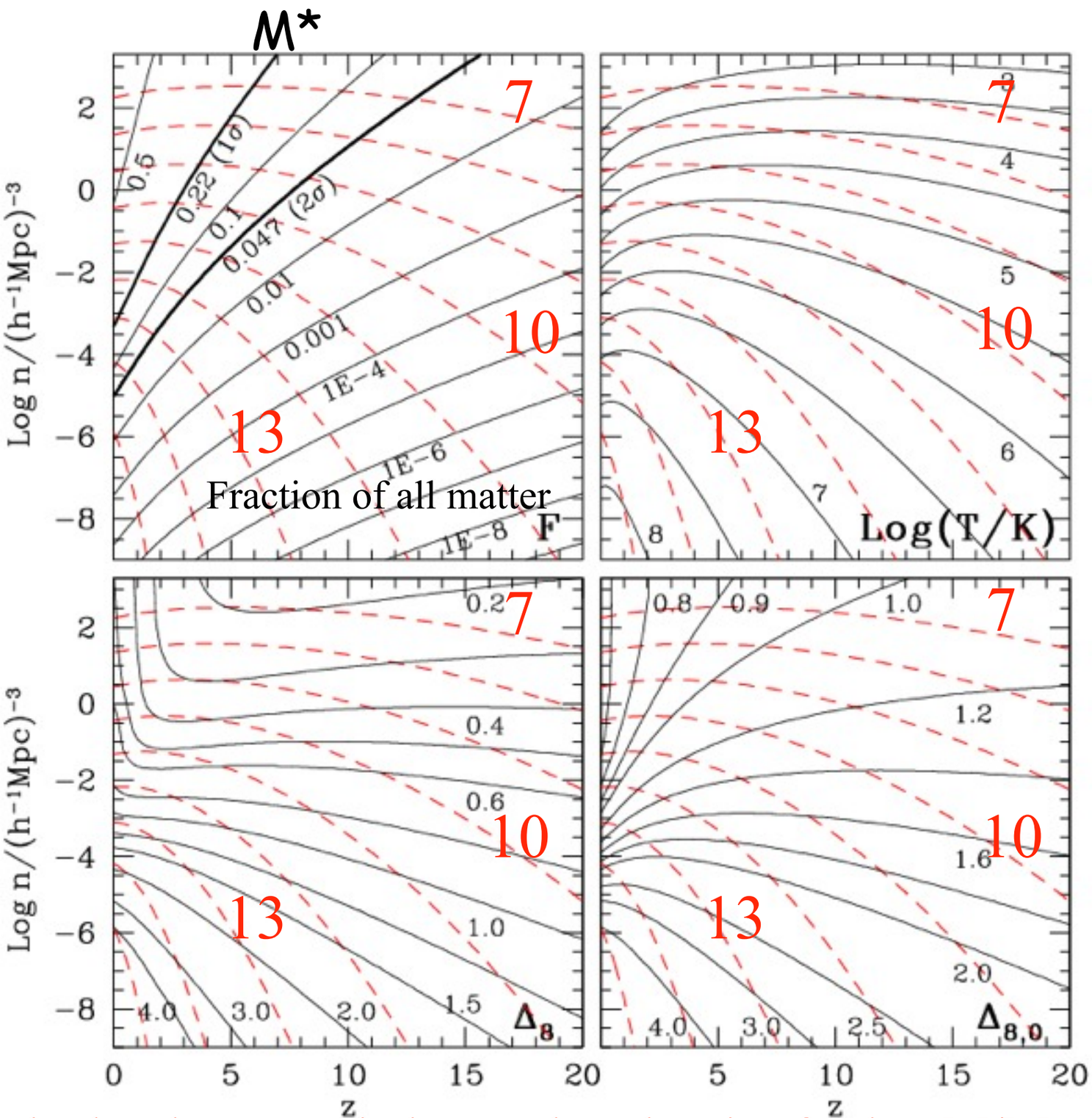

Dashed red curves: halo number density for log M/M_{sun}

Standard LCDM

Mo & White 2002

Sheth-Tormen Fails at High Redshifts

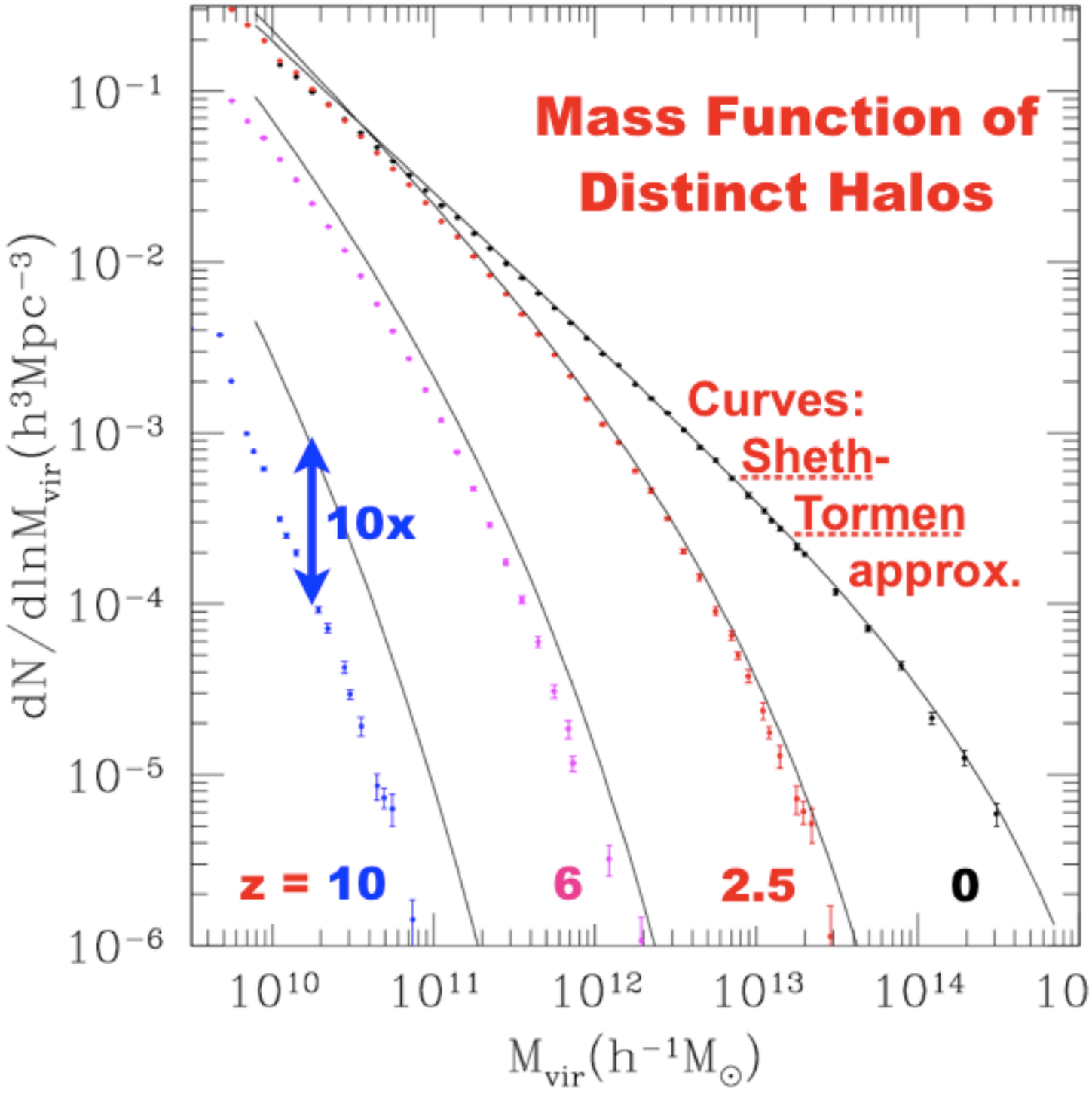

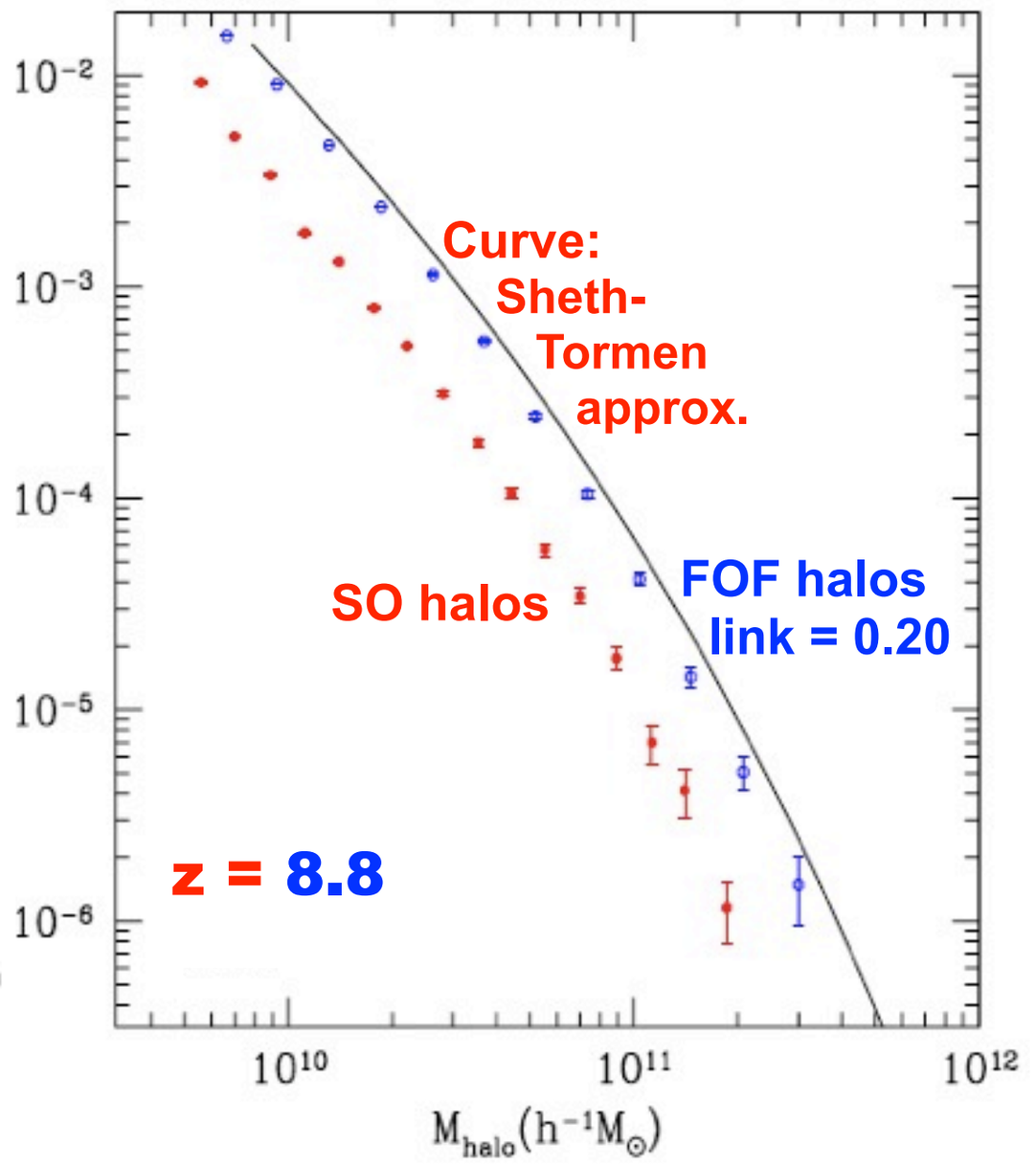

Sheth-Tormen approximation with the same WMAP5 parameters used for Bolshoi simulation very accurately agrees with abundance of halos at low redshifts, but increasingly overpredicts bound spherical overdensity halo abundance at higher redshifts.

Klypin, Trujillo, & Primack, arXiv: 1002.3660v3

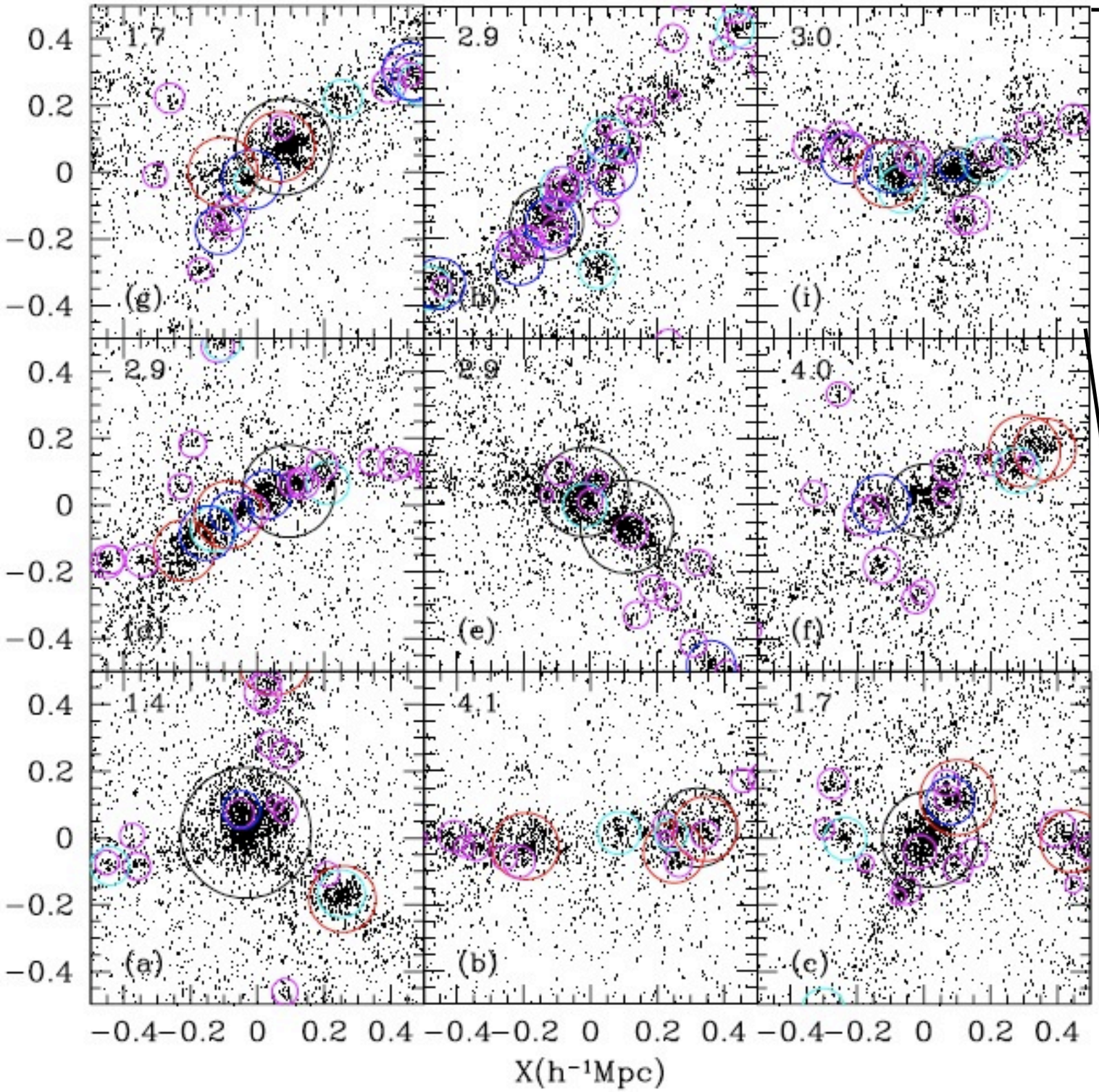

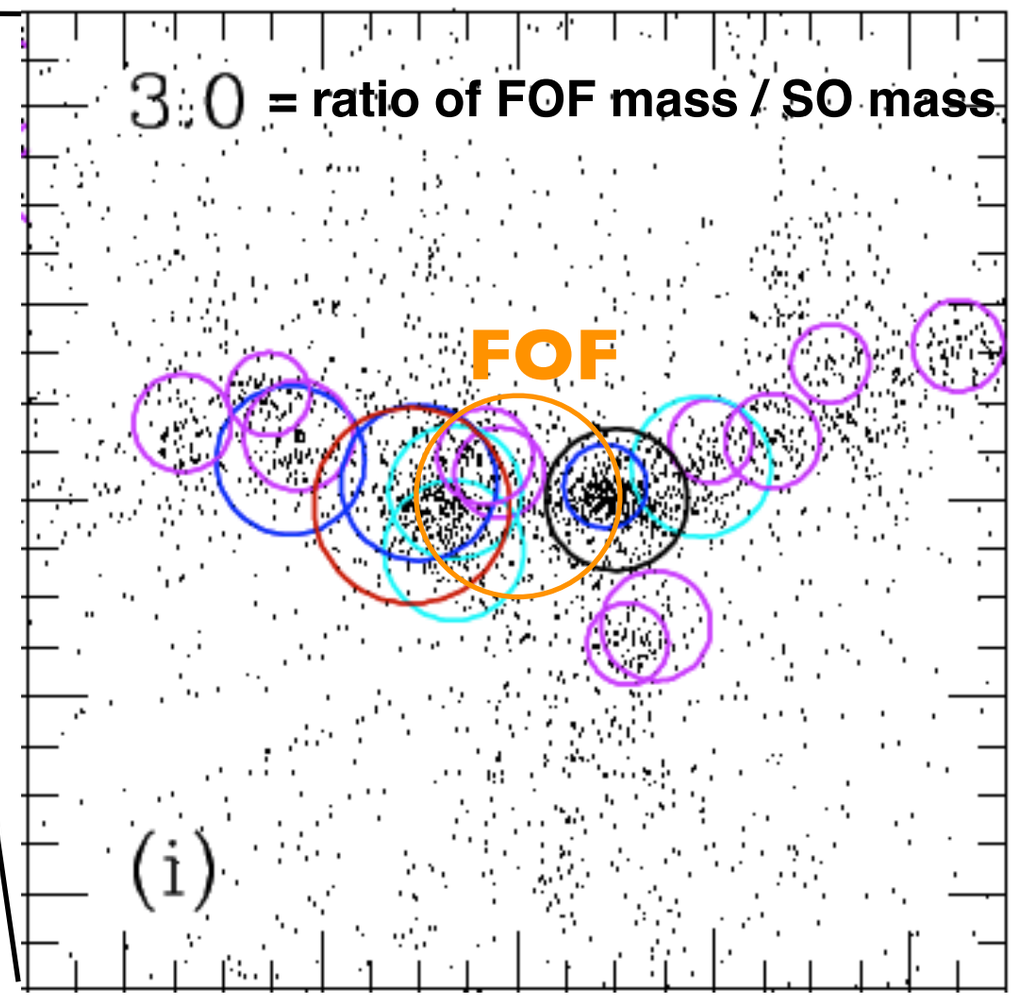

FOF linked together a chain of halos that formed in long and dense filaments (also in panels b, d, f, h; e = major merger)

Each panel shows 1/2 of the dark matter particles in cubes of $1h^{-1}$ Mpc size. The center of each cube is the exact position of the center of mass of the corresponding FOF halo. The effective radius of each FOF halo in the plots is 150 – 200 h^{-1} kpc. Circles indicate virial radii of distinct halos and subhalos identified by the spherical overdensity algorithm BDM.

Klypin, Trujillo, & Primack, arXiv: 1002.3660v3

Cosmological Simulation Methods

Dissipationless Simulations

Particle-Particle (PP) - Aarseth NbodyN, N=1,...,6
Particle Mesh (PM) - see Klypin & Holtzman 1997
Adaptive PM (P3M) - Efstathiou et al.
Tree - Barnes & Hut 1986, PKDGRAV Stadel
TreePM - GADGET2, Springel 2005
Adaptive Mesh Refinement (AMR) - Klypin (ART)

Hydrodynamical Simulations

Fixed grid - Cen & Ostriker
Smooth Particle Hydrodynamics (SPH) - GADGET2, Springel 2005
- Gasoline, Wadsley, Stadel, & Quinn
Adaptive grid - ART+hydro - Klypin & Kravtsov; ENZO - Norman et al.;
- RAMSES - Teyssier

Initial Conditions

Standard: Gaussian P(k) realized uniformly, Zel'dovich displacement
Multimass - put lower mass particles in a small part of sim volume
Constrained realization - small scale: simulate individual halos (NFW)
large scale: simulate particular region

Reviews

Bertschinger ARAA 1998; Klypin lectures 2002; U Washington website
http://www-hpcc.astro.washington.edu/

Structure of Dark Matter Halos

Navarro, Frenk, White

1996 1997 ⟶

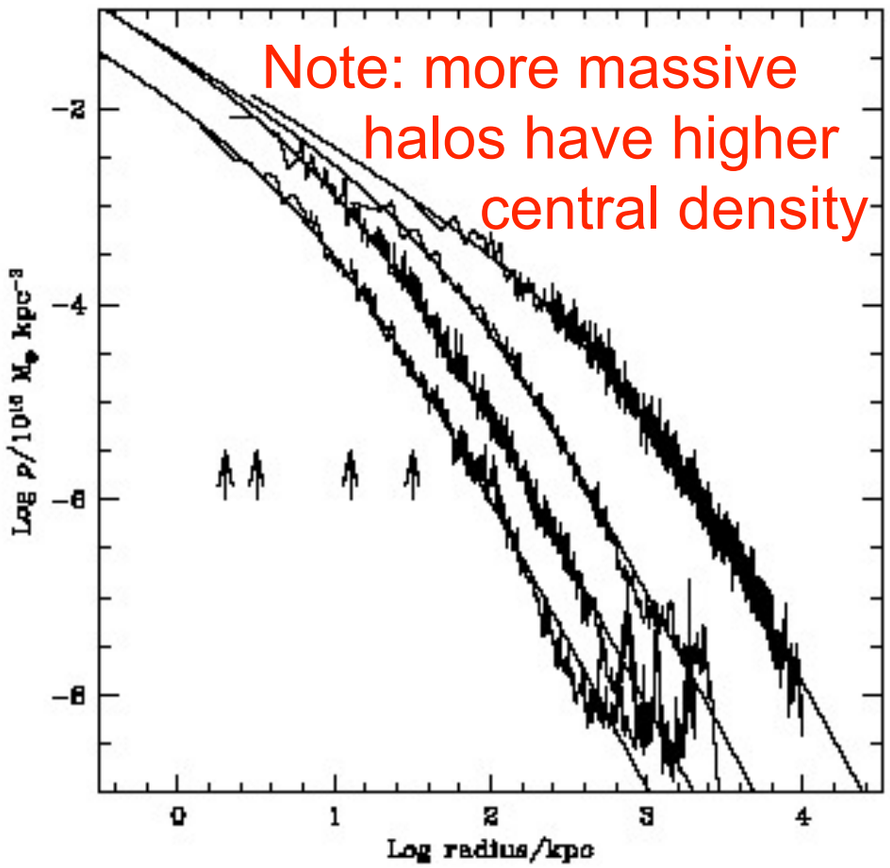

Fig. 3.— Density profiles of four halos spanning four orders of magnitude in mass. The arrows indicate the gravitational softening, h_g, of each simulation. Also shown are fits from eq.3. The fits are good over two decades in radius, approximately from h_g out to the virial radius of each system.

$$\frac{\rho(r)}{\rho_{crit}} = \frac{\delta_c}{(r/r_s)(1+r/r_s)^2}, \qquad (3)$$

NFW formula works for <u>all</u> models

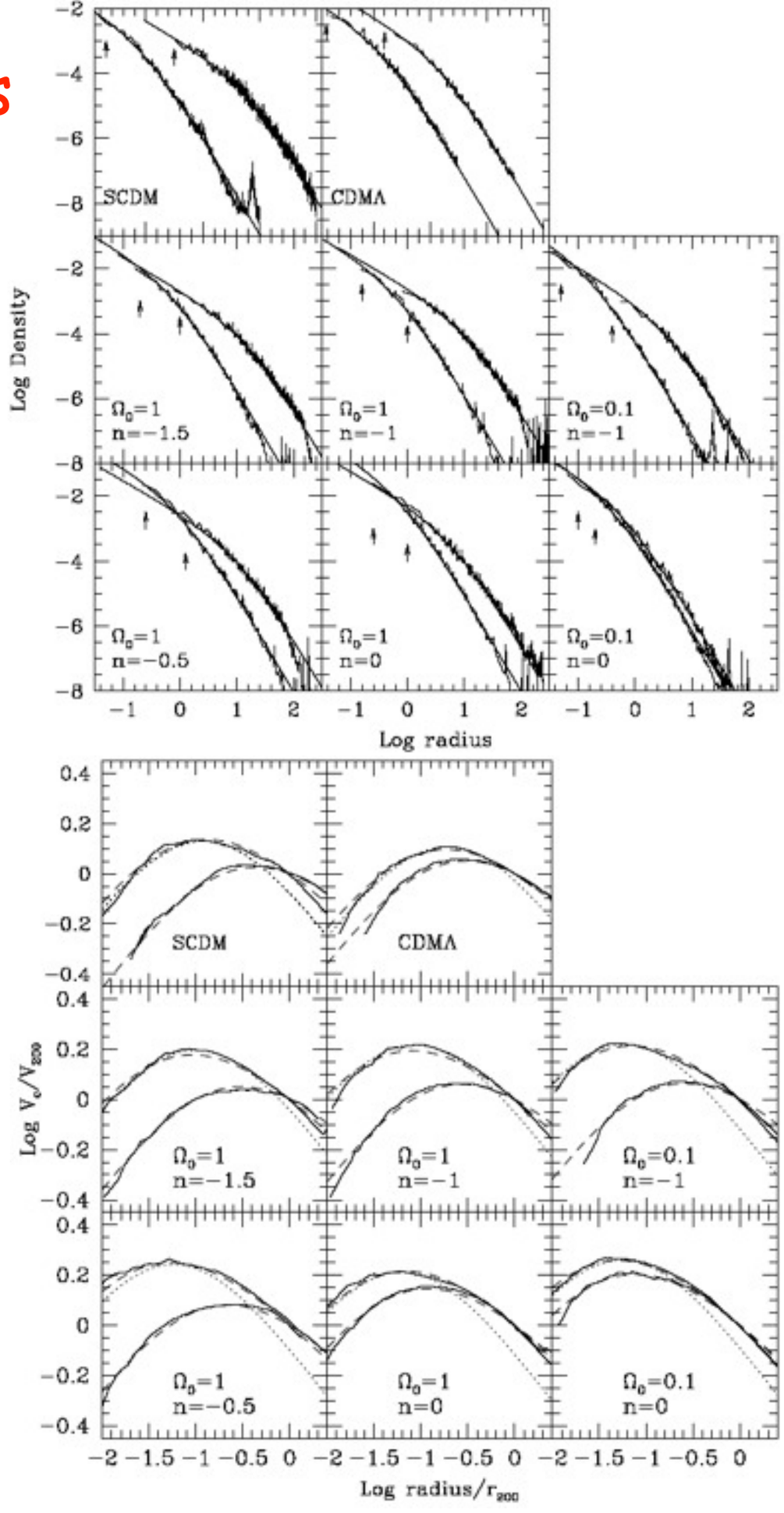

Dark Matter Halo Radial Profile

Comparison of NFW and Moore et al. profiles

Parameter	NFW	Moore et al.
Density $x = r/r_s$	$\rho = \frac{\rho_s}{x(1+x)^2}$ $\rho \propto x^{-3}$ for $x \gg 1$ $\rho \propto x^{-1}$ for $x \ll 1$ $\rho/\rho_s = 1/4$ at $x = 1$	$\rho = \frac{\rho_s}{x^{1.5}(1+x)^{1.5}}$ $\rho \propto x^{-3}$ for $x \gg 1$ $\rho \propto x^{-1.5}$ for $x \ll 1$ $\rho/\rho_s = 1/2$ at $x = 1$
Mass $M = 4\pi\rho_s r_s^3 f(x)$ $= M_{\rm vir} f(x)/f(C)$ $M_{\rm vir} = \frac{4\pi}{3}\rho_{\rm cr}\Omega_0\delta_{\rm top-hat} r_{\rm vir}^3$	$f(x) = \ln(1+x) - \frac{x}{1+x}$	$f(x) = \frac{2}{3}\ln(1+x^{3/2})$
Concentration $C = r_{\rm vir}/r_s$	$C_{\rm NFW} = 1.72 C_{\rm Moore}$ for halos with the same $M_{\rm vir}$ and $r_{\rm max}$ $C_{1/5} \approx \frac{C_{\rm NFW}}{0.86 f(C_{\rm NFW}) + 0.1363}$ error less than 3% for $C_{\rm NFW}$ =5-30 $C_{\gamma=-2} = C_{\rm NFW}$	$C_{\rm Moore} = C_{\rm NFW}/1.72$ $C_{1/5} = \frac{C_{\rm Moore}}{[(1+C_{\rm Moore}^{3/2})^{1/5} - 1]^{2/3}}$ $\approx \frac{C_{\rm Moore}}{[C_{\rm Moore}^{3/10} - 1]^{2/3}}$ $C_{\gamma=-2} = 2^{3/2} C_{\rm Moore}$ $\approx 2.83 C_{\rm Moore}$
Circular Velocity $v_{\rm circ}^2 = \frac{GM_{\rm vir}}{r_{\rm vir}}\frac{C}{x}\frac{f(x)}{f(C)}$ $= v_{\rm max}^2 \frac{x_{\rm max}}{x}\frac{f(x)}{f(x_{\rm max})}$ $v_{\rm vir}^2 = \frac{GM_{\rm vir}}{r_{\rm vir}}$	$x_{\rm max} \approx 2.15$ $v_{\rm max}^2 \approx 0.216 v_{\rm vir}^2 \frac{C}{f(C)}$ $\rho/\rho_s \approx 1/21.3$ at $x = 2.15$	$x_{\rm max} \approx 1.25$ $v_{\rm max}^2 \approx 0.466 v_{\rm vir}^2 \frac{C}{f(C)}$ $\rho/\rho_s \approx 1/3.35$ at $x = 1.25$

Klypin, Kravtsov, Bullock & Primack 2001

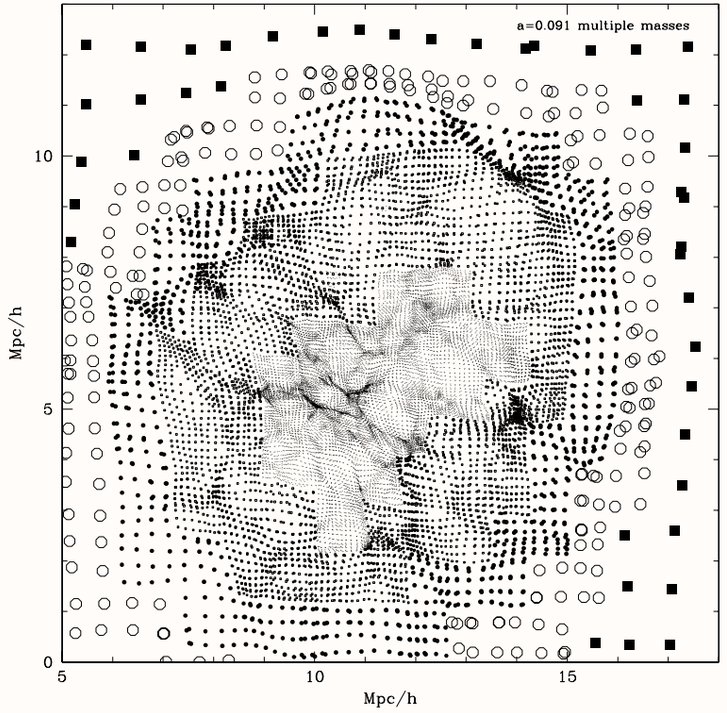

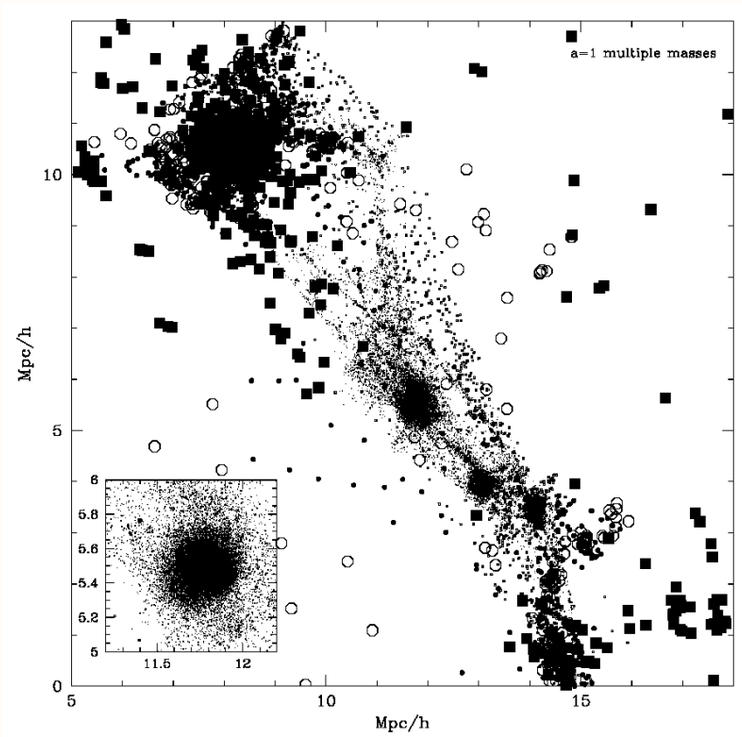

Fig. 2.— Distribution of particles of different masses in a thin slice through the center of halo A_1 (see Table 1) at $z = 10$ (top panel) and at $z = 0$ (bottom panel). To avoid crowding of points the thickness of the slice is made smaller in the center (about $30h^{-1}$kpc) and larger ($1h^{-1}$Mpc) in the outer parts of the forming halo. Particles of different mass are shown with different symbols: tiny dots, dots, large dots, squares, and open circles.

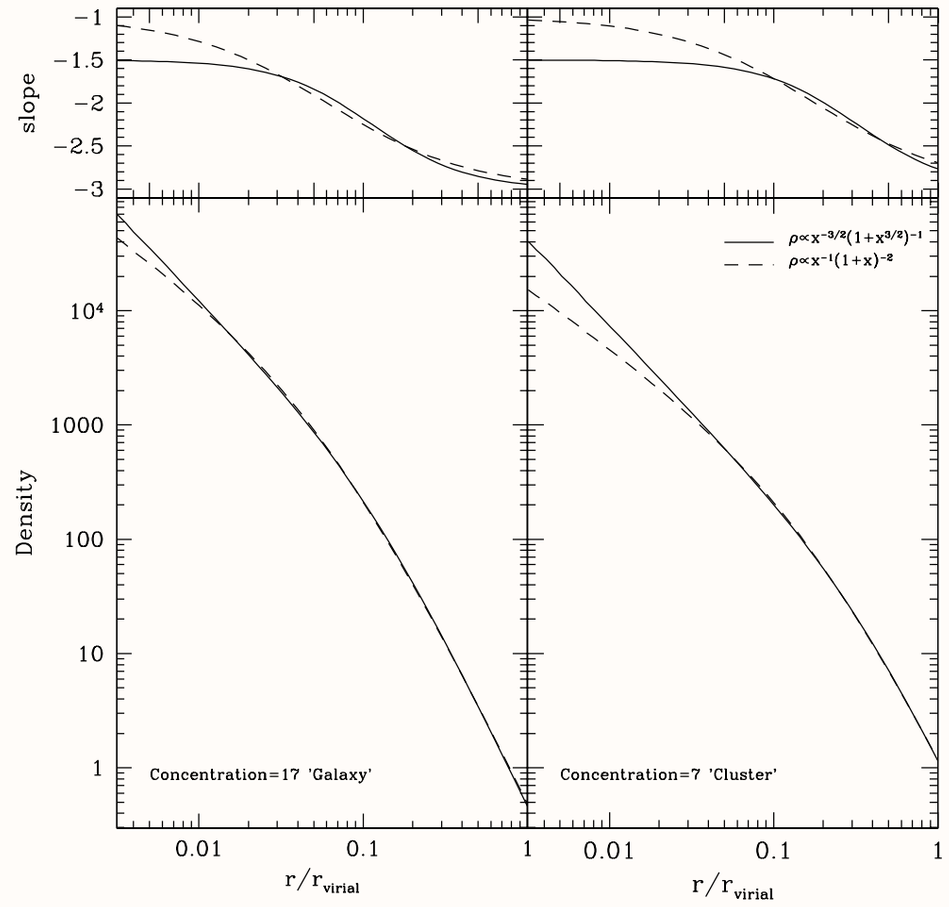

Fig. 3.— Comparison of the Moore et al. and the NFW profiles. Each profile is normalized to have the same virial mass and the same radius of the maximum circular velocity. *Left panels:* High-concentration halo typical of small galaxy-size halos $C_{\rm NFW} = 17$. *Right panels:* Low-concentration halo typical of cluster-size halos. The deviations are very small ($< 3\%$) for radii $r > r_s/2$. Top panels show the local logarithmic slope of the profiles. Note that for the high concentration halo the slope of the profile is significantly larger than the asymptotic value -1 even at very small radii $r \approx 0.01 r_{\rm vir}$.

Klypin, Kravtsov, Bullock & Primack 2001

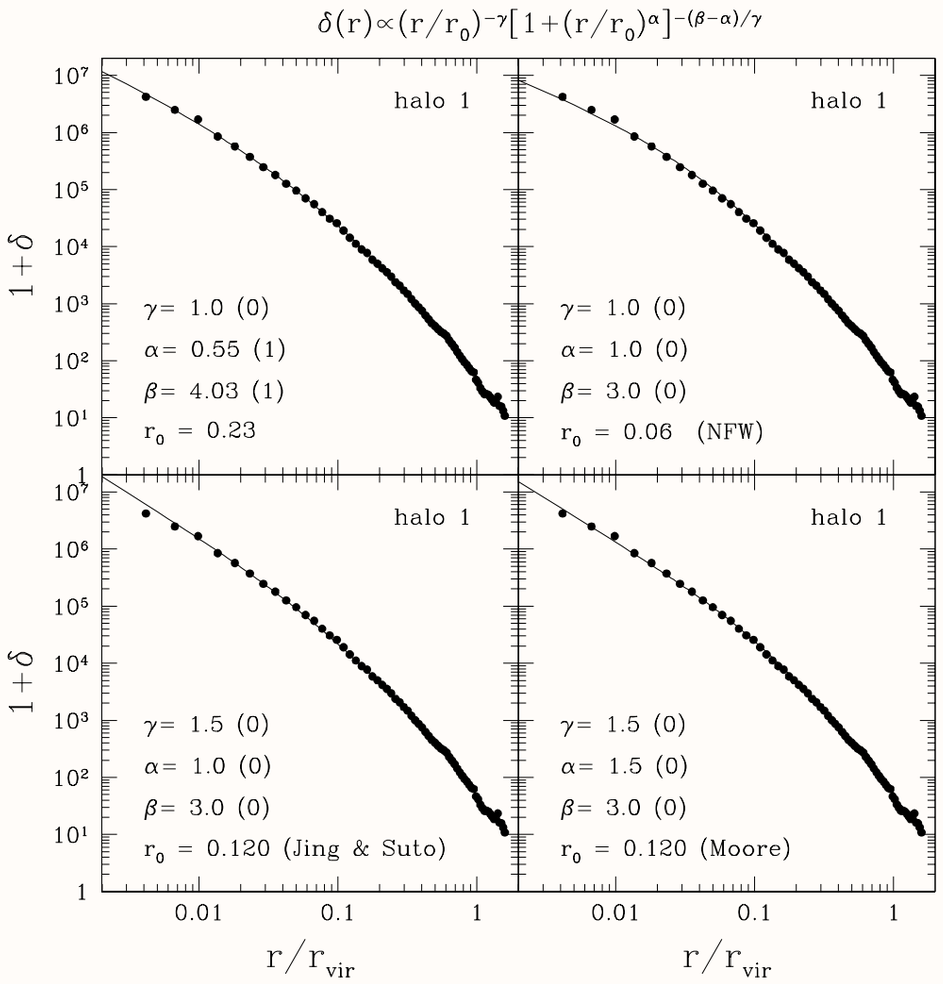

Fig. 8.— Analytic fits to the density profile of the halo A_1 from our set of simulations. The fits are of the form $\rho(r) \propto (r/r_0)^{-\gamma}[1+(r/r_0)^{\alpha}]^{-(\beta-\alpha)/\gamma}$. The legend in each panel indicates the corresponding values of α, β, and γ of the fit; the digit in parenthesis indicates whether the parameter was kept fixed (0) or not (1) during the fit. Note that various sets of parameters α, β, γ provide equally good fits to the simulated halo profile in the whole range resolved range of scales $\approx 0.005 - 1 r_{\rm vir}$. This indicates a large degree of degeneracy in parameters α, β, and γ

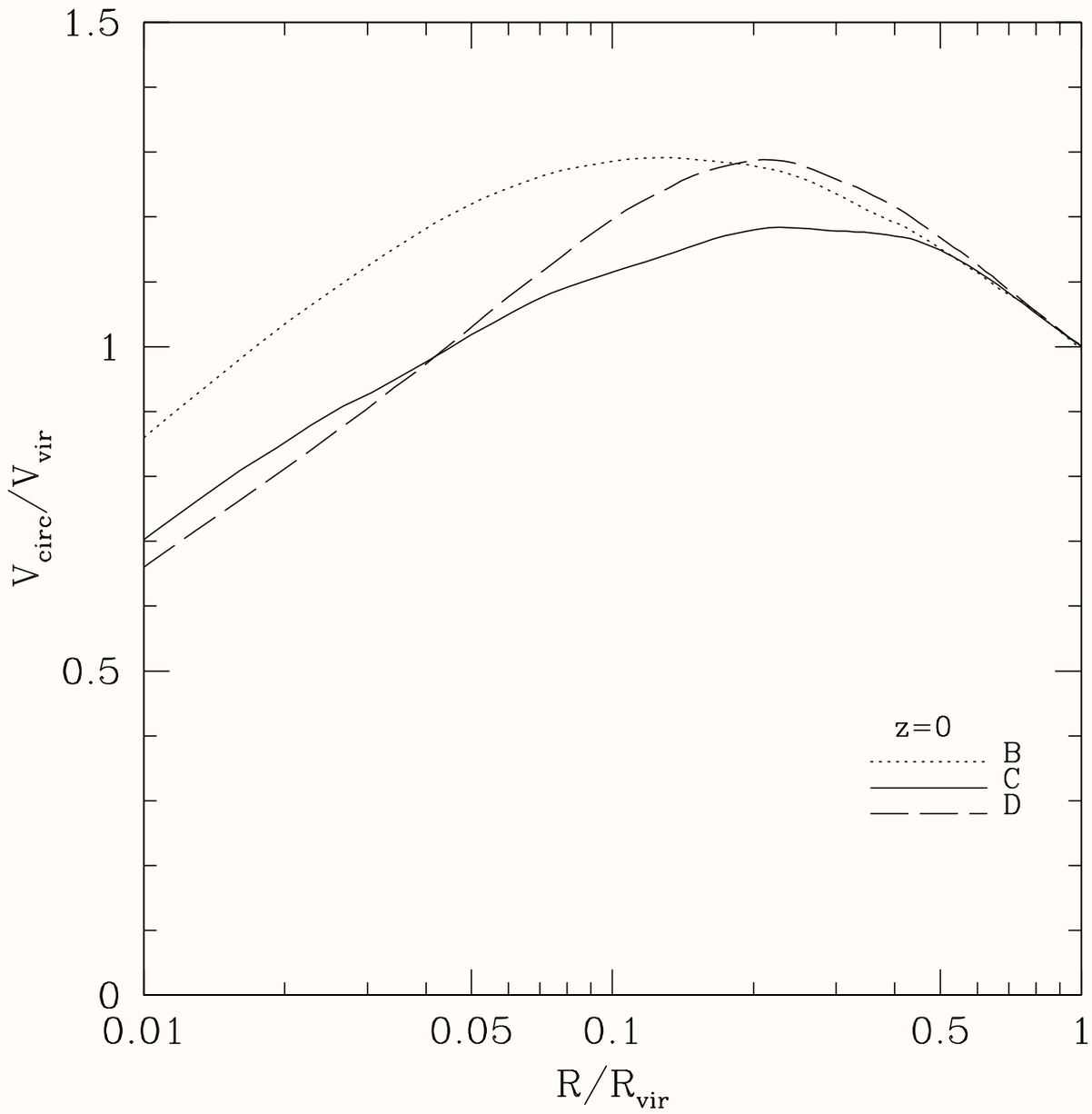

Fig. 9.— Circular velocity profiles for the halos B_1, C_1, and D_1 normalized to halo's virial velocity. Halos are well resolved on all shown scales. Although the halos have very similar masses, the profiles are very different; the differences are due to real differences in the concentration parameters.

Klypin, Kravtsov, Bullock & Primack 2001

Empirical Models for Dark Matter Halos. II. Inner profile slopes, dynamical profiles, and ρ/σ^3

Alister Graham, David Merritt, Ben Moore, Jürg Diemand, Balša Terzić

Einasto's model is given by the equation

$$\rho(r) = \rho_{\rm e} \exp\left\{-d_n\left[(r/r_{\rm e})^{1/n} - 1\right]\right\}.$$

Data on log slopes from innermost resolved radius of observed galaxies, not corrected for observational effects -- adapted from de Blok (2004).

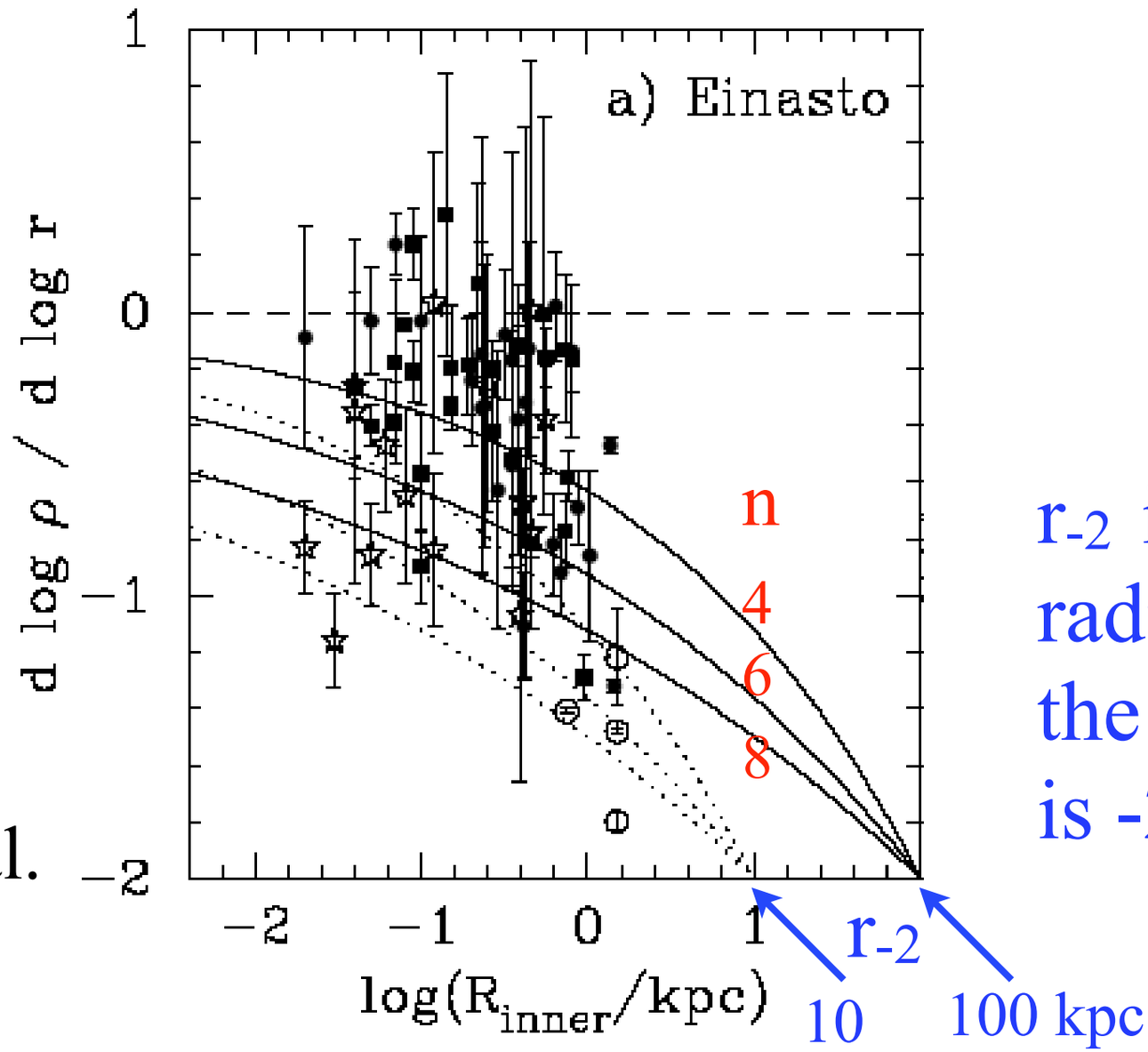

r_{-2} is the radius where the log-slope is -2

See also Navarro et al. Aquarius simulations arXiv:0810.1522

Aquarius Simulation: Formation of a Milky-Way-size Dark Matter Halo

Diameter of Milky Way Dark Matter Halo
1.6 million light years

Diameter of visible Milky Way
30 kpc = 100,000 light years

Diameter of Milky Way Dark Matter Halo
1.6 million light years

500 kpc

Volker Springel
Max-Planck-Institute
for Astrophysics

Diameter of visible Milky Way
30 kpc = 100,000 light years

Diameter of Milky Way Dark Matter Halo
1.6 million light years

500 kpc

Volker Springel
Max-Planck-Institute
for Astrophysics

Particle number in cosmological N-body simulations vs. pub date

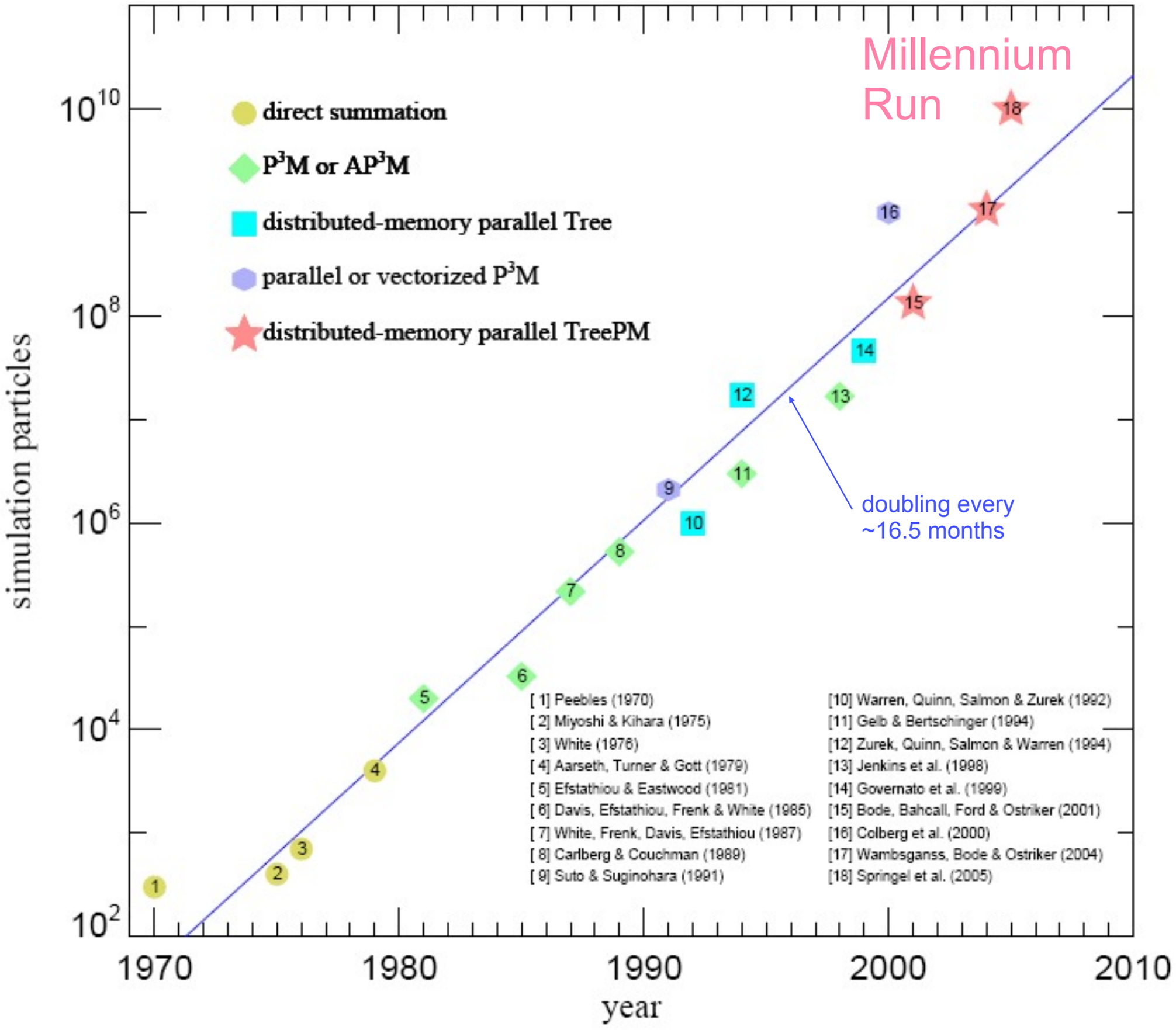

Particle number in cosmological N-body simulations vs. pub date

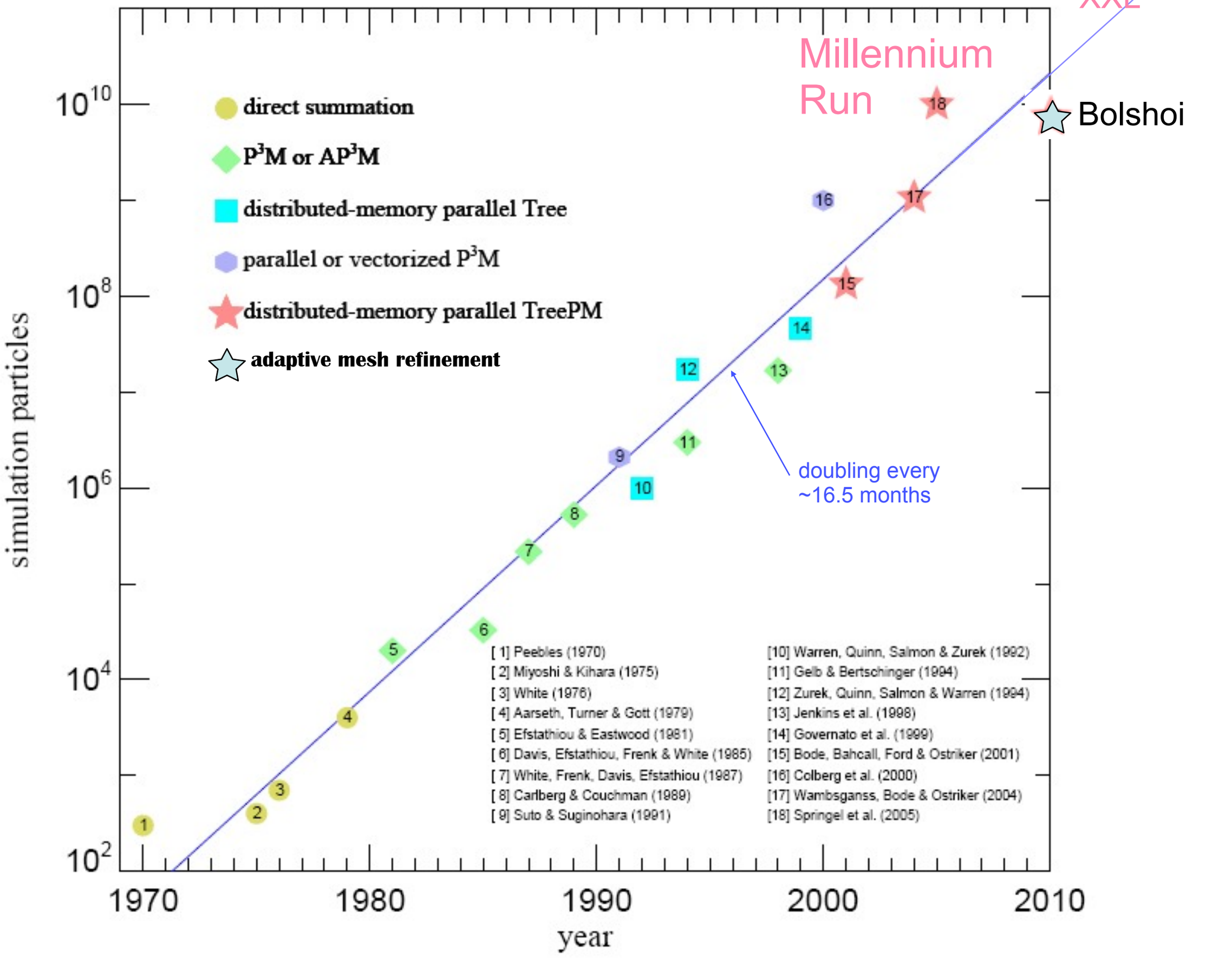

WMAP-only Determination of σ_8 and Ω_M

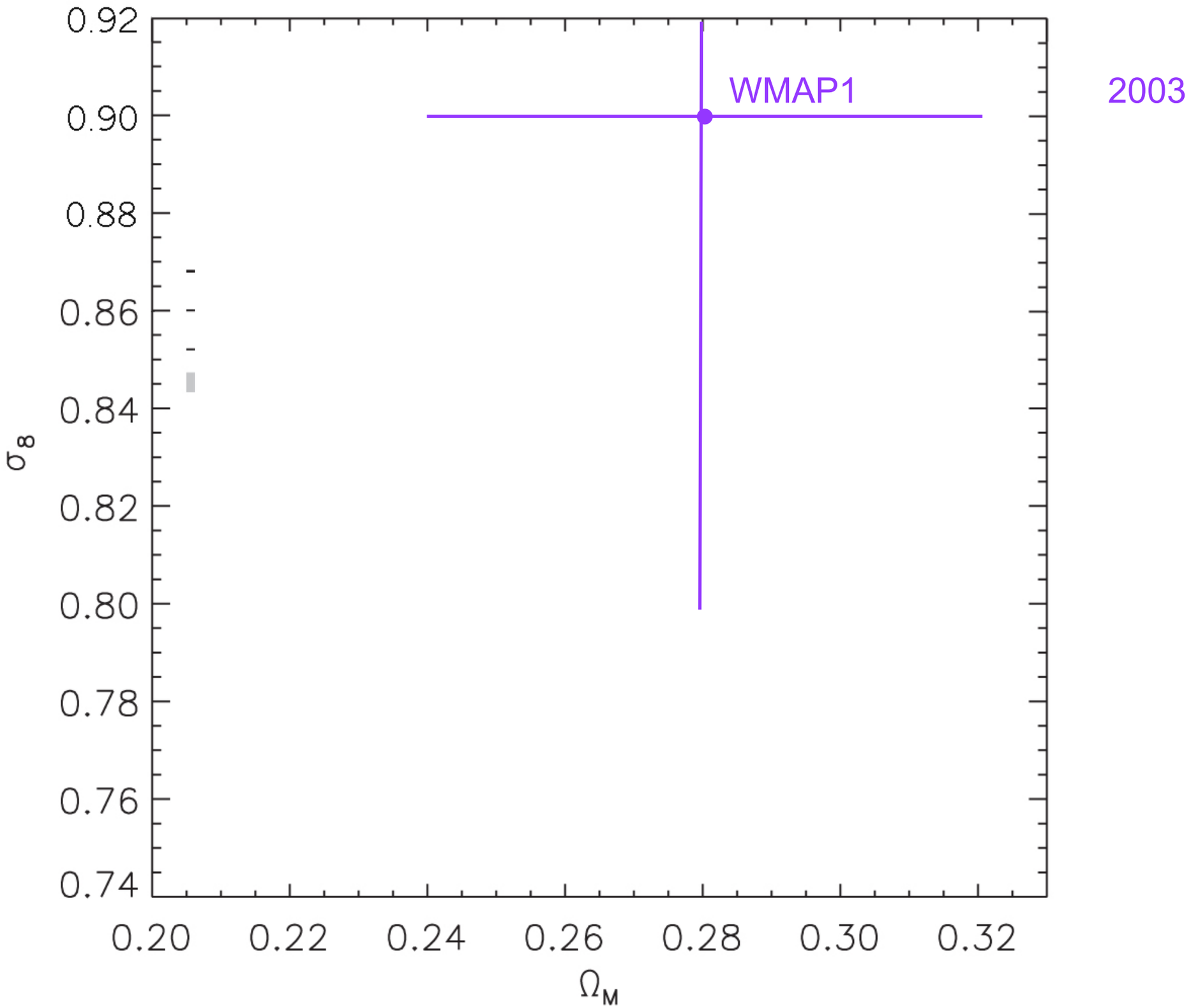

The Millennium Run

- **properties of halos** (radial profile, concentration, shapes)
- **evolution of the number density of halos**, essential for normalization of Press-Schechter- type models
- **evolution of the distribution and clustering of halos** in real and redshift space, for comparison with observations
- **accretion history of halos**, assembly bias (variation of large-scale clustering with assembly history), and correlation with halo properties including angular momenta and shapes
- **halo statistics** including the mass and velocity functions, angular momentum and shapes, subhalo numbers and distribution, and correlation with environment

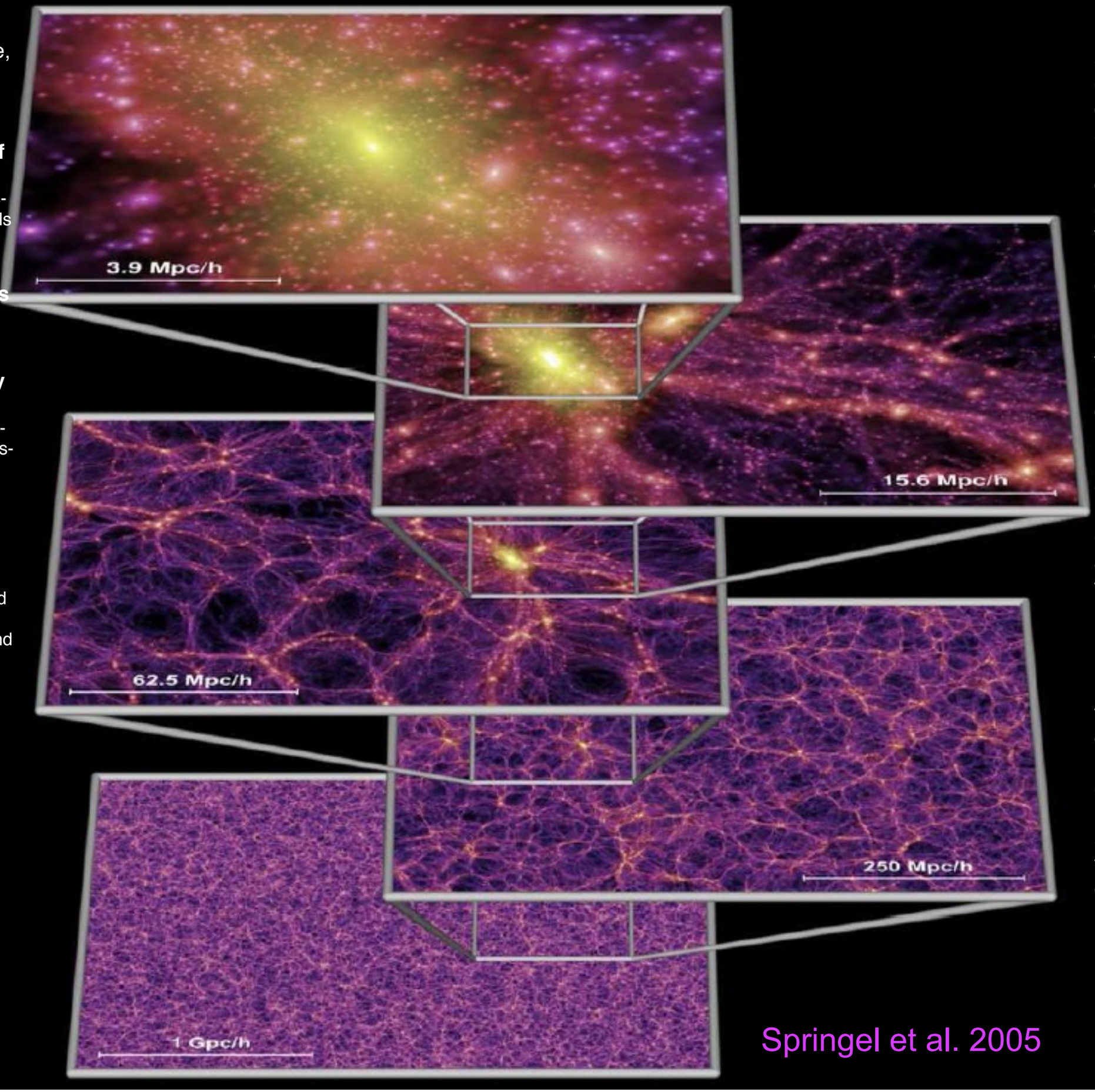

Springel et al. 2005

- **void statistics**, including sizes and shapes and their evolution, and the orientation of halo spins around voids
- quantitative descriptions of the evolving **cosmic web**, including applications to weak gravitational lensing
- preparation of **mock catalogs**, essential for analyzing SDSS and other survey data, and for preparing for new large surveys for dark energy etc.
- **merger trees**, essential for **semi-analytic modeling** of the evolving galaxy population, including models for the galaxy merger rate, the history of star formation and galaxy colors and morphology, the evolving AGN luminosity function, stellar and AGN feedback, recycling of gas and metals, etc.

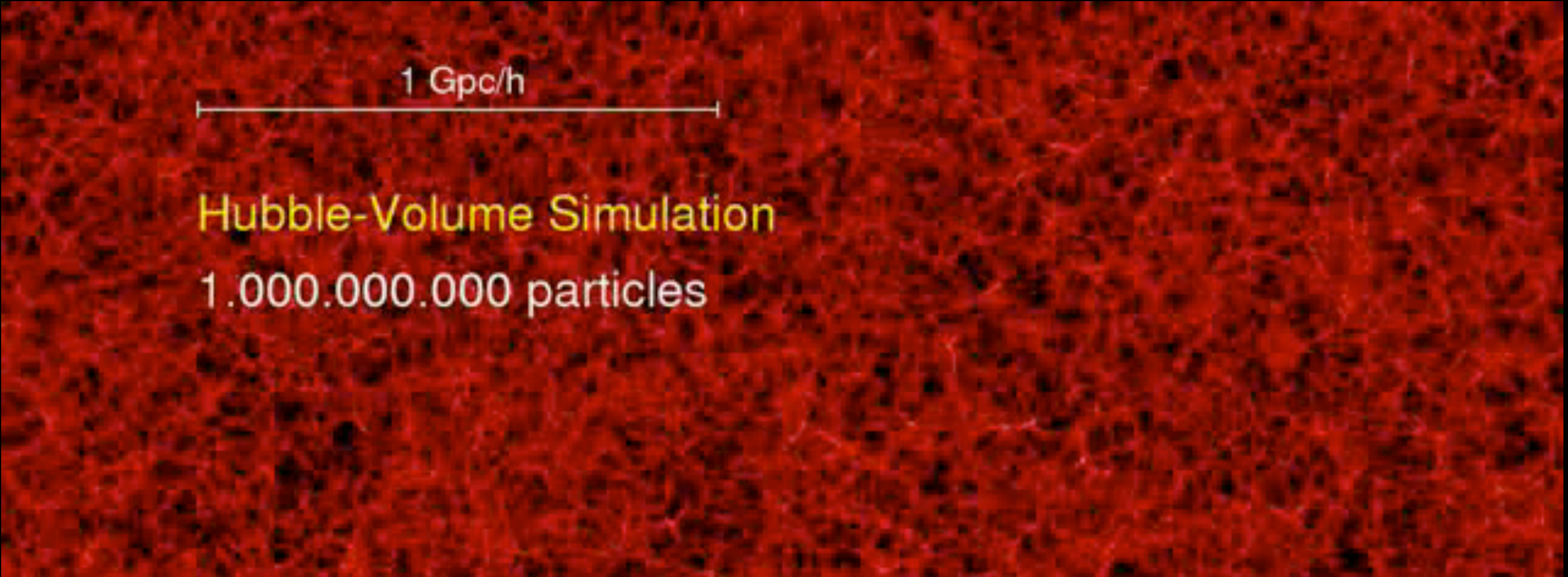
1 Gpc/h
Hubble-Volume Simulation
1.000.000.000 particles
Music: Bach, Partita No. 3
Arthur Grumiaux, violin

WMAP-only Determination of σ_8 and Ω_M

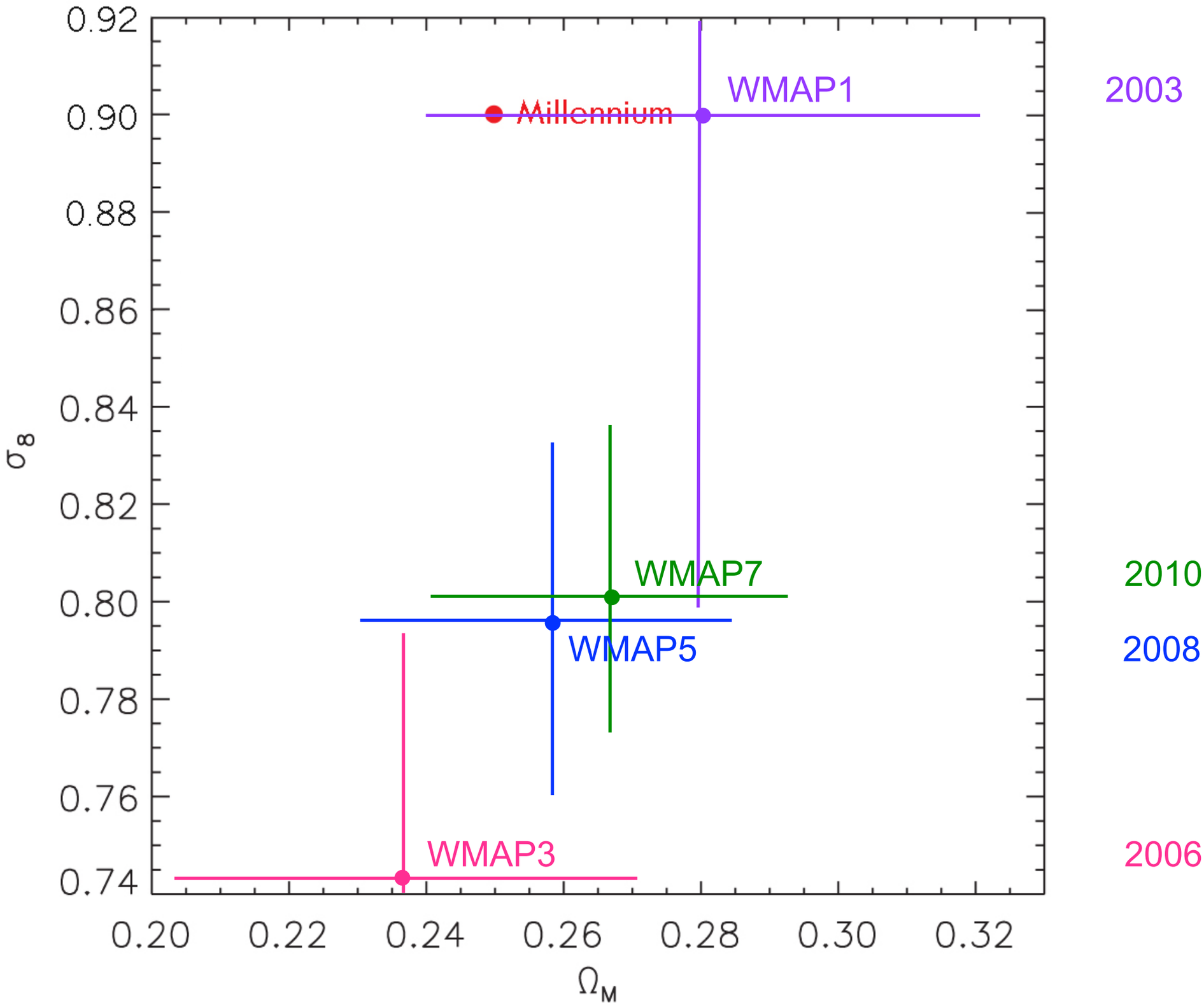

WMAP+SN+Clusters Determination of σ_8 and Ω_M

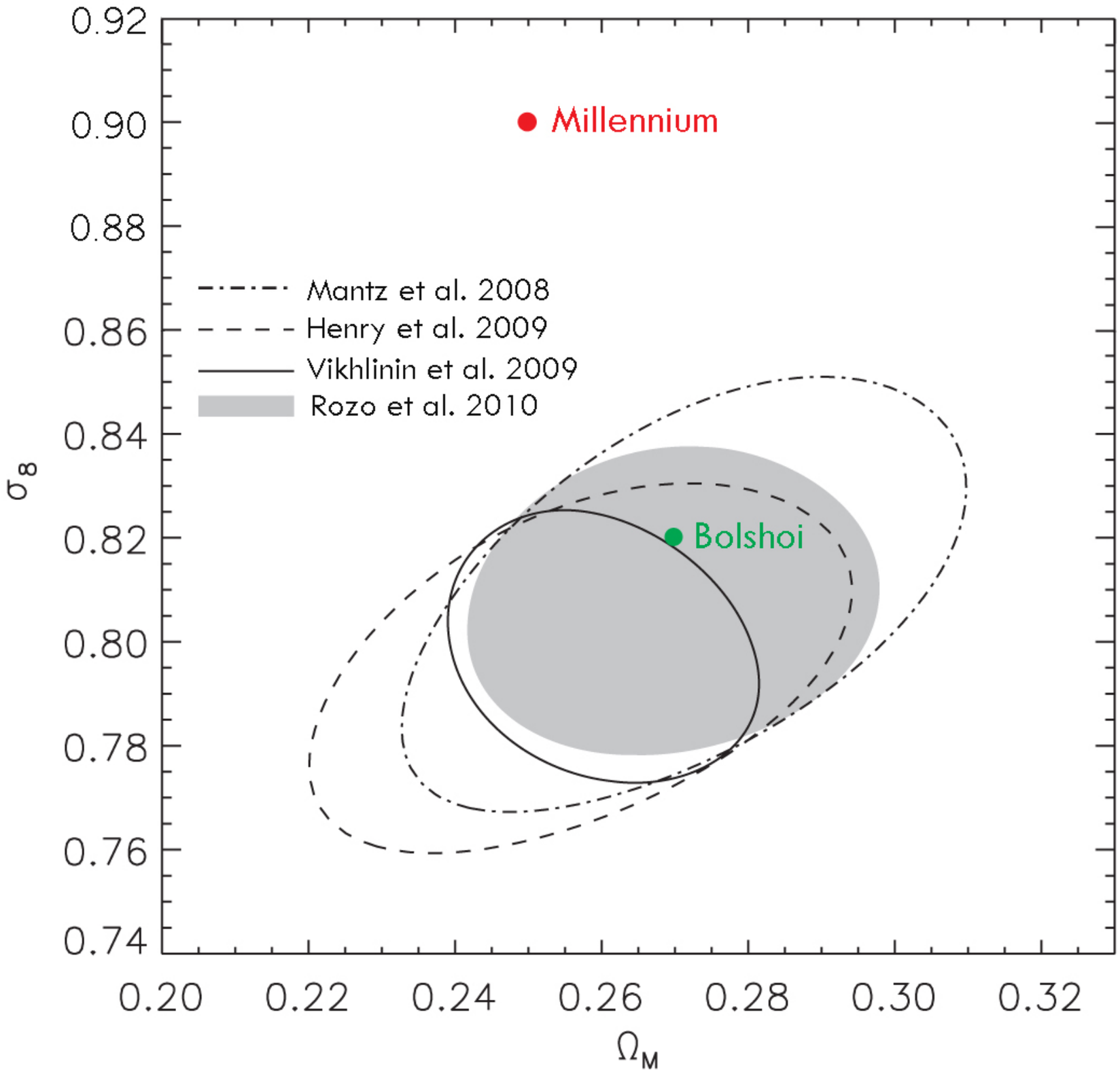

WMAP+SN+Clusters Determination of σ_8 and Ω_M

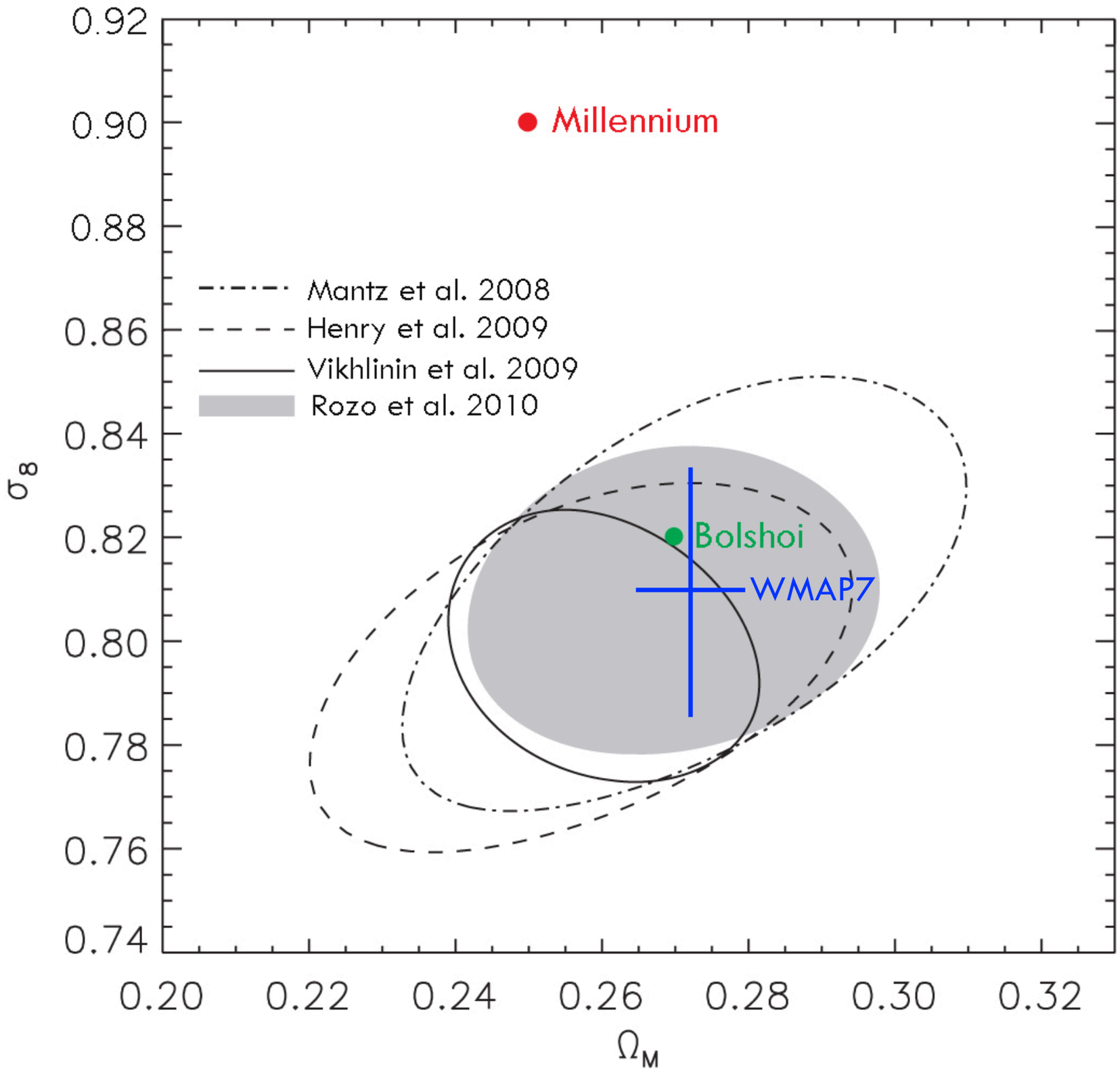

The Bolshoi simulation

ART code

250Mpc/h Box
LCDM

σ_8 = 0.82

h = 0.73

8G particles

1kpc/h force resolution

1e8 Msun/h mass res

dynamical range 262,000

time-steps = 400,000

NASA AMES
supercomputing center
Pleiades computer
13824 cores
12TB RAM
75TB disk storage
6M cpu hrs
18 days wall-clock time

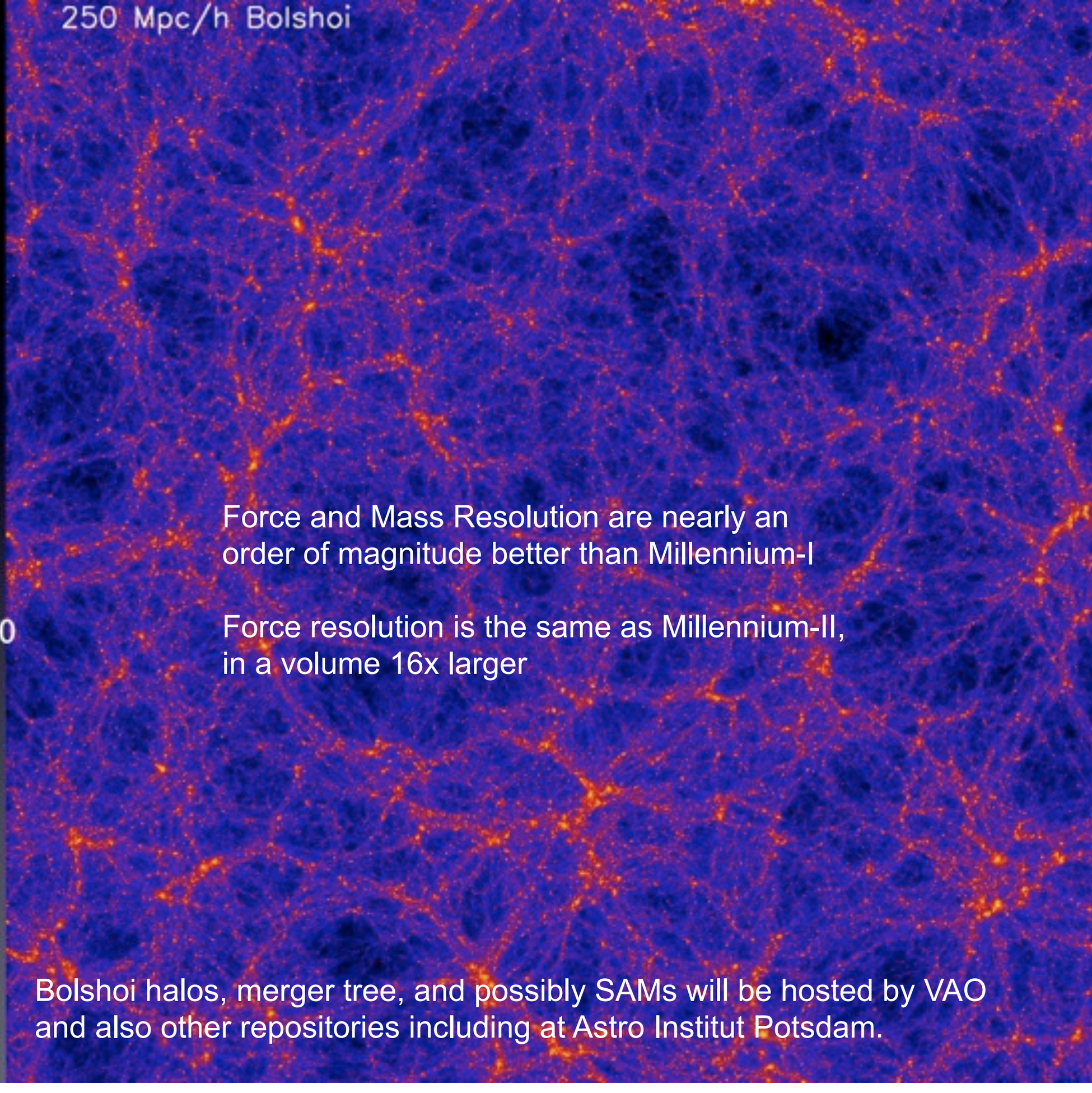

Force and Mass Resolution are nearly an order of magnitude better than Millennium-I

Force resolution is the same as Millennium-II, in a volume 16x larger

Bolshoi halos, merger tree, and possibly SAMs will be hosted by VAO and also other repositories including at Astro Institut Potsdam.

250 Mpc/h Bolshoi

BOLSHOI SIMULATION ZOOM-IN

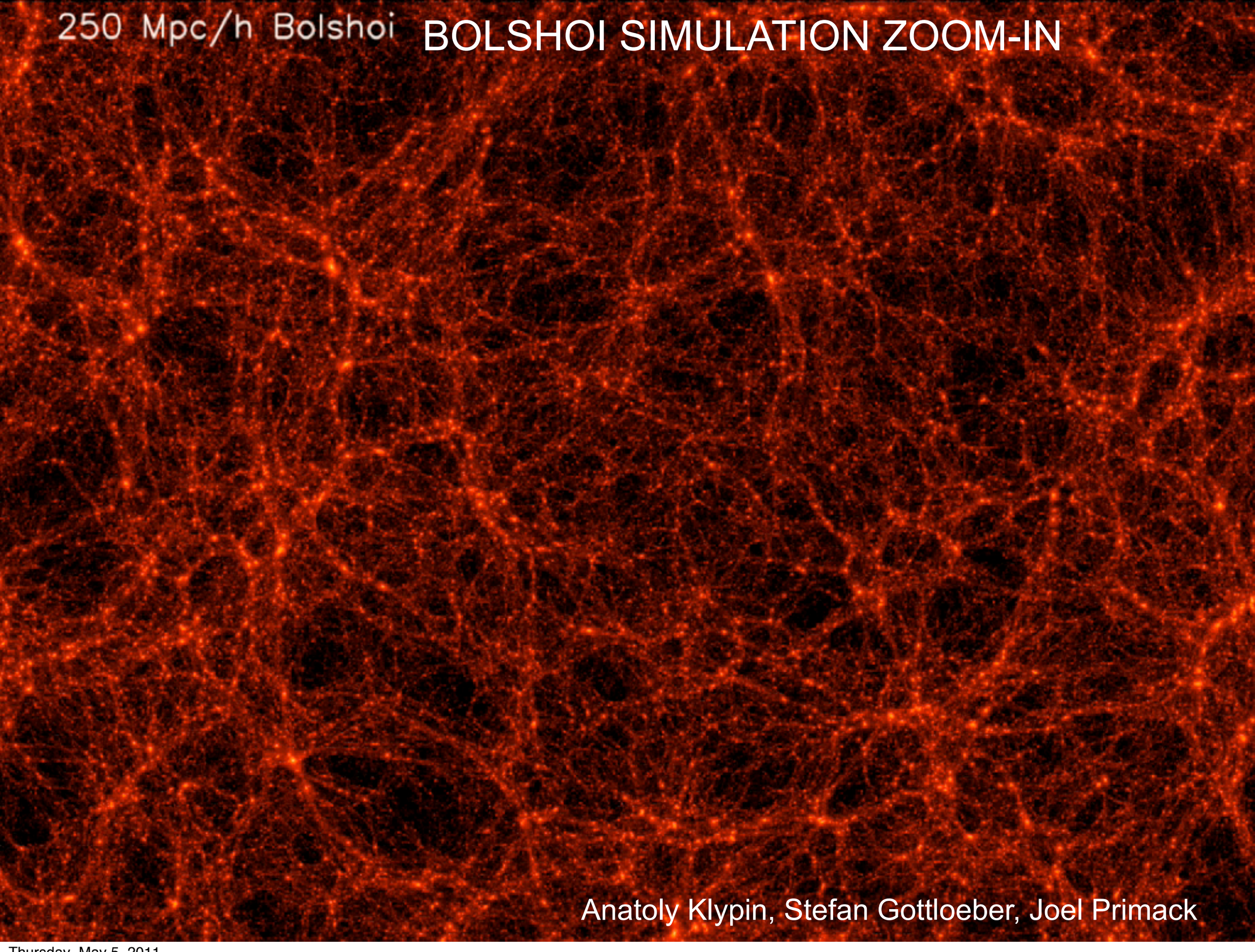

Anatoly Klypin, Stefan Gottloeber, Joel Primack

Halos and galaxies: results from the Bolshoi simulation

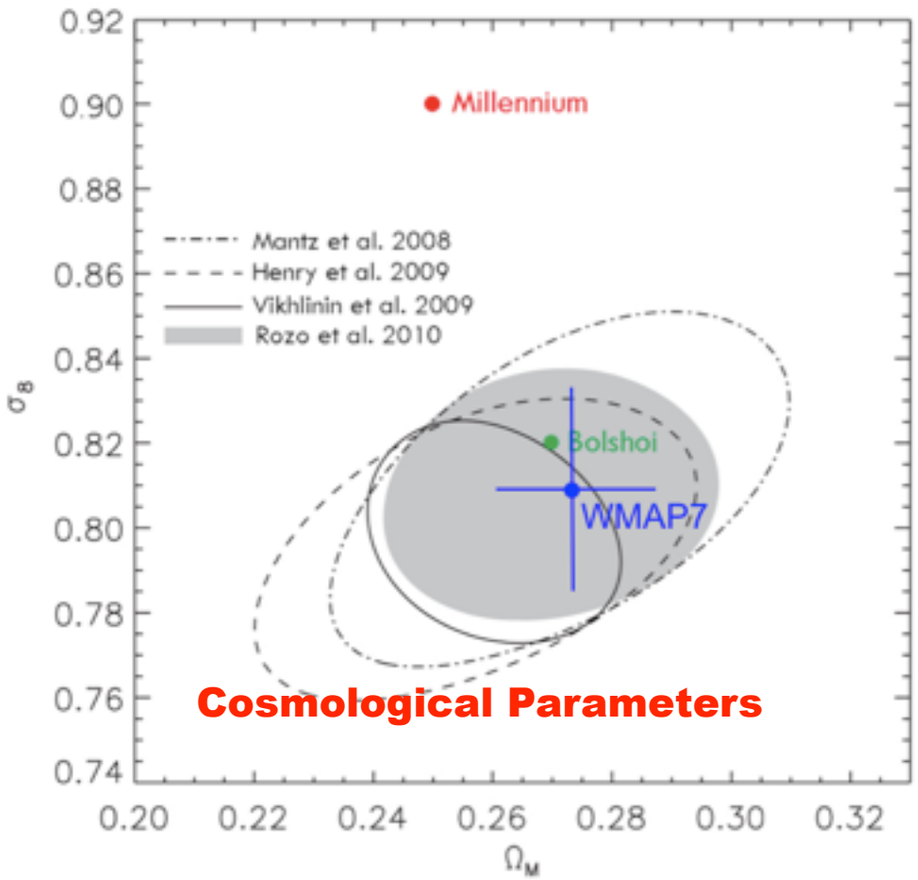

The Millennium Run (Springel+05) was a landmark simulation, and it has been the basis for ~300 papers. However, it and the new Millennium-II simulations were run using WMAP1 (2003) parameters, and the Millennium-I resolution was inadequate to see many subhalos. The new Bolshoi simulation (Klypin, Trujillo & Primack 2010) used the WMAP5 parameters (consistent with WMAP7) and has nearly an order of magnitude better mass and force resolution than Millennium-I. We have now found halos in all 180 stored timesteps, and we have complete merger trees based on Bolshoi.

Klypin, Trujillo-Gomez, & Primack, arXiv:1002.3660 ApJ in press

Subhalos follow the dark matter distribution

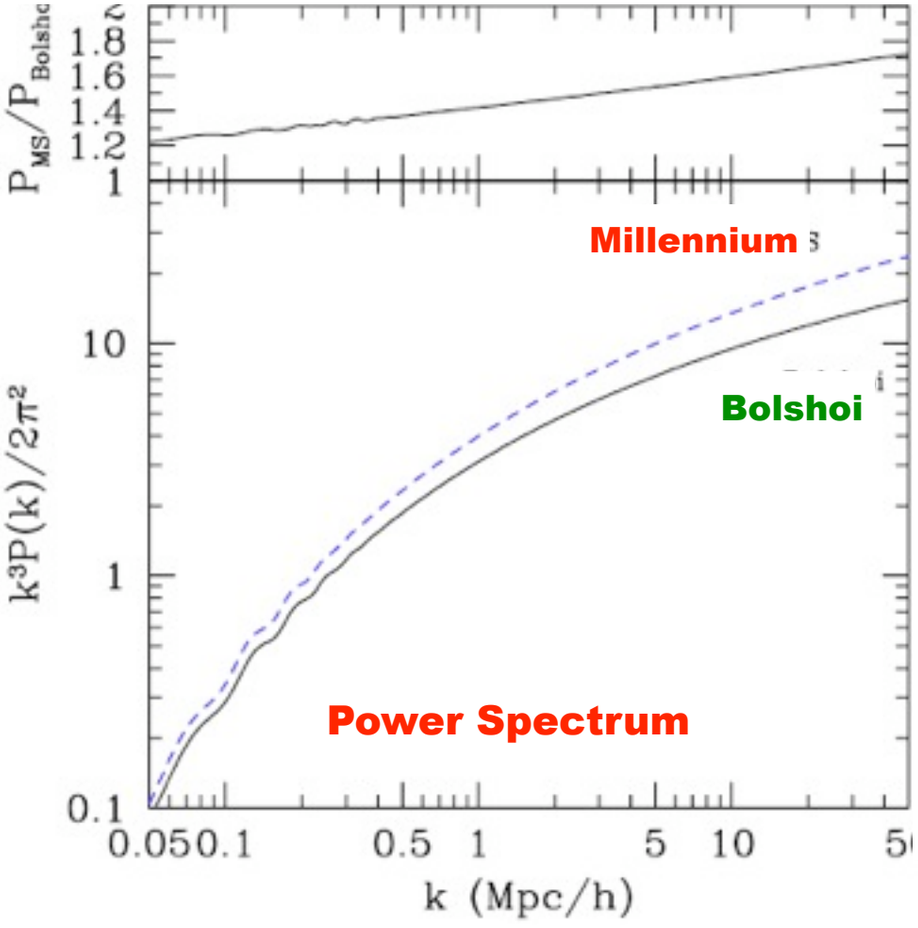

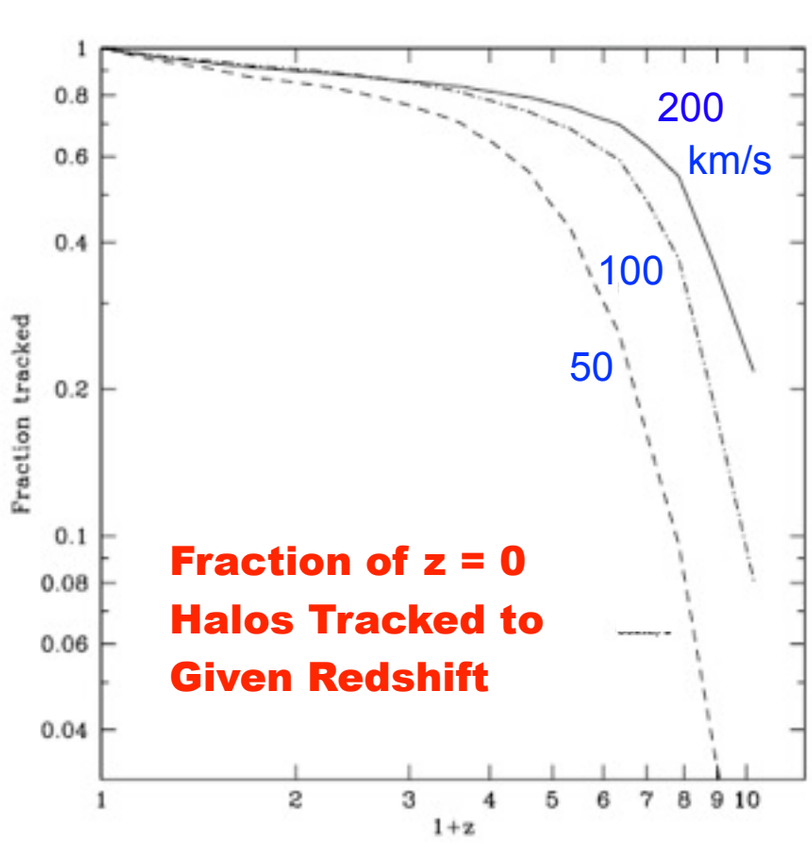

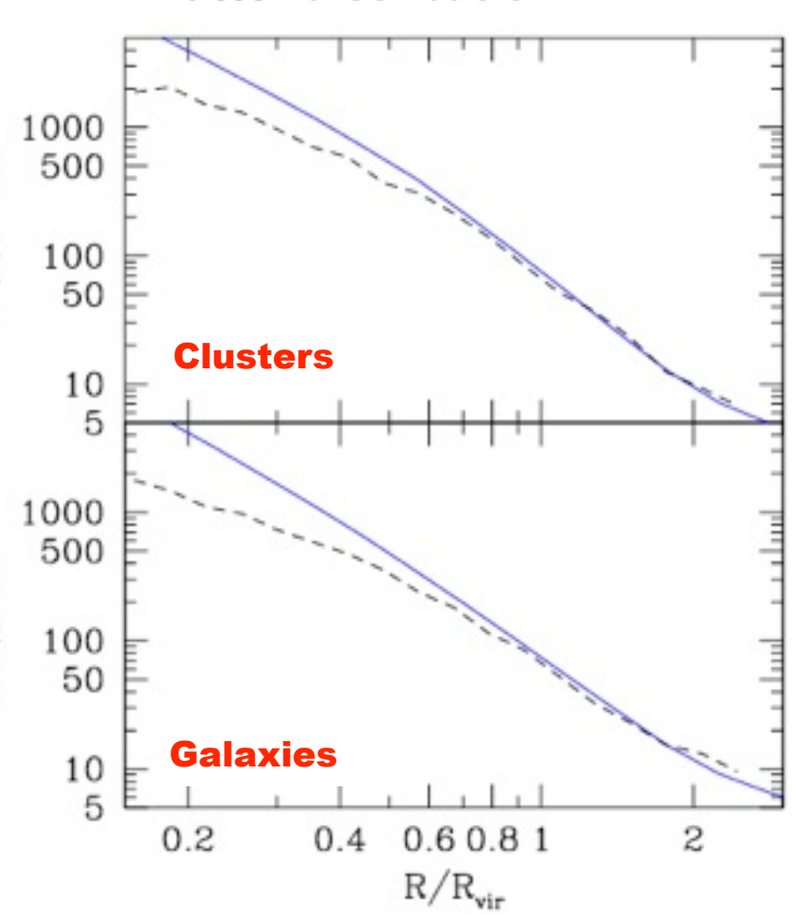

BOLSHOI SIMULATION FLY-THROUGH

$<10^{-3}$
of the
Bolshoi
Simulation
Volume

UNDERSTANDING GALAXY CORRELATIONS

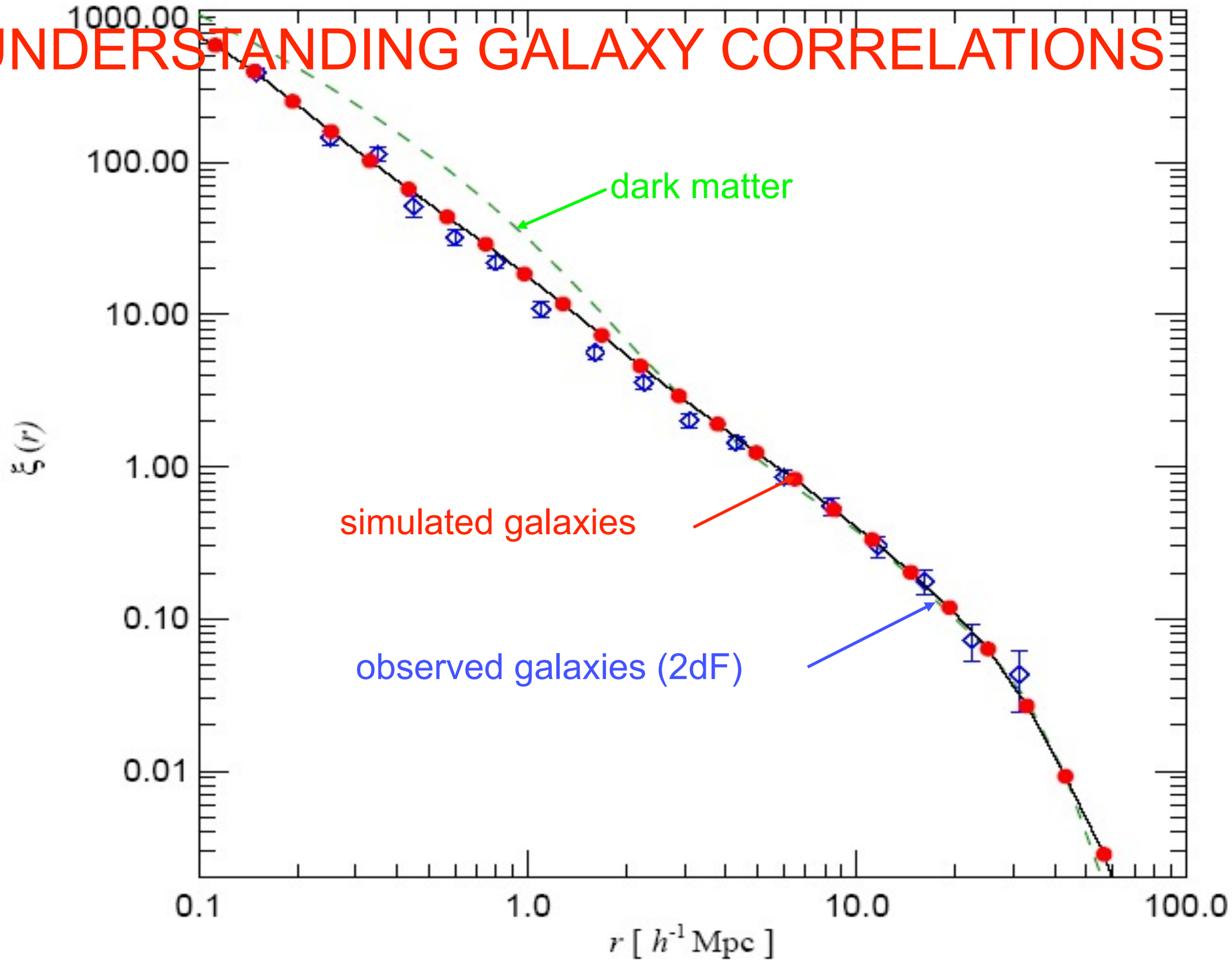

Galaxy 2-point correlation function at the present epoch.

Springel et al. 2005

Millennium-I and II $w_p(r_p)$ by SAM vs. SDSS Observations

——— MS

---------- MS-II

The correlations are seriously overestimated at small separations for lower masses because the high σ_8 = 0.90 produces too many massive halos, which contain pairs of such subhalos.

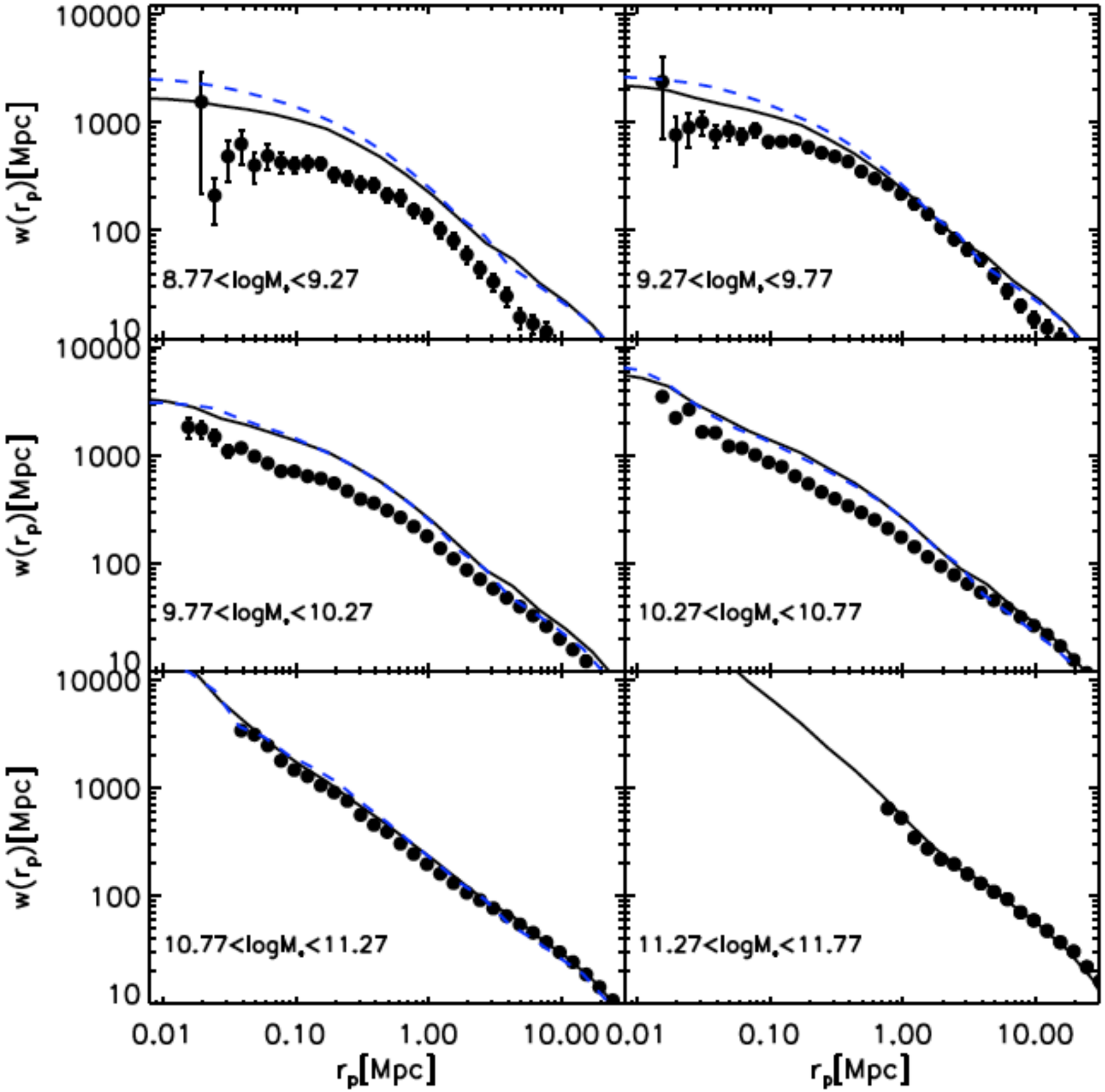

Guo, White, et al. 2011 MN in press

Bolshoi $w_p(r_p)$ by Halo Abundance Matching vs. SDSS Observations

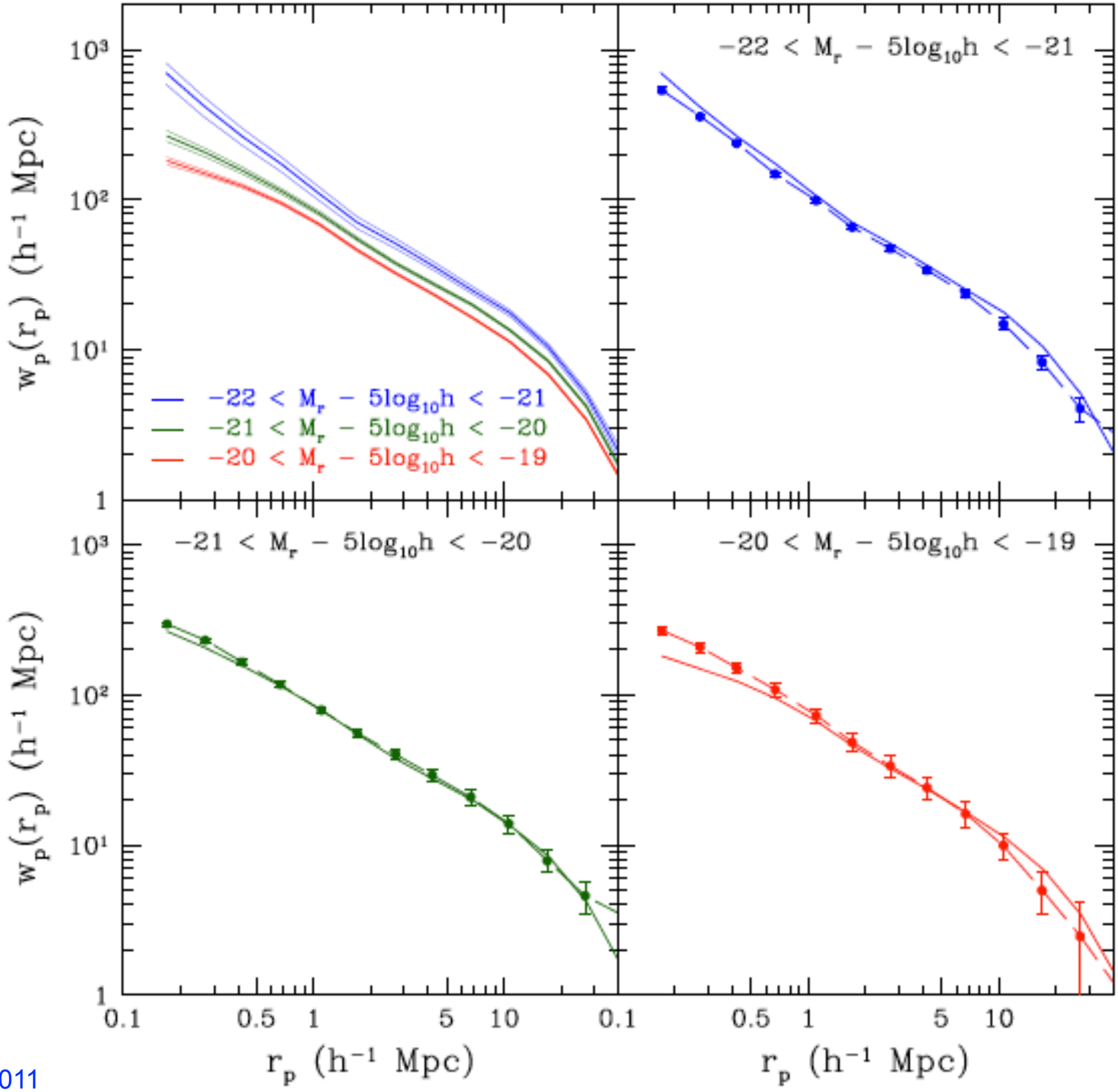

Trujillo-Gomez, Klypin, Primack, & Romanowsky 2011

ΛCDM PREDICTS EVOLUTION IN THE GALAXY CORRELATION FUNCTION

$\xi_{gg}(r)$

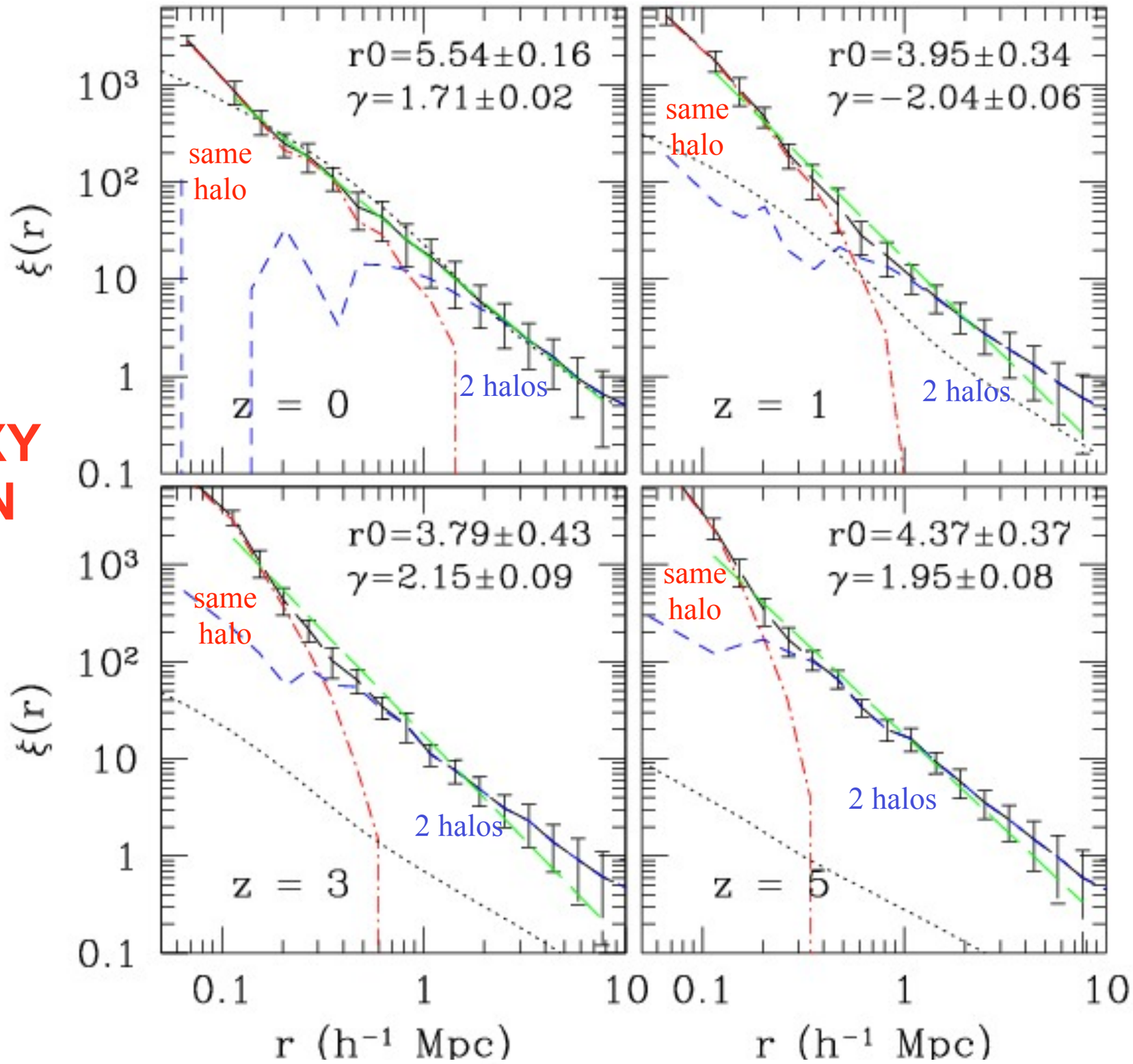

FIG. 8.— Evolution of the two-point correlation function in the $80h^{-1}$ Mpc simulation. The solid line with error bars shows the clustering of halos of the fixed number density $n = 5.89 \times 10^{-3}h^3$ Mpc^{-3} at each epoch. The error-bars indicate the "jack-knife" one sigma errors and are larger than the Poisson error at all scales. The dot-dashed and dashed lines show the corresponding one- and two-halo term contributions. The long-dashed lines show the power-law fit to the correlation functions in the range of $r = [0.1 - 8h^{-1}$ Mpc$]$. Although the correlation functions can be well fit by the power law at $r \gtrsim 0.3h^{-1}$ Mpc in each epoch, at $z > 0$ the correlation function steepens significantly at smaller scales due to the one-halo term.

Kravtsov, Berlind, Wechsler, Klypin, Gottloeber, Allgood, & Primack 2004

Galaxy clustering in SDSS at z~0 agrees with ΛCDM simulations

$n(>V_{\mathrm{max,acc}})=n(>L)$

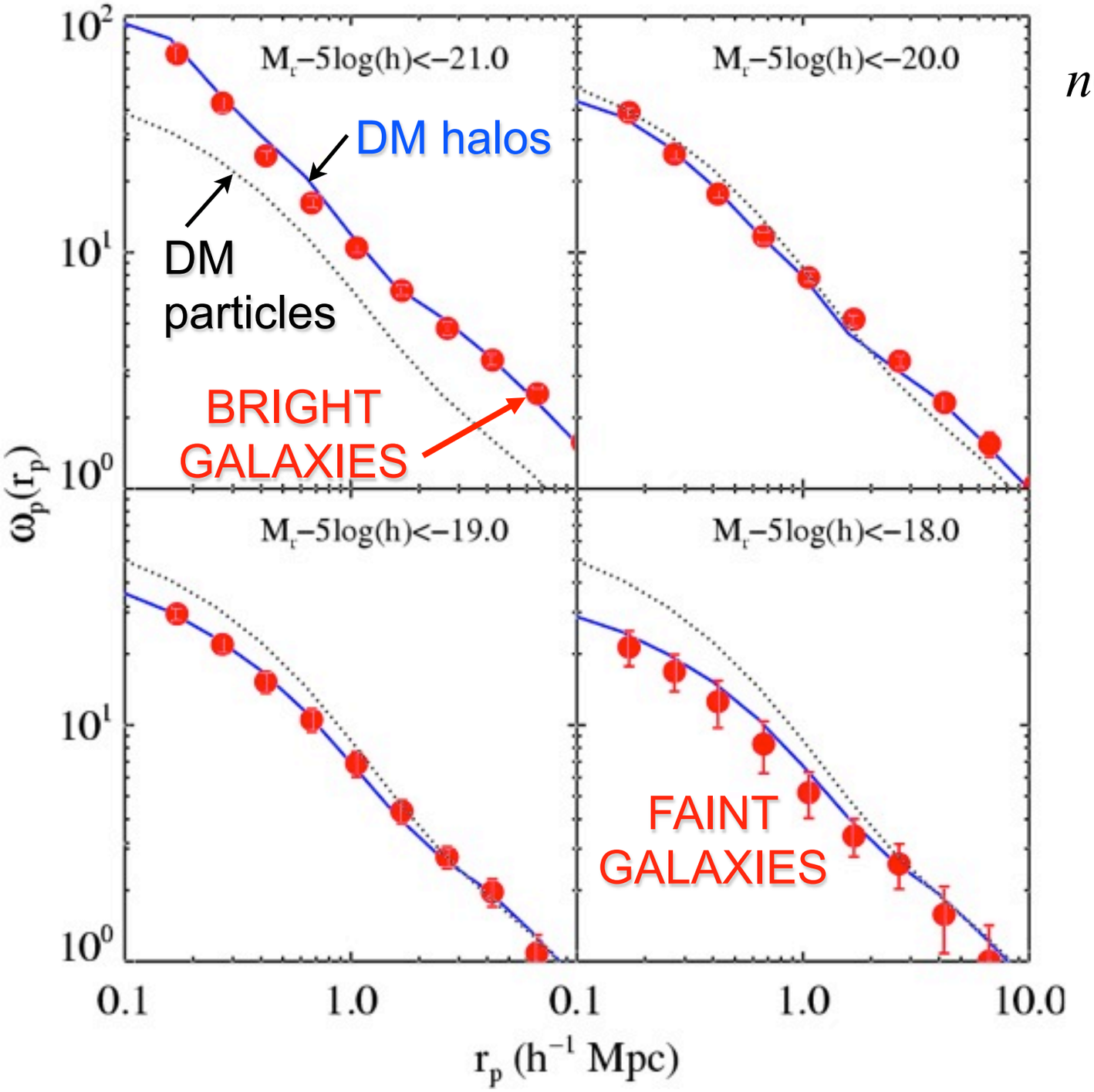

projected 2-point correlation function

projected separation

Conroy, Wechsler & Kravtsov 2006, ApJ 647, 201

and at redshift z~1 (DEEP2)!

$$n(>V_{\mathrm{max,acc}})=n(>L)$$

projected 2-point correlation function

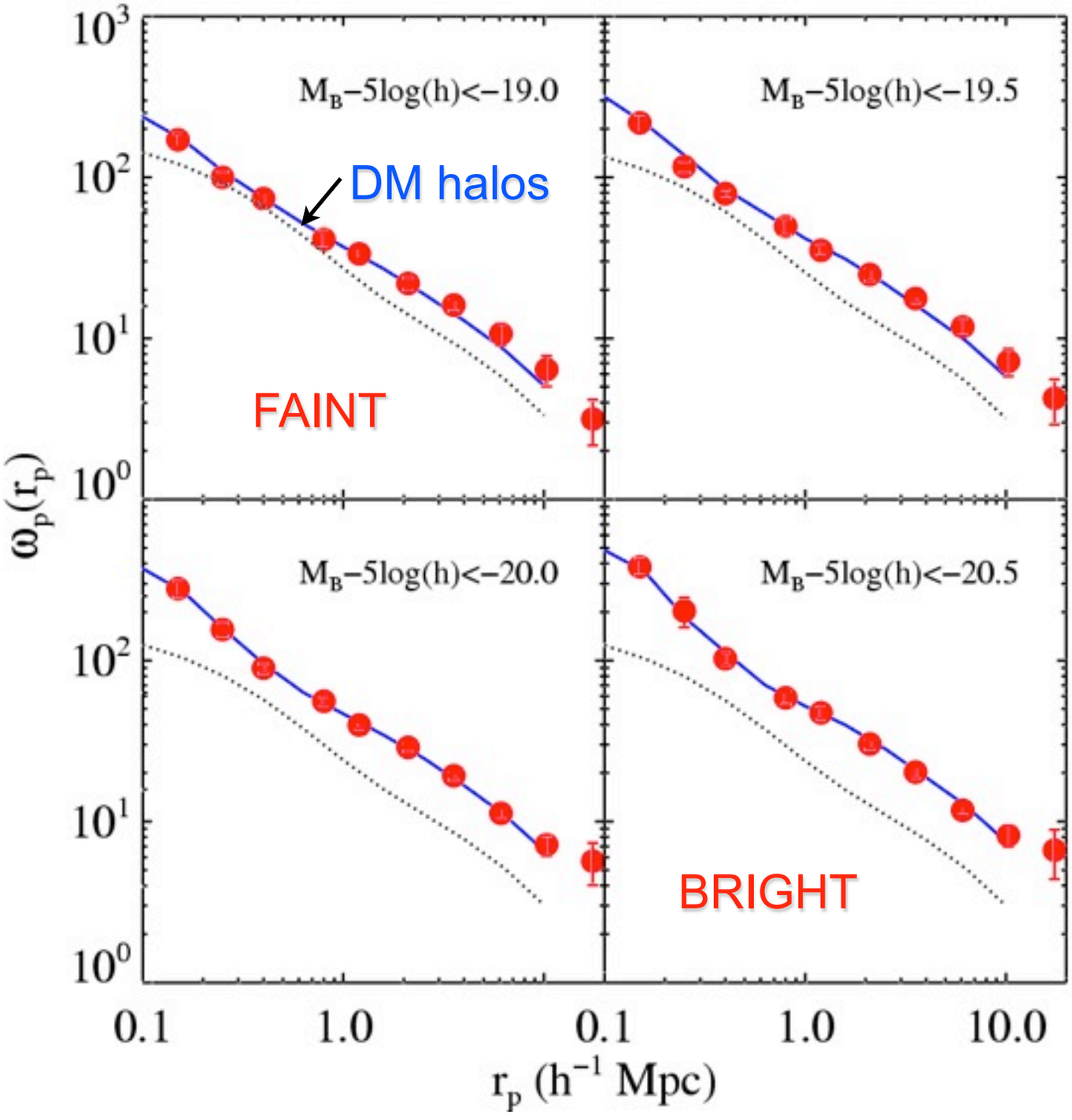

projected separation

Conroy, Wechsler & Kravtsov 06

and at z~4-5 (LBGs, Subaru)!!

angular 2-point correlation function

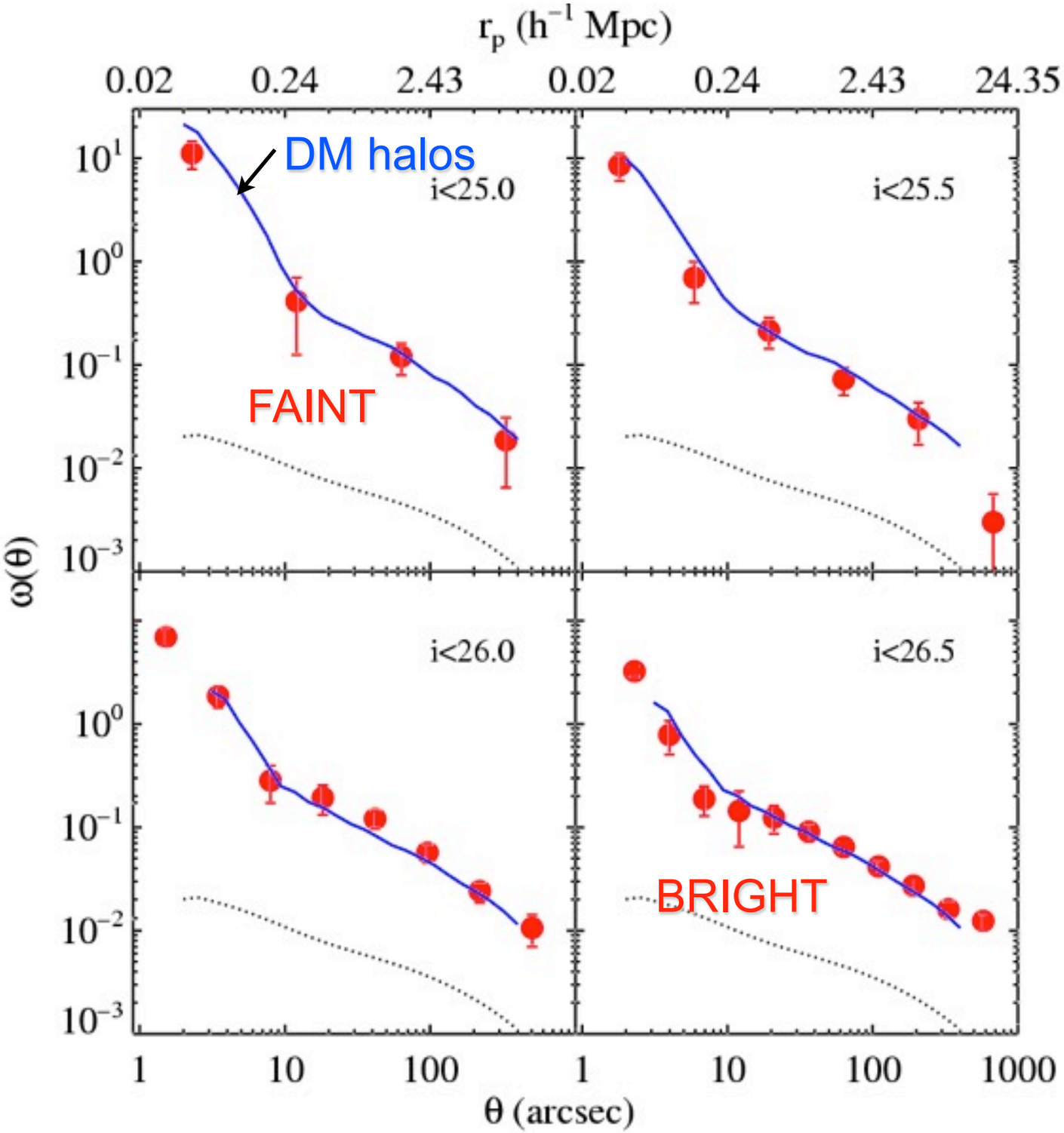

$n(>V_{\mathrm{max,acc}})=n(>L)$

Conroy, Wechsler & Kravtsov 06

projected separation